Award Number: DE-EE0003842

Project Title: RECOVERY ACT: DEVELOPMENT OF A HIGH PERFORMANCE COLD CLIMATE HEAT PUMP

Awardee: PURDUE UNIVERSITY

Reporting Period Ending: 12/31/2013

Acknowledgment: "This material is based upon work supported by the Department of Energy under Award Number DE-EE0003842."

Disclaimer: "This report was prepared as an account of work sponsored by an agency of the United States Government. Neither the United States Government nor any agency thereof, nor any of their employees, makes any warranty, express or implied, or assumes any legal liability or responsibility for the accuracy, completeness, or usefulness of any information, apparatus, product, or process disclosed, or represents that its use would not infringe privately owned rights. Reference herein to any specific commercial product, process, or service by trade name, trademark, manufacturer, or otherwise does not necessarily constitute or imply its endorsement, recommendation, or favoring by the United States Government or any agency thereof. The views and opinions of authors expressed herein do not necessarily state or reflect those of the United States Government or any agency thereof."

1 Introduction and Summary

The primary goals of the proposed project were to develop, test, and evaluate a high performance and cost-effective vapor compression air-source heat pump for use in cold climate regions. Vapor compression heat pumps are a proven technology, and have been used for many years to meet heating requirements for buildings in residential, commercial, and industrial applications. However, in climate regions that experience very low outdoor ambient temperatures both the heating capacity and coefficient of performance (COP) of traditional air-source vapor compression heat pumps drops dramatically with a decrease in the outdoor air temperature. The efficiency of heat pumping equipment has improved substantially over the past 20 years; however, the efficiencies of the highest rated equipment on the market are approaching practical limits that cannot be surpassed without modifications to the basic cycle and possibly the use of additional hardware.

In this report, three technologies to improve the efficiency of vapor compression systems are described. These are a) vapor injected compression, b) oil flooded compression and c) hybrid flow control of the evaporator.

Compressor prototypes for both, oil flooded and vapor injected compression were developed by Emerson Climate Technologies. For the oil flooded compressor, the oil injection port location was optimized and an internal oil separator was added using several design iterations.

After initial testing at Emerson Climate Technologies, further testing was done at Purdue University, and compressor models were developed. These models were then integrated into a system model to determine the achievable improvement of seasonal energy efficiency (SEER) for Minneapolis (Minnesota) climate. For the oil flooded compression, a 34% improvement in seasonal energy efficiency was found while a 21% improvement in seasonal energy efficiency ratio was found for the vapor injected compression. It was found that one benefit of both tested compression technologies is a lower discharge temperature, which allows for continued operation at lower ambient temperatures.

A bin analysis of the vapor injected prototype cold climate heat pump predicts a 6% improvement in HSPF for Minneapolis. This improvement is mainly a result of the increased capacity of the system for active vapor injection. For the oil flooded system, a slightly larger performance improvement is predicted, in this case mostly caused by an increase in heating COP. Based on an economic analysis of these results, the maximum additional cost of the system changes, for the Minneapolis location, are $430 for the vapor injected system and $391 for the oil flooded system. These estimates assume that a 3-year simple payback period is accepted by the customer.

For the hybrid flow control of evaporators, a new type of balancing valve was developed together with Emerson Climate technologies to reduce the cost of the control scheme. In contrast to conventional stepper motor valves, this valve requires less cables and can be driven by a cheaper output circuit on the control board. The correct valve size was determined in a dedicated test stand in several design iterations.

The performance benefits of the hybrid control of the evaporator coil were determined for clean coil conditions as well as with partial blockage of the air inlet grille and under frosting conditions. For clean

coil conditions, the benefits in terms of COP and capacity are negligible. However, significant benefits were noted for severely air-maldistributed operating conditions. For the H2-test, the maximum COP improvement of 17% along with a capacity improvement of nearly 40% was observed. Overall, the hybrid control scheme leads to a significant amount of performance improvement, if the air inlet conditions to the evaporator are maldistributed.

2 System and component modeling and development

In this task, the numerical models that are necessary to fully evaluate the proposed technologies are developed. These models are then used to assess their performance potential for low temperature heat pumping applications and to develop prototype designs.

2.1 Liquid flooded compressor modeling

The primary objectives of this task are to develop and expand the numerical models that are necessary to fully evaluate the proposed technologies, and to use those models to assess their performance potential for low temperature heat pumping applications and to develop prototype designs.

Subtasks 2.2 and 2.3 describe the modeling of the multi-port vapor injection and subtask 2.4 shows the results of system level modeling.

2.1.1 Isentropic Efficiency Model

The isentropic efficiency model is used for the system modeling and considers a constant isentropic efficiency of the compressor. The homogeneous mixture model is used to evaluate the combined properties of refrigerant and injected oil. Several simplifying assumptions are utilized for the mixture properties. It is assumed that the oil and refrigerant are in thermal and mechanical equilibrium; thus the oil and refrigerant mixture are at the same temperature and pressure. For the cycle analysis, the necessary thermodynamic mixture properties are the mixture enthalpy and mixture entropy as functions of temperature and pressure. Thus, the mixture enthalpy and mixture entropy can be expressed as

$$h_m = x_l h_l + (1 - x_l) h_g \text{ and} \tag{2.1}$$

$$s_m = x_l s_l + (1 - x_l) s_g , \tag{2.2}$$

which is simply an oil-mass-flow-fraction weighted average of the properties of the oil and refrigerant vapor. The oil mass fraction x_l is given as the ratio of mass flow rates of oil to total mass flow rate of oil and refrigerant, defined by

$$x_l = \frac{\dot{m}_l}{\dot{m}_l + \dot{m}_g} , \tag{2.3}$$

and the gas mass fraction is given by

$$x_g = 1 - x_l . \tag{2.4}$$

The inlet state point of the compressor is given by

$$h_1 = h_m \left(T_1, P_1, x_{l,1} \right) \text{ and} \tag{2.5}$$

$$s_1 = s_m \left(T_1, P_1, x_{l,1} \right) . \tag{2.6}$$

The isentropic outlet enthalpy can be determined from

$$h_{2s} = h_m\left(P_2, s_1, x_{l,1}\right). \tag{2.7}$$

For compressors flooded with large amounts of oil, it is assumed that there is no external heat transfer since the oil will tend to decrease the discharge temperature of the compressor and therefore the amount of heat lost to the ambient through convection and radiation.

The discharge entropy is given by

$$s_2 = s_m(P_2, h_2, x_{l,2}), \tag{2.8}$$

where the inlet $x_{l,1}$ and outlet $x_{l,2}$ oil mass fractions are the same. The compressor power is given by

$$\dot{W}_{comp} = (\dot{m}_l + \dot{m}_g)\left(h_{2m} - h_{1m}\right), \tag{2.9}$$

and for the isentropic case as

$$\dot{W}_{is} = (\dot{m}_{ref} + \dot{m}_l)(h_{2s,m} - h_{1,m}) \tag{2.10}$$

The isentropic efficiency of the compressor is then given by

$$\eta_{is} = \frac{\dot{W}_{is}}{\dot{W}_{el}}. \tag{2.10}$$

The regenerator is modeled using the effectiveness approach.

Figure 1 a) shows that model and experiment agree well for the dependency on the discharge temperature for -20°C evaporation temperature. A typical limit for compressor operation is 130°C (403 K) discharge temperature. This limit is exceeded without oil injection while operation can be continued if more than 10% oil is injected. Figure **1** b) shows the isentropic efficiency. The experiments showed an increase of the isentropic efficiency with increased oil injection. This effect was not captured by the isentropic efficiency model.

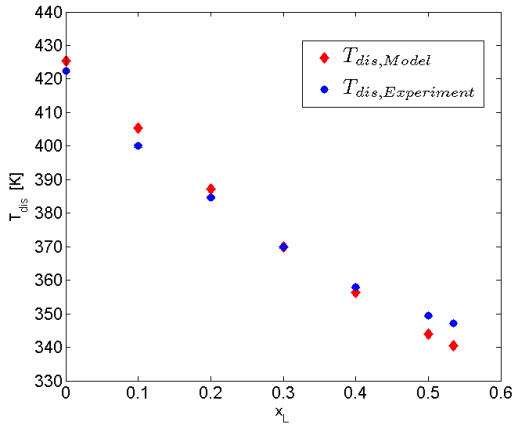

a) Discharge temperature as function of oil mass fraction.

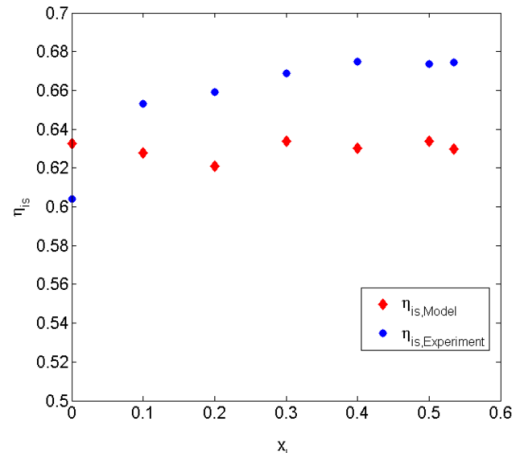

b) Isentropic efficiency as function of oil mass fraction.

Figure 1: Validation of scroll model for experimental conditions at T_{evap}=-20°C, T_{cond}=43.3°C, T_{oil_inj}=25°C.

2.1.2 Semi-empirical model

A set of semi-empirical models was developed for the oil flooded compressor, which can be used for the prediction of discharge temperature, mass flow rate, and power consumption. These can be used for system level simulations. The benefit of the semi-empirical model is that it captures additional effects which were not captured accurately by the isentropic efficiency model. The coefficients of the semi-empirical model were tuned according to the experimental results. The employed discharge temperature T_{2m} is calculated as

$$T_{2m} = (C_3 + C_4 \cdot x_L + C_5 \cdot x_L^{\ 2} + C_6 \cdot x_L^{\ 3}) \cdot EXP\left((C_7 \cdot \frac{T_{1m}}{T_C} + C_8 \cdot \frac{P_2}{P_1}) \cdot (C_9 \cdot x_L + C_{10}) \right), \qquad (2.11)$$

where C_3 to C_{10} are empirical coefficients, P_1 is the suction pressure, P_2 is the discharge pressure, and T_c is the critical pressure of the refrigerant. T_{1m} is the correlated mixture suction temperature, which is calculated as

$$T_{1m} = \frac{C_2 \cdot x_L \cdot T_{oil,1} + C_1 \cdot (1 - x_L) \cdot T_{gas,1}}{C_1 \cdot (1 - x_L) + C_2 \cdot x_L}, \qquad (2.12)$$

where C_1 and C_2 are empirical coefficients, x_L is the oil mass fraction (= oil/total mass flow rate), $T_{oil,1}$ and $T_{gas,1}$ are the temperature of the injected oil and suction side refrigerant, respectively.

For the calculation of mass flow rate and power consumption, the polytropic exponent n, calculated as

$$n = \ln\left(\frac{P_2}{P_1}\right) / \ln\left(\frac{\rho_{2m}}{\rho_{1m}}\right), \qquad (2.13)$$

is needed. ρ_{1m} and ρ_{2m} are the suction and discharge mixture densities. These are calculated as

$$\rho_{im} = \frac{\rho_{oil,i} \cdot \rho_{gas,i}}{(1-x_L)\cdot \rho_{oil,i} + x_L \cdot \rho_{gas,i}}, \tag{2.14}$$

where the index *i* is used to indicate suction (i=1) or discharge location (i=2). $\rho_{oil,i}$ and $\rho_{gas,i}$ are the oil and gas densities at these locations.

The mass flow rate $\dot{m}$ is calculated with the empirical coefficients C_{11} to C_{16} as

$$\dot{m} = \rho_{1m}\left(C_{11} + C_{12}\cdot\left(\frac{P_2}{P_1}\right)^{\frac{1}{n}} + C_{13}(P_2 - P_1)\cdot(C_{14} + C_{15}\cdot x_L + C_{16}\cdot x_L{}^2)\right). \tag{2.15}$$

The compressor power consumption $\dot{W}$ is calculated with the empirical coefficients C_{17} to C_{21} as

$$\dot{W} = \frac{n}{n-1}\cdot\frac{\dot{m}}{\rho_{1m}}\cdot(C_{17} + C_{18}\cdot x_L + C_{19}\cdot x_L{}^2)(C_{20}\cdot P_1 + C_{21})\cdot\left(\left(\frac{P_2}{P_1}\right)^{\frac{n-1}{n}} - 1\right). \tag{2.16}$$

Figure 2 shows that most of the measured discharge temperatures are predicted with an accuracy close to 2 K, and an RMS of 1.7 K. Figure 3 shows that most of the points with mass flow rates above 0.06 kg/s are predicted with an accuracy of 2%, the RMS of the entire population was 0.0009 kg/s. Figure 4 shows that most of the power consumption data is predicted within an accuracy of 2% while the RMS was 46 W.

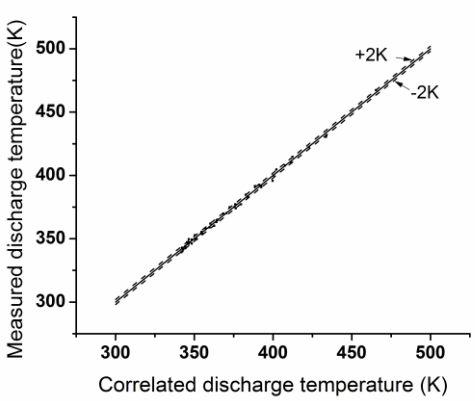

Figure 2: Measured and predicted discharge temperature

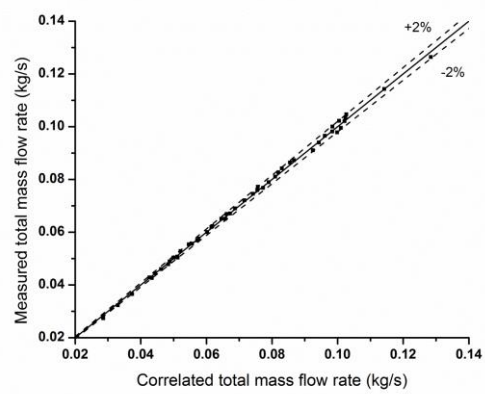

Figure 3: Measured and predicted mass flow rate

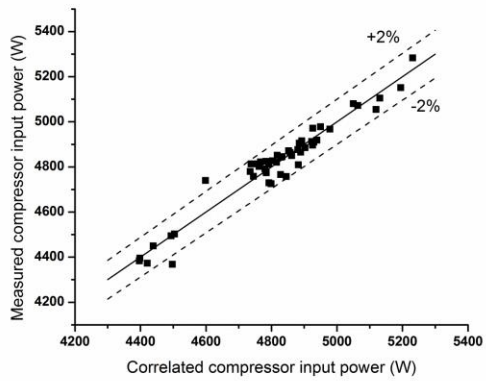

Figure 4: Measured and predicted power consumption

The determined empirical coefficients for the correlation are shown in Table 1.

Table 1: Empirical coefficients for compressor correlations

C_1 = 0.9469	C_8 = 0.02698	C_{15} = -5.185
C_2 = 1.053	C_9 = -1.234	C_{16} = 5.466
C_3 = 161	C_{10} = 1.099	C_{17} = 42.29
C_4 = 68.71	C_{11} = 0.003971	C_{18} = -8.066
C_5 = 143.4	C_{12} = -0.00004128	C_{19} = 23.45
C_6 = -28.76	C_{13} = -0.0000001404	C_{20} = 28.71
C_7 = 0.8153	C_{14} = 0.6863	C_{21} = 3352

2.2 Multiple port vapor injected compressor modeling

In this task, models to predict the behavior of scroll compression mechanisms with multiple vapor injection ports and economizing were modeled. Modeling results from this subtask will be used to develop prototype scroll compressor designs for the vapor injection with economizing concept. This work was carried out by Purdue University in collaboration with Emerson Climate Technologies.

2.2.1 Isentropic efficiency model

An isentropic efficiency model was developed for the system modeling. The main assumptions in the model are a constant isentropic efficiency of the compression process which is modeled as a parallel compression process as shown in Figure 5. The isentropic efficiency is therefore weighted according to the mass flow rate and defined as

$$\eta_{isen} = \frac{\dot{m}_s(h_{2s} - h_1) + \dot{m}_{inj,1}(h_{3s} - h_3) + \dot{m}_{inj,2}(h_{4s} - h_4)}{\dot{m}_s(h_2 - h_1) + \dot{m}_{inj,1}(h_2 - h_3) + \dot{m}_{inj,2}(h_2 - h_4)} \tag{2.17}$$

.

The volumetric efficiency is calculated based on the inlet density to the suction as

$$\eta_{vol} = \frac{\dot{m}_s}{\rho_{in} * \dot{v}}, \tag{2.18}$$

where the displacement of the suction is based on the suction displacement and the compressor rotational frequency:

$$\dot{v} = V_{disp} * f \ . \tag{2.19}$$

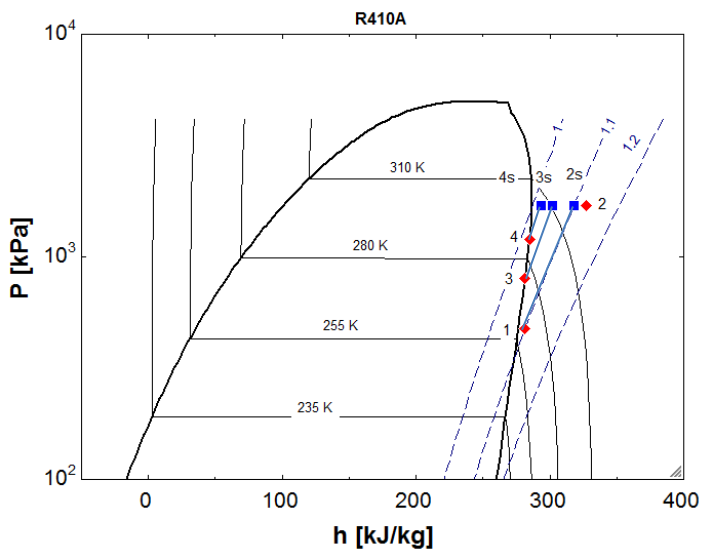

Figure 5: Log(p)-h plot of isentropic compression in vapor injection

2.2.2 Physics based model

A physics based model was developed to better understand the compression process with vapor injection. Figure 6 shows that the model is composed out of 4 sub-models. The model was implemented in Matlab.

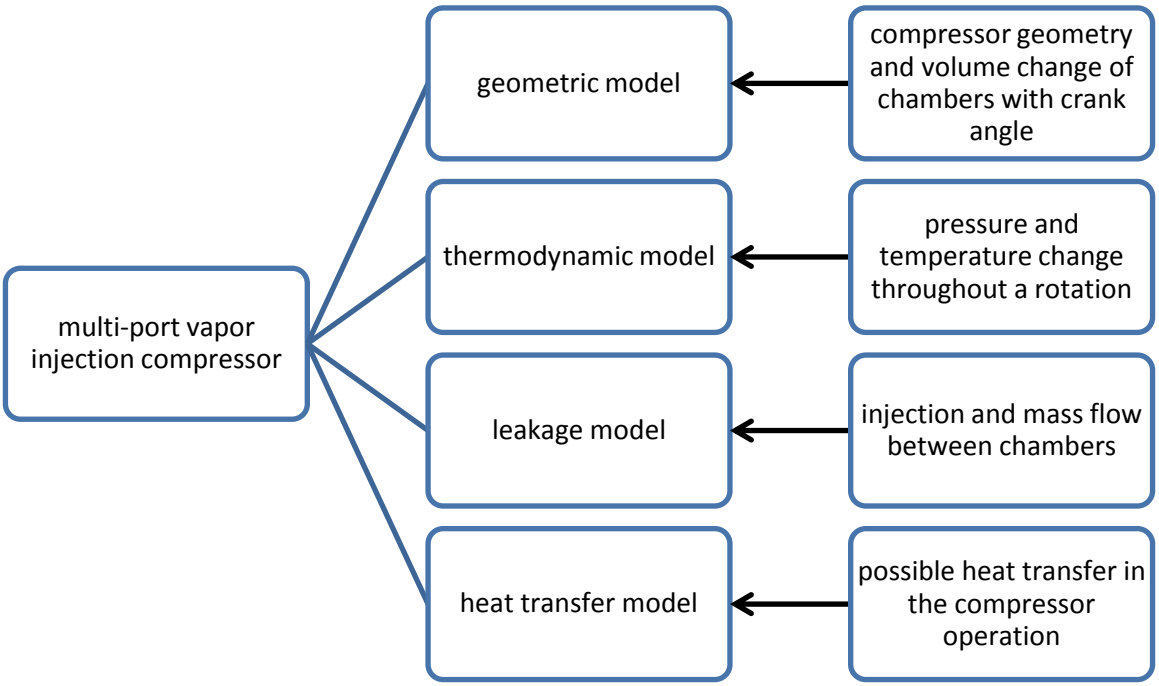

Figure 6: Model of multi-port vapor injection compressor

The geometric model has been built up to include geometric parameters at a given crank angle. Specifically, it calculates the parametric equations of the inner and outer scroll wraps of both fixed and orbiting scrolls, as well as the discharge region as shown in Figure 7. The volume of each chamber can be calculated based on the parametric equations of the wraps at any crank angle, which is necessary in analyzing thermodynamic parameters.

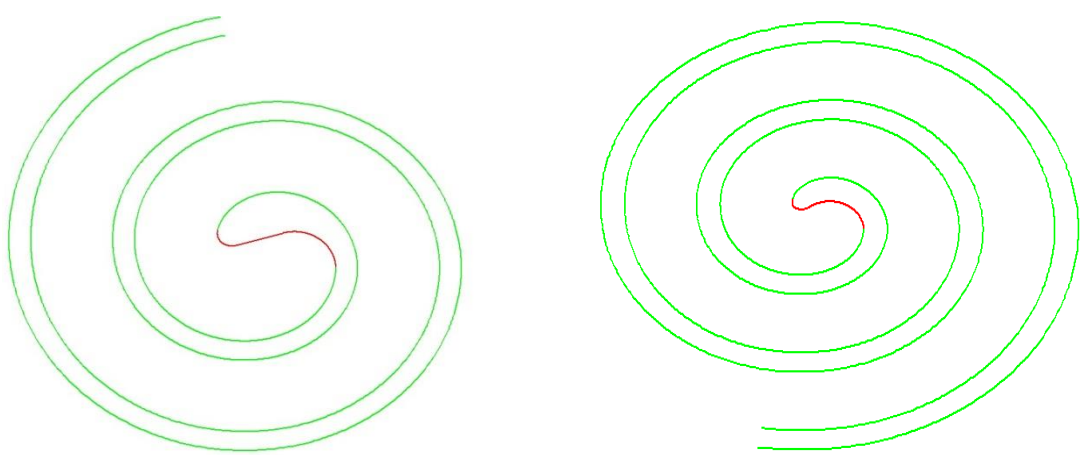

Figure 7: Scroll wraps with different discharge region generated in MATLAB.

Since the state of the refrigerant at every angle of a rotation is determined, two parameters are calculated to fix all the state parameters in the operation of the compressor. In the mathematical model of the compressor, the variation of temperature and mass flow rate with crank angle can be expressed with two ordinary differential equations derived from conservation equations. The Euler method was initially used to solve these equations but the results showed that this not accurate enough. Therefore an adaptive Runge-Kutta 5th order method was selected, which gives a good prediction of the state parameters when heat transfer and leakage are neglected. The scroll geometry generation code has been validated against the Copeland ZPI29K5E-PFV compressor shown in Figure 8.

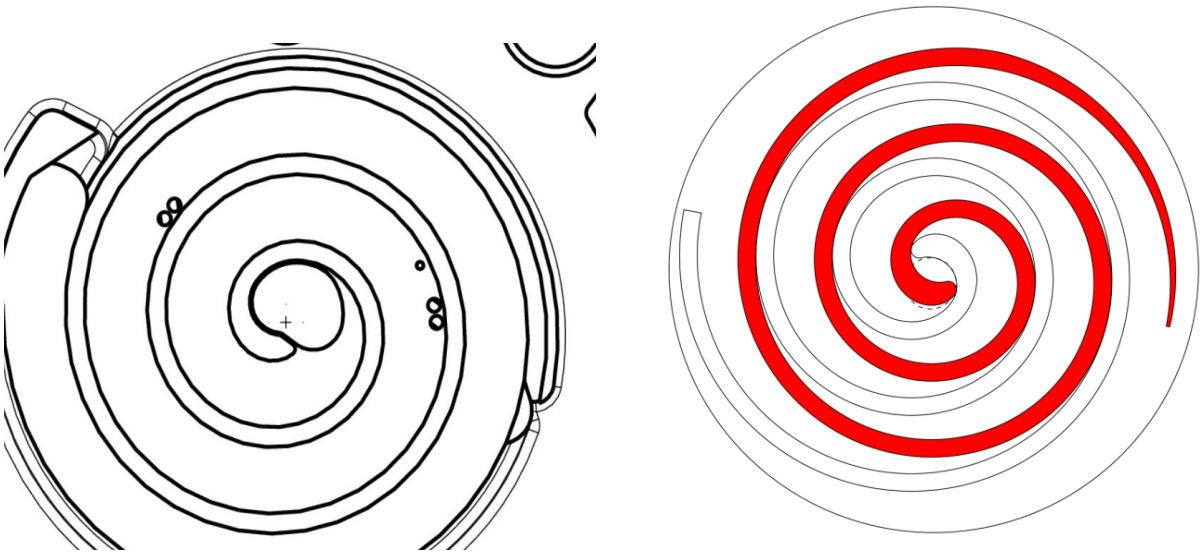

a) Manufacturer supplied drawing. b) Scroll geometry generated using Matlab.

Figure 8: Copeland ZPI29K5E-PFV compressor scroll geometry and model results.

In order to model the compressor with vapor injection, the detailed scroll compressor model developed for oil flooding has been modified to handle vapor injection. The injection line is modeled as being at a constant pressure and temperature, which is taken to be 5 K superheated above the saturation temperature at injection pressure.

It was found that the injecting economized refrigerant during the compression process cools the refrigerant that is being compressed. Furthermore the economized refrigerant does not need to be compressed from the suction pressure. These factors lead to reduced compression work. Although the economization may slightly decrease the heating capacity of the cycle, the decrease in power consumption is more significant. Therefore the coefficient of performance (COP) of the cycle, which is defined as the ratio of heating capacity to power consumption, will improve with economizing. To maximize the benefits of economization, the injected refrigerant should be used to provide as much cooling to the compressed refrigerant as possible. However, the amount of cooling that can be supplied by economization is generally limited by the desire to maintain a vapor state in the compressor, and thus the refrigerant in the compressor should not be cooled beyond the saturated vapor point.

The compression process tends to increase the superheat of the refrigerant. Therefore, it would be ideal to inject a two-phase mixture of refrigerant in order to return the refrigerant in the compressor at the injection port to the saturated vapor state. While the performance improvements provided by two-phase refrigerant injection are significant, there is also substantial complexity associated with controlling the quality and flow rate of the injected refrigerant.

As an alternative, saturated vapor can be injected during the compression process to provide cooling. The superheat of the refrigerant in the compressor will continue to increase during the compression process because the vapor will provide less cooling than two-phase refrigerant. However, vapor injection is expected to be much easier to control. In addition, this method of economization only uses the saturated vapor generated during the expansion process without drawing off any liquid, which leaves a larger mass flow rate in the evaporator. Thus, there is no reduction in the heat gained in the evaporator and the only reduction in the cycle heating capacity is due to the decrease in the compressor exit temperature.

Figure 9 shows the COP of the heat pump with economization relative to the unmodified heat pump cycle as a function of evaporating temperature. Solid lines show the performance of the cycle with continuous injection of two-phase refrigerant, while dashed lines show the performance with continuous injection of saturated vapor. These results assume a compressor isentropic efficiency of 70% and consider three different condensing temperatures. The two-phase injection provides greater performance improvements; the difference between the improvements in COP with saturated vapor injection versus two-phase injection is between approximately 25 and 30% relative to the baseline cycle.

The difference between the performance with two-phase refrigerant injection and saturated vapor injection becomes less pronounced for lower ambient temperature applications. In addition, Figure 10 shows that this difference becomes smaller when fewer injection ports are used. The horizontal lines in Figure 10 represent the performance of the two economized cycles with continuous refrigerant injection for an evaporating temperature of -20°C and a condensing temperature of 50°C. The plotted points show the cycle performance as a function of the number of injection ports. With one injection port, the difference between cycle performance with two-phase and saturated vapor injection is negligible. With two, three or four injection ports, the two-phase injection offers less than a 3% improvement in performance over the cycle with saturated vapor injection. The benefit of reduced overall cycle complexity far outweighs the slight reduction in performance when saturated vapor injection is used in place of two-phase refrigerant. Therefore, the development of a scroll compressor with multiple injection ports should initially focus on using saturated vapor.

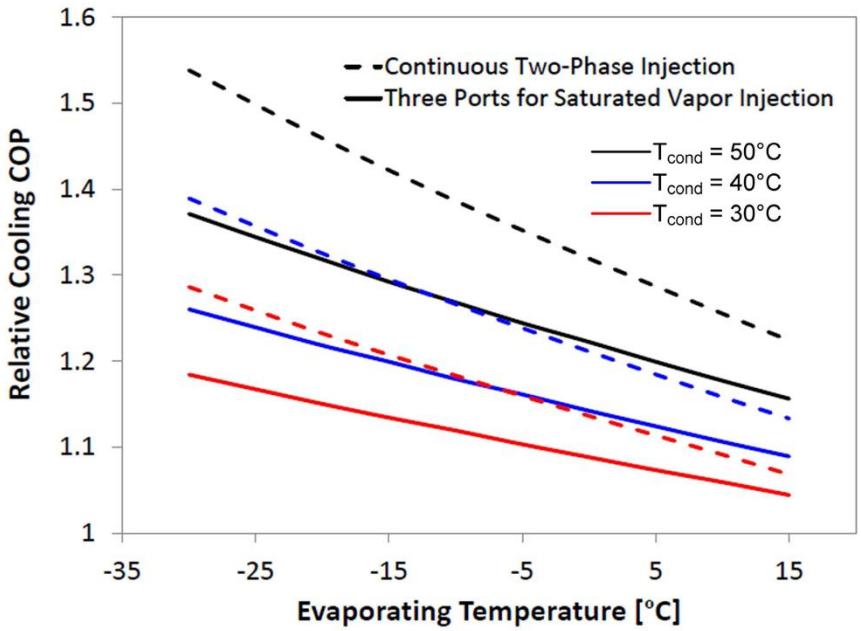

Figure 9: Comparison of economized cycle performance with continuous injection of two-phase refrigerant versus saturated vapor refrigerant (Mathison, 2011).

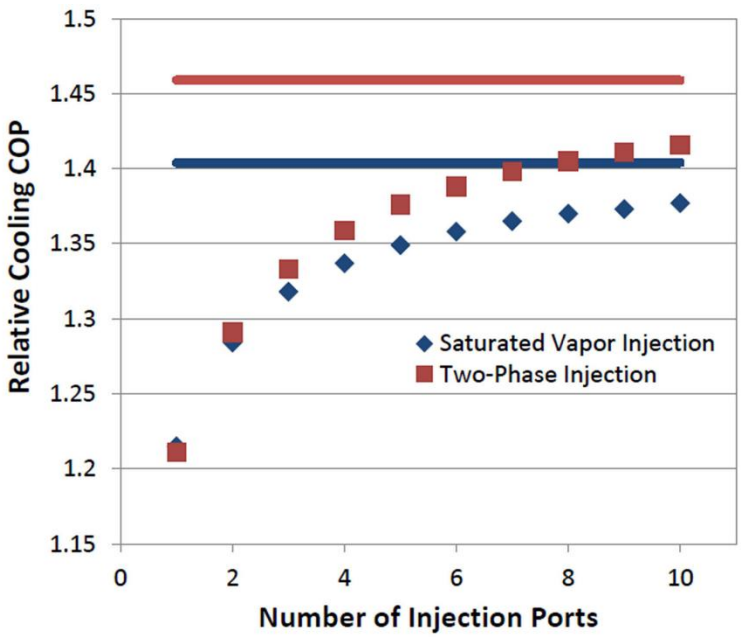

Figure 10: Comparison of economized cycle performance with injection of two-phase refrigerant versus saturated vapor refrigerant through a varying number of ports (Mathison, 2011).

2.2.3 Empirical Model

The test results of the experiments were mapped for system simulation purposes using an empirical correlation,

$$X = a_0 + a_1 \cdot \left(\frac{P_d}{P_s}\right)^{a_2} \cdot \left(\frac{P_{VI,h}}{P_s}\right)^{a_3} \cdot \left(\frac{P_{VI,l}}{P_s}\right)^{a_4}, \quad (0.1)$$

where a_0 to a_4 are empirical coefficients, X is the correlated property, and P_d, $P_{VI,H}$, and $P_{VI,L}$ are the discharge, high vapor injection and low vapor injection pressures in kPa. The coefficients for these correlations along with the coefficient of determination are shown in Table 9.

Table 2: Coefficients and coefficient of determination for regressed properties

X	Units	Description	a_0	a_1	a_2	a_3	a_4	R^2
$\dot{m}_{VI,H} / \dot{m}_{suc}$	[-]	Dimensionless mass flow of high pressure injection	-0.1262	0.157	-0.1592	1.097	0.02495	0.998
$\dot{m}_{VI,L} / \dot{m}_{suc}$	[-]	Dimensionless mass flow of low pressure injection	-0.4597	0.3204	-0.04321	-0.1482	0.8981	0.999
$\dot{m}_{suc}$	[kg/s]	Mass flow at compressor suction	-11.82	11.99	-0.0043	-0.00095	-0.00057	0.991
$\dot{W}$	[kW]	Compressor power consumption	5.766	19.70	-3.144	1.154	1.268	0.833
T_{disc}	[C]	Discharge temperature	98.64	0.002351	4.268	0.6079	-0.2864	0.973

In addition to the empirical model, a physics based model was developed to determine possible experimental issues and to better understand the compression process. The main result of the physics based model, which was tuned to the experimental data, was a good agreement between experiment and simulation.

2.3 Evaporator balancing valve modeling

Develop numerical models for the two different evaporator refrigerant flow control concepts. The models will help to accomplish two steps in the design process: 1) determining the range of valve openings to achieve the desired range of pressure drops under steady-state conditions and 2) designing the valve mechanism to provide an appropriate control response for the expected boundary conditions. This work will be carried out by Purdue University in collaboration with Emerson Climate Technologies.

During the discussion with Emerson Climate Technologies, it became clear that the valve concepts of the proposal were not favorable in terms of cost and manufacturability. Therefore a number of new valve concepts were developed with a number of to be fulfilled characteristics. The balancing valves should fulfill the following requirements:

- Cheap: cheaper than conventional TXV valves,
- Reliable: expected lifetime is 7 years or more,
- Small: the sizing of the HX housing should be kept the same,
- Efficient: little or no energy use.

A number of valve concepts seemed to be promising, but initial design calculations as well as material limitations (self-powered valve) showed that they were not viable. The calculations are shown in greater

detail in the phase 1 report. The linear bimetallic valve was the most promising passive concept and is shown in Figure 11. In the valve, two counteracting bimetallic washer sets are used to measure the superheat and adjust the needle position to regulate the flow rate. The shaft of the needle needs to be sealed, since it poses a possible leakage path from evaporator inlet to evaporator outlet. The seal, in this case an O-ring, leads to friction and by that to hysteresis of the valve. The hysteresis of the valve was estimated for PTFE coated O-rings and standard rubber O-rings, Figure 12. While the PTFE-coated O-ring lead to an acceptable hysteresis of 0.4 K superheat, the hysteresis for the standard O-rings was unacceptably high. Since the Teflon coating might wear off within the lifetime of the system, the hysteresis was found to be unacceptable. Therefore the passive valve concepts were entirely removed from the list of possible valve designs.

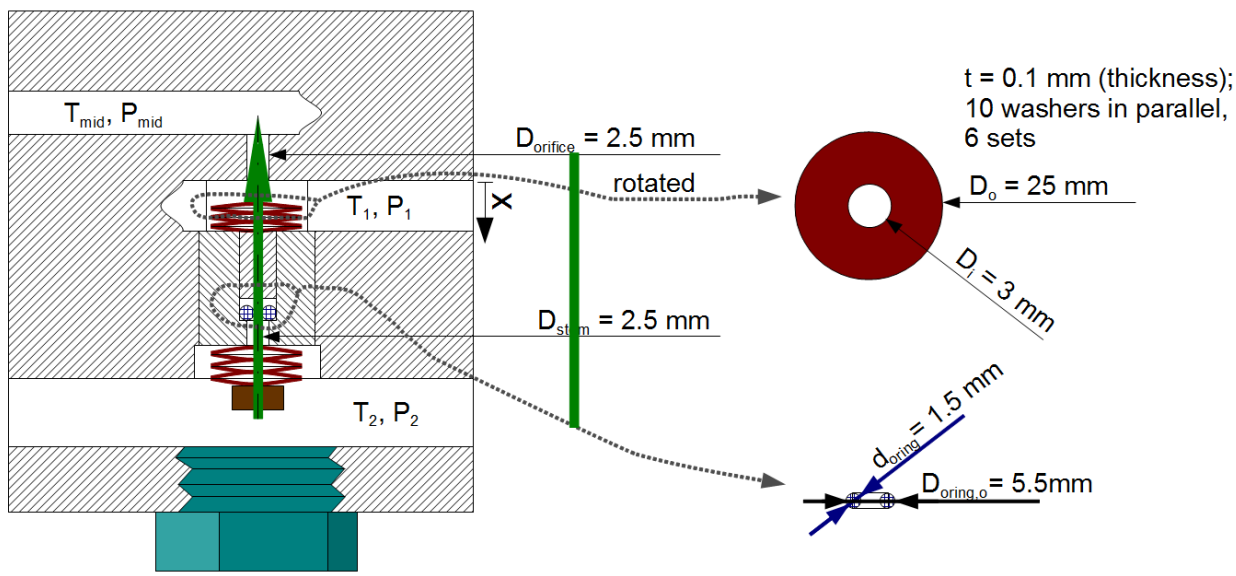

Figure 11: Dimensions used for the bimetallic valve with linear action

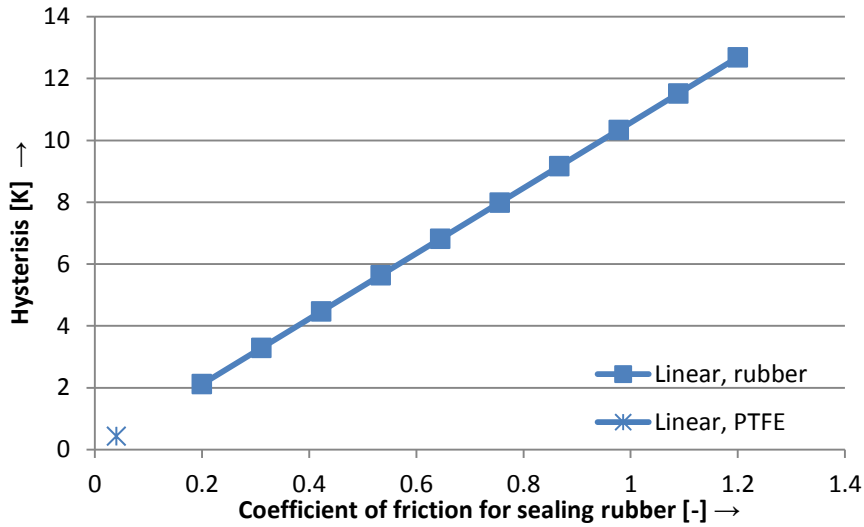

Figure 12: Hysteresis of the valve concept for different friction coefficients

The required characteristics were best matched for the 2-step balancing valves with and without self-hold. For this project, 2-step balancing valve prototypes were designed and build by Emerson Climate Technologies, as shown in paragraph 3.1.3. These 2-step prototype valves are based on conventional solenoid technology.

Test data was obtained according as outlined in paragraph 3.1.3. For the development of the flow correlation, the data of the valve modifications V1 and V2, as shown in Table 3, was used.

Table 3: Valve data used for correlations

modification	height groove 1	diameter groove 1	height groove 2	diameter groove 2
V1*	1.4	7.85	1.14	8.6
V2	1.4	7.22	1.14	8.65

* = tested also in PWM-mode according to previous test plan

Equation 1 was developed to correlate the measurement data. The dimensionless PI-groups 4 and 8 of the correlation represent the effects of cross-sectional area for the flow and the pressure difference across the valve, respectively. The dimensionless PI-group 1 represents the mass flow rate and accounts for the effects of inlet pressure. The constant c_0 is employed to capture the effects of leakage around the valve plunger. Figure 13 shows the simulated inlet and exit pressure of the valve together with the selected points for the test plan. Linear interpolation between the flow area of the open and closed position was used for the points with pulse width modulation. The points are equally spaced over the operating range of the valve test stand. Figure 14 shows the performance of the correlation, the majority of the points are predicted within a deviation of 15%.Table 4 shows the employed constants, PI-groups, the goodness of fit parameters and the definition of the hydraulic area. .

$$PI_1 = c_L + c_0 \cdot PI_{14}^{C_4} \cdot PI_8^{C_8} = \frac{\dot{m}}{A_{hydraulic} \cdot \sqrt{\rho_f \cdot p_{in}}} \tag{1}$$

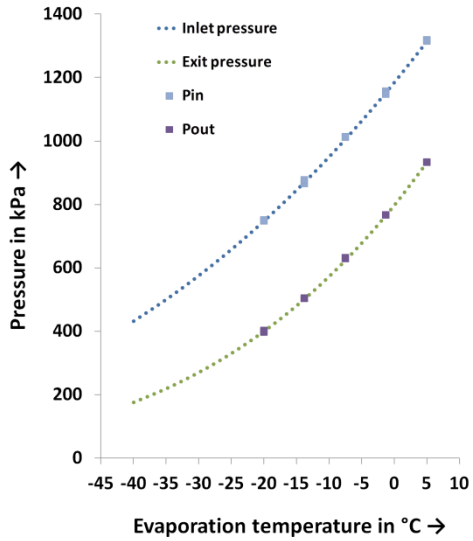

Figure 13: Operating conditions for valve and test points.

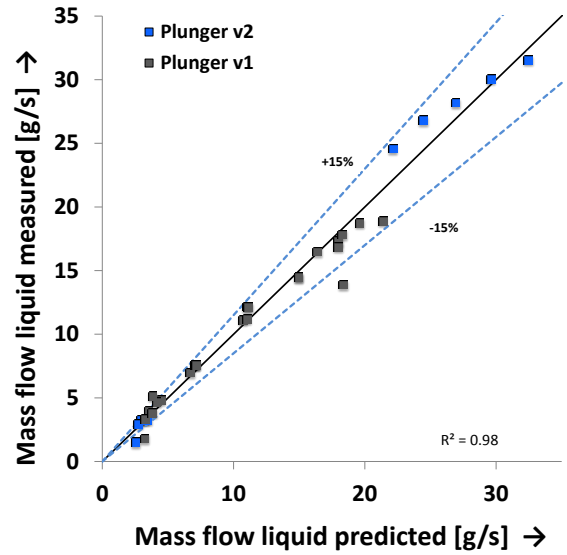

Figure 14: Correlation results.

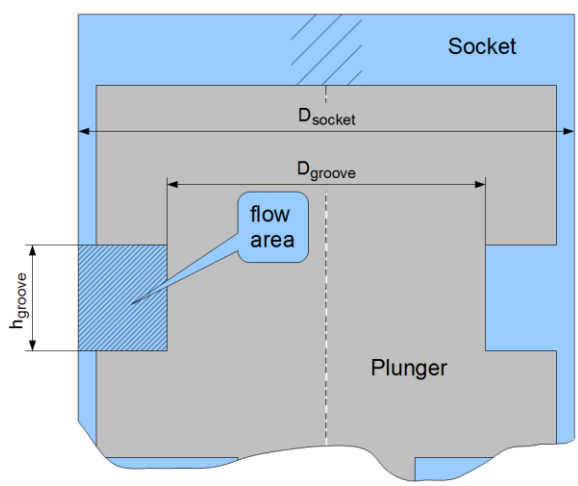

Figure 15: Plunger dimensions as used for correlation

Table 4: Constants, Pi groups and correlation performance

c_L		c_0	c_8	c_{14}
-4.03696471		3.420794827	-0.1484192972	-0.05448275105
R^2	sigma	bias	Pi_8	Pi_{14}
0.98	1.24 g/s	0.04 g/s	$\frac{D_{hydraulic}^2}{D_{socket}^2}$	$\frac{P_{in} - P_{out}}{P_{crit}}$
$d_{hydraulic}$		$A_{hydraulix}$	D_{socket}	
$\frac{4 \cdot h_{groove} \cdot (D_{socket} - D_{groove})}{4 \cdot h_{groove} + 2 \cdot (D_{socket} - D_{groove})}$		$\frac{\pi \cdot D_{hydraulic}^2}{4}$	8.9 mm	

After several design iterations, acceptable dimensions for the 2-step valves, which will be used as balancing valves for the hybrid control scheme, were found. For the valve in low flow rate position we targeted 25% of the flow rate required to best match the building heat load within the limitations of the compressor speed. For the high flow rate we required the maximum of either the flow rate at 60 Hz compressor frequency or 150% of the flow rate required to match the building heating requirement. Figure 16 shows the measured flow rates for the target as well as measured flow rates. The low flow rate valve position matches the target of 25% flow rate very well. The high flow position of the valve leads to a larger flow rate than required. However, this will be of benefit if maldistribution is prevalent when rapid heating of the building is required. The found dimensions are therefore acceptable and the subtask is therefore finished.

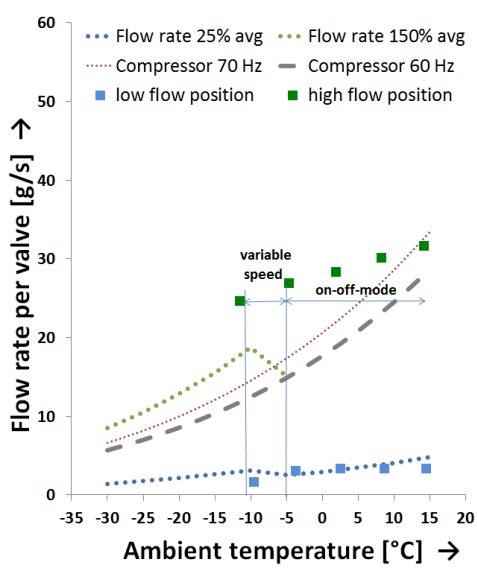

Figure 16: Target flow rates and actual flow rates.

2.4 System level modeling

System modeling was done for baseline single stage system, 2-port vapor injected compression and oil flooded compression. The previously described isentropic efficiency models for the compressor were used for the system level models, where constant isentropic efficiencies were assumed for the compressors. For all systems, a pinch point approach was chosen to obtain the saturation temperatures at the heat exchangers.

The components of the oil flooded model use the enthalpy values of the oil mixture in each component, and oil solubility is considered for the oil-stream leaving the oil separator. For each point, the oil injection rate is optimized to gain the highest possible COP. For the internal heat exchanger, a constant effectiveness was assumed.

Equal vapor pressure ratios for all three compression stages were used for the 2-port injected vapor injected compression. It was assumed that all vapor generated during the expansion process is injected into the injection ports.

A parametric study was conducted in order to evaluate the effects of ambient temperature, refrigerant selection and control scheme onto the performance indices COP and heating capacity. Figure 17 shows the COP of the two technologies compared to the baseline COP. The relative COP generally increases as ambient temperature decreases. For R32 and R410A, vapor injection is predicted to lead to a larger performance improvement than oil flooding. The largest performance improvement is predicted for R1234yf. Figure 18 show the normalized capacity – saturated vapor injection generally leads to a decrease in capacity at higher ambient temperatures while it increases the capacity at lower ambient temperatures. For oil flooded compression, the capacity change with temperature is smaller and observes the opposite trend for R32 and R410A.

Another parametric study (Bell, 2011), came to the conclusion that achievable performance improvements using oil flooding for alternative refrigerants such as CO2, propane, and ammonia are higher than for R410A. However, these refrigerants have drawbacks: CO2 is a high pressure refrigerant, propane is flammable, and ammonia is has a pungent smell that can cause panic in case of small leaks. Therefore, these refrigerants were not followed up further in the current study.

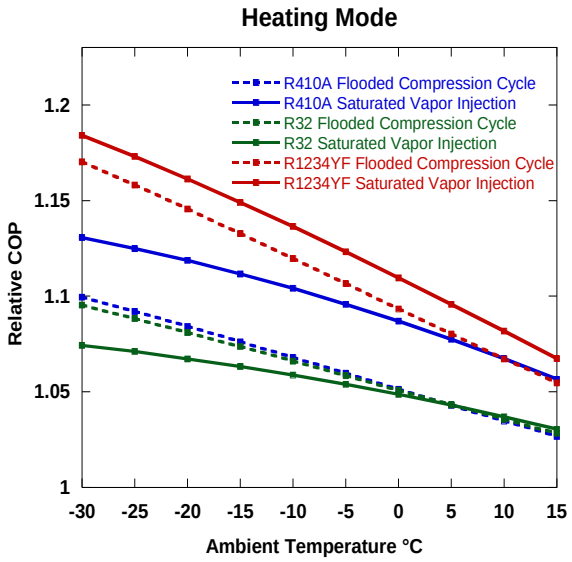

Figure 17: Normalized Heating COP

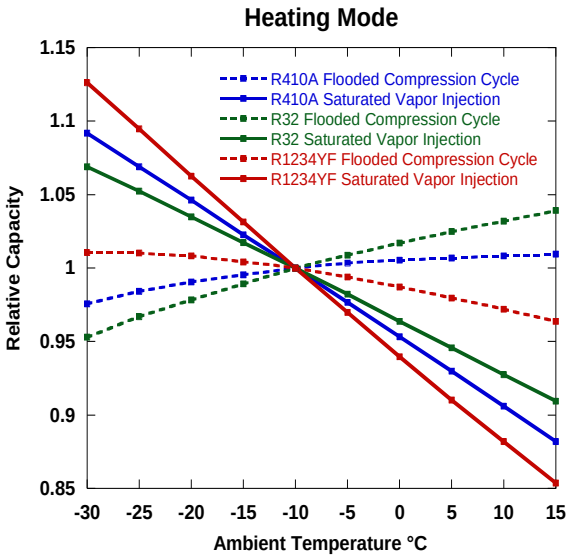

Figure 18: Normalized heating Capacity

3 Experimental testing and model/performance validation

This task was completed as the second project phase. The aims of this task were to evaluate component performance and validate and improve the numerical models developed in Task 2. Prototypes were developed in cooperation with the industrial partners and tested in the laboratory.

3.1 Development of compressor and valve prototypes

Prototype compressors for each of the two compression concepts will be developed along with prototypes for each of the evaporator refrigerant flow control valve ideas, based on the results and outcome of Task 2. This work will be carried out by Emerson Climate Technologies in close cooperation with Purdue University.

3.1.1 Oil flooded compressor prototype

The prototype oil flooded compressor was manufactured by Emerson Climate Technologies and uses standard components. The ZPI72KCE running gear with special modifications for R410A capability is used. Also, the compressor uses a ZS45K4E shaft and rotor for better compressor balance and ZS45K4E scroll set to provide 4in3 (6.56e-05 m^3) volumetric displacement and a volume ratio of 3.29. ZPI72KCE and ZS45K4E are the Emerson/Copeland part number designations. The oil injection ports are located at the suction chamber of the compressor rather than within the compression process as it is the case for the vapor injected compressor, as shown in Figure 19. The compressor runs on a 200/230V three phase supply and rotates at 3500 rpm under load. Figure 20(a) shows a schematic of the R410A scroll compressor with dual oil injection ports and Figure 20(b) shows the compressor cross-section. Figure 4.8 shows the oil flooded compressor installed in the test stand. An oil level indicator is connected to the compressor shell to monitor the oil sump level in the compressor

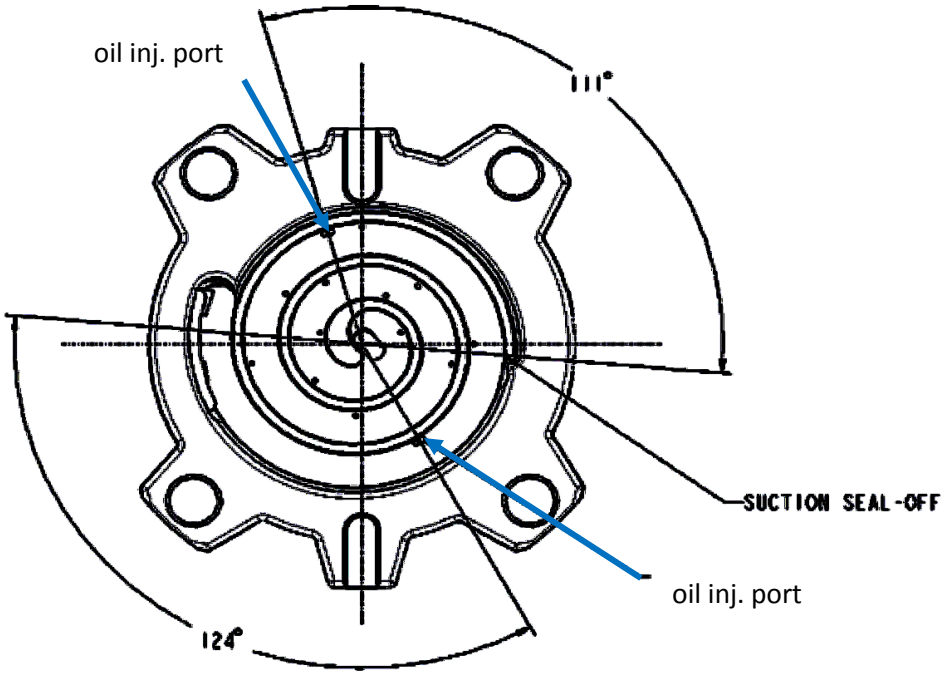

Figure 19: Location of oil injection ports

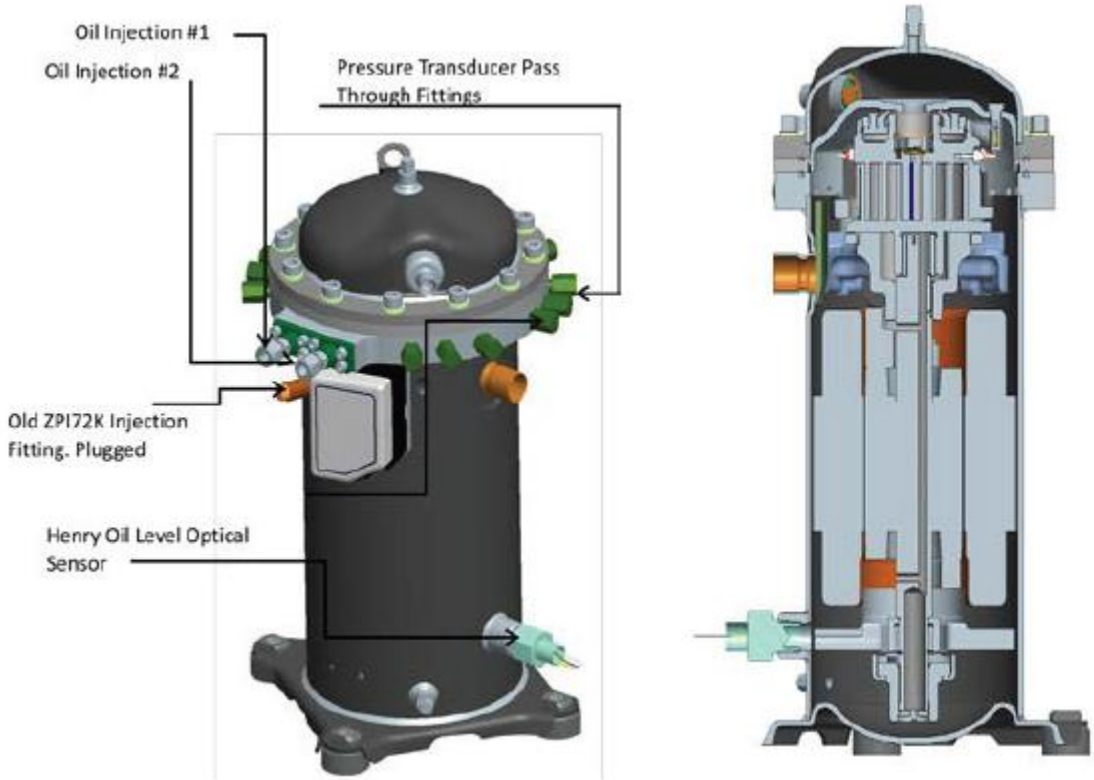

a) Overview and port locations

b) cross-sectional view

Figure 20: Prototype R410A compressor with dual oil injection ports

3.1.2 Vapor injected compressor prototype

The prototype vapor injected compressor was manufactured by Emerson Climate Technologies. It utilizes the Model ZPI72KCE running gear and the ZS45K4E shaft and rotor for better compressor balance. The ZF13K4E scroll set was modified to include injection ports. It has 4 in^3 (6.56e-05 m^3) volumetric displacement and a volume ratio of 3.29. The compressor is powered by a 200/230V three-phase AC motor, which rotates at 3500 rpm under load. Figure 21 (a) shows a schematic of the R410A scroll compressor with dual oil injection ports and Figure 21 (b) shows the compressor cross-section. The higher-pressure saturated vapor is injected into the injection port #1 labeled (INJPORT B 1..3 in Figure 22, inner compression path) while the lower-pressure saturated vapor is injected into the injection port #2 labeled as INJ-PORT A 1..3 and used for the outer compression path in Figure 21.

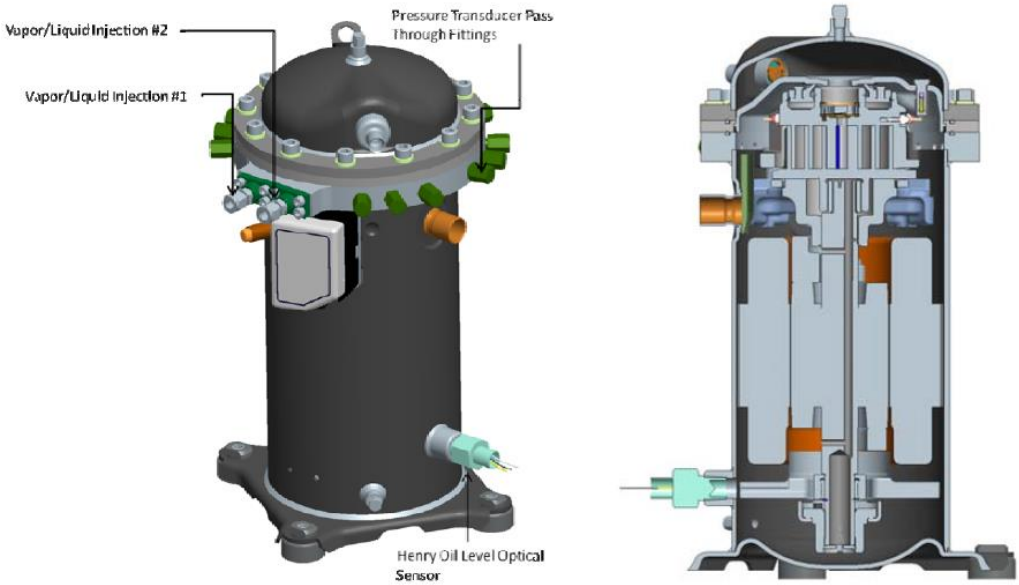

a) Overview and port locations b) cross-sectional view

Figure 21: : Prototype R410A compressor with dual vapor injection ports

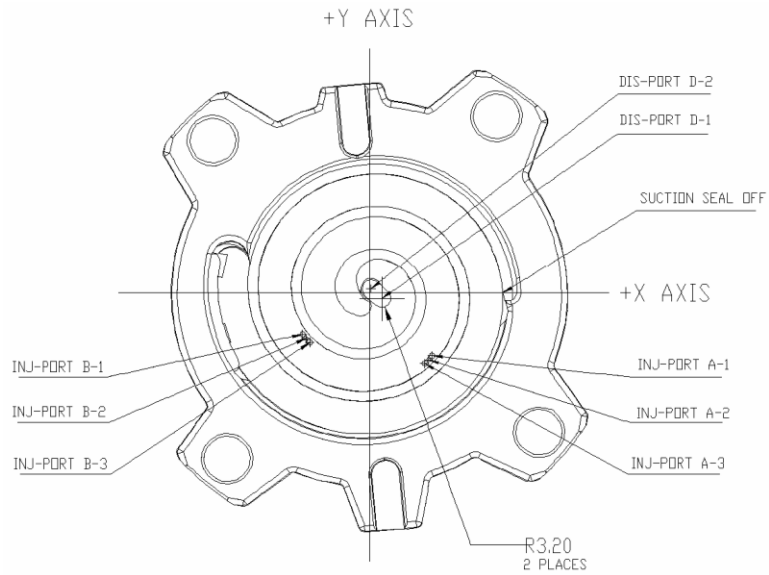

Figure 22: Location of vapor injection ports

3.1.3 Refrigerant flow valve prototypes

It was found that the initial valve concepts were not viable. Therefore different valve concepts were developed and it was found that solenoid technology was most promising. Figure 23 shows one of these solenoid valve. Figure 24 shows the explosion view of the same valve. A spring-loaded plunger with 2 grooves of different depth is used to control the flow through the valve body. In open position, the coil is deactivated, the spring pushes the plunger in such that the larger groove is active, and the plunger only leads to a minor restriction of the flow. This is also the default position of the valve that would result from a broken coil or cable and by that a fail-safe feature: It ensures that the performance of a heat pump with that type of valve as balancing valve does not drop below the performance of a conventional distribution system in case of valve failure. To bring the valve into throttled position, the solenoid has to be activated. The plunger is pulled up and the now active smaller groove leads to a smaller flow rate.

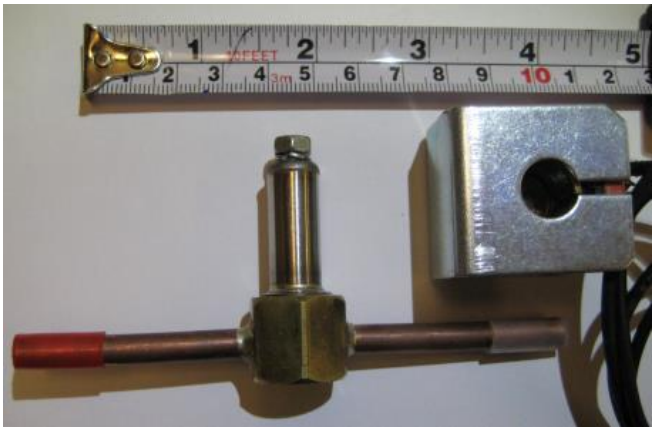

Figure 23. Prototype solenoid 2-step expansion valve

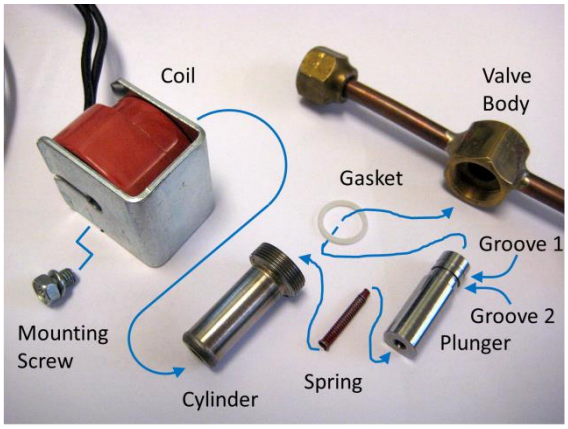

Figure 24: Prototype 2-step valve,exploded view

3.2 Experimental testing of compressor and valve prototypes

Each of the proposed prototype components will be tested over a range of conditions representative of heat pumps in cold climates. This will require utilization of specialized test stands at Purdue University. Existing test stands will be modified to allow testing of these concepts. Test results will be compared with model predictions to provide validation and refinements to the modeling tools. The prototype performance and modeling results will be used to update the assessments of the benefits of the various technologies that are studied. This work will be carried out by Purdue University in collaboration with Emerson Climate Technologies and Carrier Corporation.

3.2.1 Experimental testing of oil flooded compressor

The oil flooded compressor was tested in a dedicated valve test stand, Figure 25. The test stand is designed as a hot gas bypass test stand. In addition to the hot gas bypass part, a primary and an auxiliary oil separator are used. The compressor oil level is maintained by metering oil from the primary oil separator into the compressor sump. The auxiliary oil separator is used to capture the oil injected to achieve a closer to isothermal compression process. The refrigerant flow can be adjusted between the two separators in order to capture sufficient amounts of oil for oil injection and compressor sump.

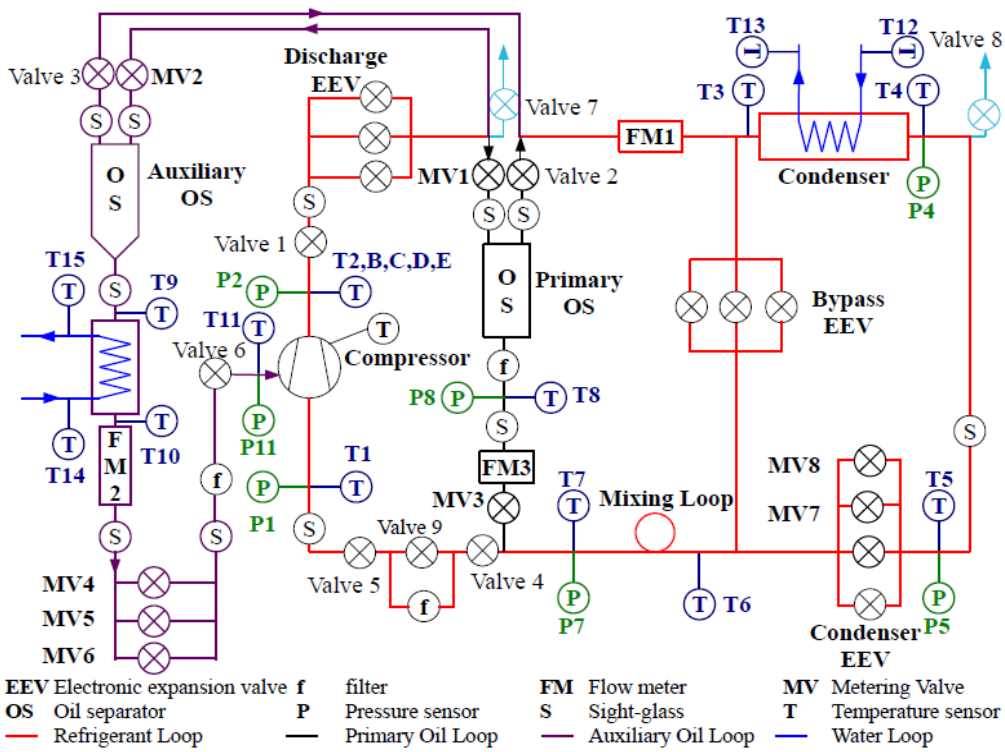

Figure 25: Schematic of load system modified for oil flooding with instrumentation

Most air conditioning and heat pump applications on the market today use R410A as the refrigerant. Therefore, this project focused on validating efficiency improvements with oil flooding for R410A. R410A

is most commonly known in the US under its trade name Puron and is a near-azeotropic mixture of difluoromethane (CH2F2, or R32) and pentafluoroethane (CHF2CF3, or R125). R410A has no chlorine content, no ozone depletion potential, and a global warming potential (GWP) of 1890. The oil employed in this experimental testing program is polyolester (POE) oil; with the Copeland model number 32-3MAF. The manufacturer recommends this oil for this compressor when operating with refrigerant R410A.

Some data from the manufacturer had been provided for the oil flooded compressor. The oil flooded compressor was tested by the manufacturer at the rated conditions without oil flooding. Table 5 gives the test data of oil flooded compressor without oil injection.

Table 5: Test data of the compressor.

Refrigerant	R410A
T_{evap}, F	45
T_{cond}, F	100
$\Delta T_{superheat}$, F	20
$\Delta T_{subcooling}$, F	15
$T_{ambient}$, F	95
Mass flow, lb/hr	949
Capacity, BTU/hr	77131.9
EER	13.16
Power, W	5861.1
Current, A	18.36
Motor speed, RPM	3515

To develop an understanding of the performance of the compressor with oil flooding, the compressor was run at a selection of test points. Since the motivation for this experimental testing is to evaluate liquid-flooding and regeneration for low-temperature heat pumping applications, low evaporation temperatures were employed. The goal was to test the compressor down to evaporator saturation temperatures as low as -30°C. An indoor air temperature of 31.33°C is required to be supplied by the heating system. Therefore a condensation temperature of 43.3°C was implemented and tested on the load stand. The superheat was varied such that the refrigerant inlet temperature and the oil inlet temperature to the compressor were maintained at 25°C. This would be approximately the conditions achieved in a system having a regenerator and an oil cooler that rejects heat to the indoor air. Large superheat is used for testing the oil flooded compressor because of the use of regenerator, which is a key component in the system operation.

The combinations shown in Table 6 were used to test the compressor. For all combinations, the oil flow rate was varied in order to yield nominal increments in the oil mass fraction of 0.1. The highest mass fraction in each set was the maximum amount of oil that could be injected in the compressor with all the oil injection valves fully open. The mass flow rate of the injected oil is given as a fraction of the total (refrigerant and oil) mass flow rate through the scroll compressor. Since the valves were undersized, it was difficult to achieve evaporation temperatures higher than -5°C in steady state.

During the test runs it took approximately 1-2 hours to reach a steady state. This waiting time was caused on one side by the manual control of the superheat with the needle valves for the condenser and on the other side by changing water temperatures in the laboratories building water system. The changing water temperature made the control of the oil temperature challenging.

Table 6: Test matrix for oil flooded compressor.

T_{evap} °C	T_{cond} °C	$\Delta T_{superheat}$ °C	$T_{oil\text{-}injection}$ °C
-30	43.3	55	25
-20	43.3	45	25
-10	43.3	35	25
-20	43.3	15-55	25

Calculations for evaluating the experimental results

The saturation evaporator and condenser temperatures are found from the measured compressor suction and discharge pressures. Then the compressor inlet superheat is defined as

$$T_4 = T_{\text{sink}} + \Delta T_{pinch} \,. \tag{3.1}$$

The mass flow rates of refrigerant ($\dot{m}_{ref}$) and oil with dissolved refrigerant ($\dot{m}_l$) are directly measured and thus the liquid mass fraction can be given by

$$x_l = \frac{\dot{m}_l}{\dot{m}_l + \dot{m}_{ref}} \tag{3.2}$$

The total isentropic power is given by the sum of the isentropic power required to compress the refrigerant to the discharge pressure and the power needed to isentropically compress the injected mixture of oil and refrigerant oil to the discharge pressure

$$\dot{W}_{is} = (\dot{m}_{ref} + \dot{m}_l)(h_{2s,m} - h_{1,m}) \tag{3.3}$$

where h_{2s} and $h_{2s,inj}$ are the exit refrigerant and oil enthalpies associate with isentropic processes between the inlet conditions (refrigerant and oil) and the discharge pressure. The injected mixture is modeled based on homogeneous oil-refrigerant mixture properties. Therefore the overall isentropic efficiency and volumetric efficiency are calculated by:

$$\eta_{is} = \frac{\dot{W}_{is}}{\dot{W}_{el}} \,, \tag{3.3}$$

$$\eta_{vol} = \frac{\dot{m}_{total}}{\rho_{in} * \dot{v}} \,, \tag{3.4}$$

$$\dot{m}_{total} = \dot{m}_{ref} + \dot{m}_l \,, \tag{3.5}$$

$$\dot{v} = V_{disp} * f \,, \tag{3.6}$$

$$\rho_{in} = \frac{x_{ref} + S*(1-x_{ref})}{x_{ref} * v_{ref} + S*(1-x_{ref})*v_l} \,. \tag{3.7}$$

Each point in the test matrix was tested at least twice on different days to demonstrate repeatability in the experimental measurements. The atmospheric pressure was taken into account, since gauge pressure transducers were used for the refrigerant side pressure measurements. At least 5 minutes of steady state data was acquired at each state point. The data was then post-processed to calculate all parameters not directly measured. Figure 26 shows the performance of the compressor as a function of evaporator saturation temperature, 43.3°C condenser saturation temperature and 25°C oil inlet temperature. It can be seen that the discharge temperature is very high when there is no oil flooding (for $x_L = 0$). As the oil is injected, the discharge temperature of the compressor decreases monotonically with larger oil mass fractions. The discharge temperature is higher for lower evaporator saturation temperatures due to higher pressure ratios. In addition, the refrigerant mass flow rate tends to increase as the oil injection rate is increased. This increase in refrigerant mass flow rate may be due to better sealing between higher and lower pressure pockets and lower temperatures in the suction chamber as a result of lower overall compressor temperatures. The refrigerant mass flow rate also increases with the improved sealing of leakage gaps with oil flooding. It can be observed that the mass flow rate of the refrigerant decreases for higher oil mass fraction due to pressure drop caused by pumping high flow rates of oil. Also, the mass flow rate of refrigerant is higher for high T_{evap}. The compressor power consumption is highest with no flooding and decreases significantly with small amounts of oil injection. However, the compressor power consumption increases with oil mass flow rate at higher mass fractions. The overall compressor isentropic and volumetric efficiencies increase with oil injection rate except at high mass fractions. At an evaporating temperature of -30°C and condensing temperature of 43.3°C, the compressor isentropic efficiency increases by 24% and volumetric efficiency increases by 14% for an oil injection mass fraction of 0.5 when compared to no oil flooding.

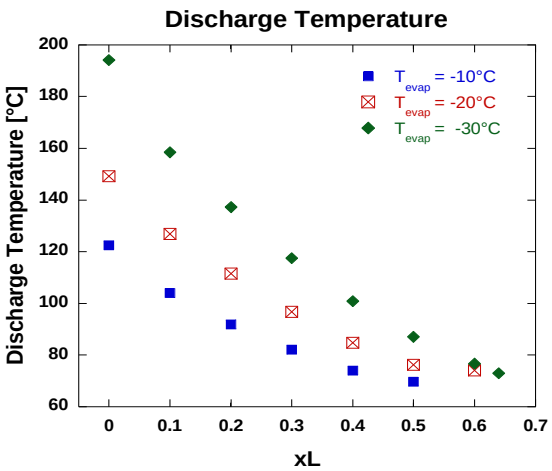

a) Discharge Temperature

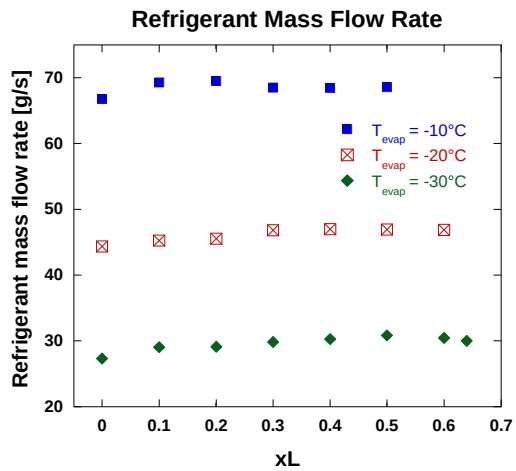

b) Refrigerant Mass Flow Rate

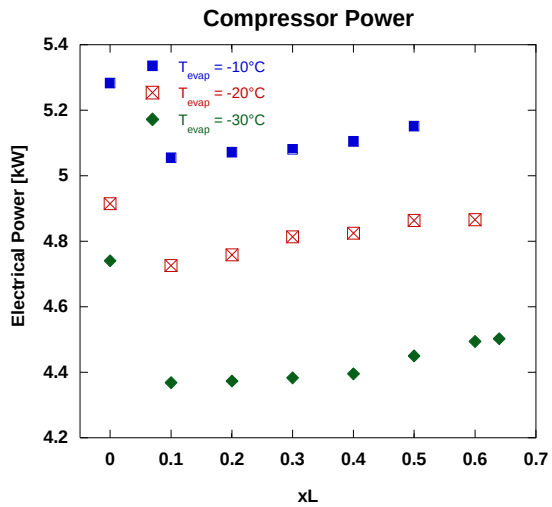

c) Compressor Power Consumption

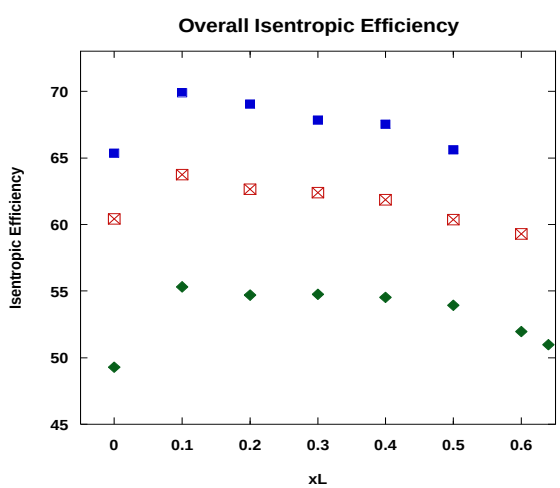

d) Overall Isentropic Efficiency

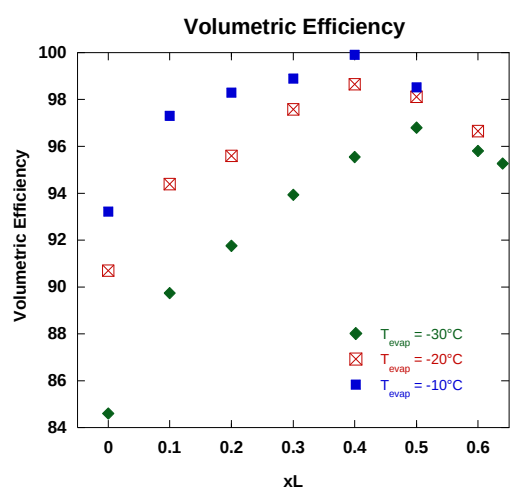

e) Volumetric Efficiency

Figure 26: Performance of compressor for varied T_{evap} and T_{cond}=43.3°C with and without oil injection.

Figure 27 shows the performance of the compressor with oil flooding for varied suction superheat, -20°C T_{evap}, 43.3°C $T_{cond,}$ and 25°C oil inlet temperature. It can be observed that the performance of the compressor with increasing oil injection rate for varied superheat is qualitatively similar to the performance with varied T_{evap}. As the superheat is increased, the refrigerant mass flow rate decreases due to the decrease in refrigerant density at higher temperature. The discharge temperature of the compressor also increases due to the higher suction temperature. The compressor power consumption is higher for lower superheat due to higher mass flow rate of refrigerant. There is a large improvement in the overall isentropic efficiency and volumetric efficiency for higher superheat.

The oil inlet temperature is expected to be important factor for the performance of the compressor with oil flooding. However, the achievable minimum oil temperature for heat pump applications is fixed to be above the return air temperature of the heated builing. Therefore 25°C oil inlet temperature condition was used in the experiments.

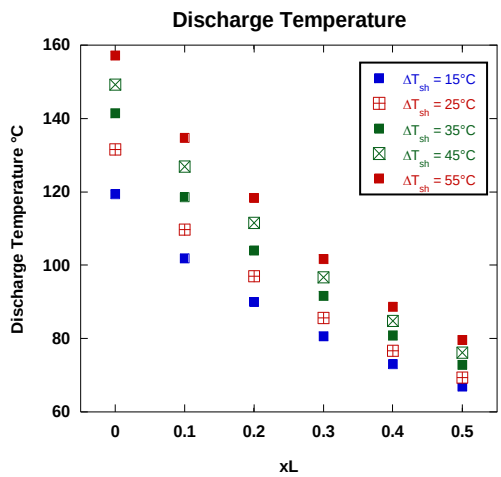

a) Discharge Temperature

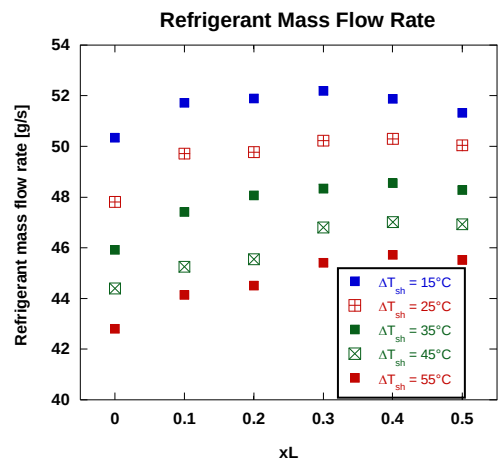

b) Refrigerant Mass Flow Rate

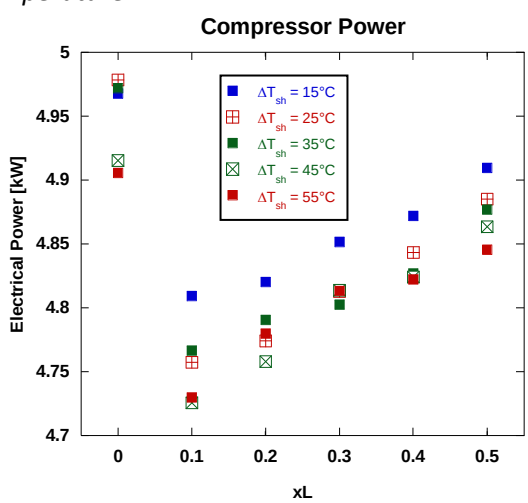

c) Compressor Power Consumption

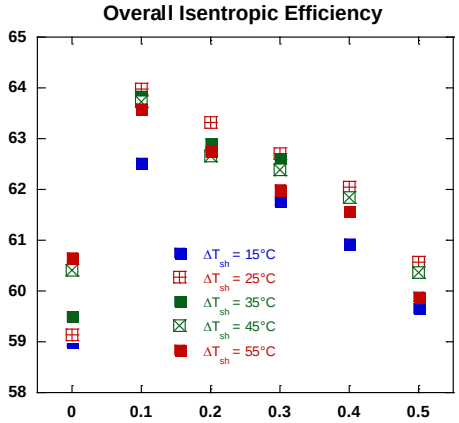

d)

Overall Isentropic Efficiency

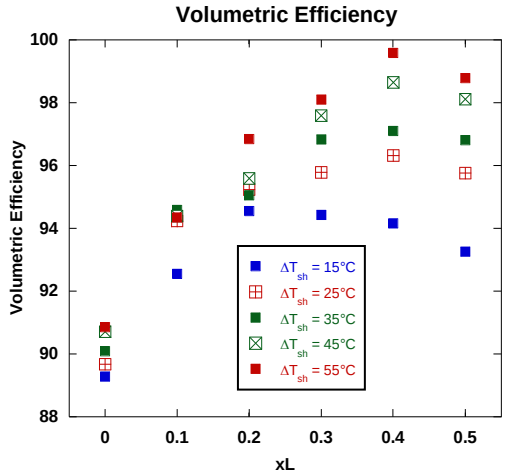

e) Volumetric Efficiency

Figure 27: Performance of compressor for varied superheat (T_{evap} =-20°C, T_{cond}=43.3°C, $Toil_{_inj}$=25°C)

3.2.2 Experimental testing of vapor injected compressor

Initial testing for the prototype multi-port vapor injected compressor was conducted at Emerson Climate Technologies, which was followed up by testing according to Table 7 at Purdue University. The test matrix contains 8 different injection pressure pairs which are combined with 3 different suction pressures (24 points total). A wide range of different injection pressures was chosen to be able to obtain a well-defined mapping of the compressor.

Testing was conducted on a modified version of the hot gas bypass test stand, Figure 28. Discharge gas is taken after the oil separator and cooled to near saturated condition in dedicated heat exchangers for both injection ports.

The resulting test data was then used to obtain a regression model for simulation purposes and to tune the physics-based model in order to check its accuracy.

Table 7: Test matrix for vapor injected compressor

Parameter	Nominal Values Used	Unit
Condensing Temperature	43.3	°C
Evaporating Temperature	-10, -20, -30	°C
Compressor Suction Superheat	11.1	°C
High/Low Vapor Injection Pressure	1100/900, 1300/900, 1300/1100, 1500/1300, 1500/1100, 1500/900, 1700/1500, 1700/1300	kPa

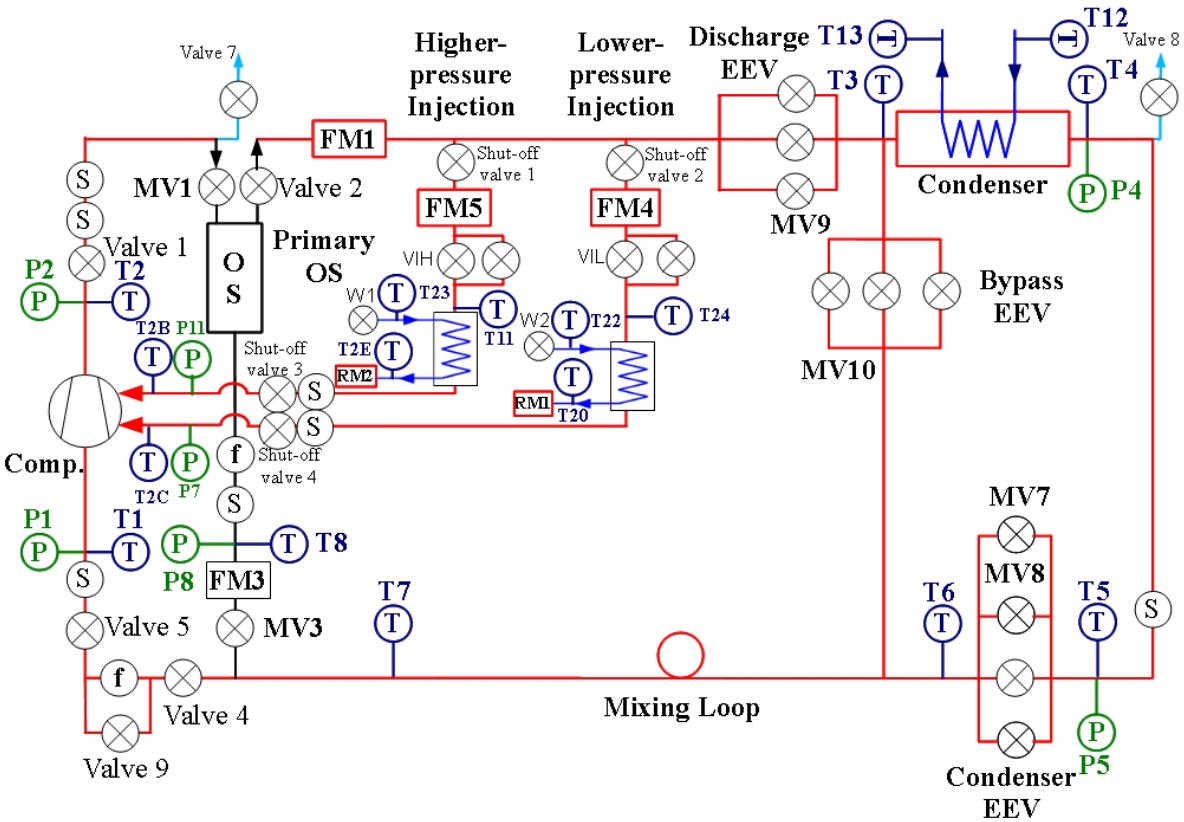

Figure 28: System schematic for the hot-gas bypass stand with vapor injection.

3.2.3 Experimental testing of valve prototypes

The valve was tested with different plunger diameters to obtain the required flow rates. Figure 3 shows the test section of the test stand. A modified flanged oil separator is used as refrigerant liquid/vapor separator. One of the ports is used to drain the saturated liquid trough the 2 step valve while the other port will is used in conjunction with the former oil exit port and an external capacitive level probe to measure the liquid level in the separator. The former vapor inlet and outlet are used as two phase inlet and gas outlet, respectively.

To allow for quicker testing, the 3 step valve is followed by a stepper valve R1.3 so that the exit pressure can be regulated without the need for a change in the actual system evaporation temperature. The existing bypass branch in the expansion valve test stand is then used to compensate for the reduced mass flow rate through the test branch.

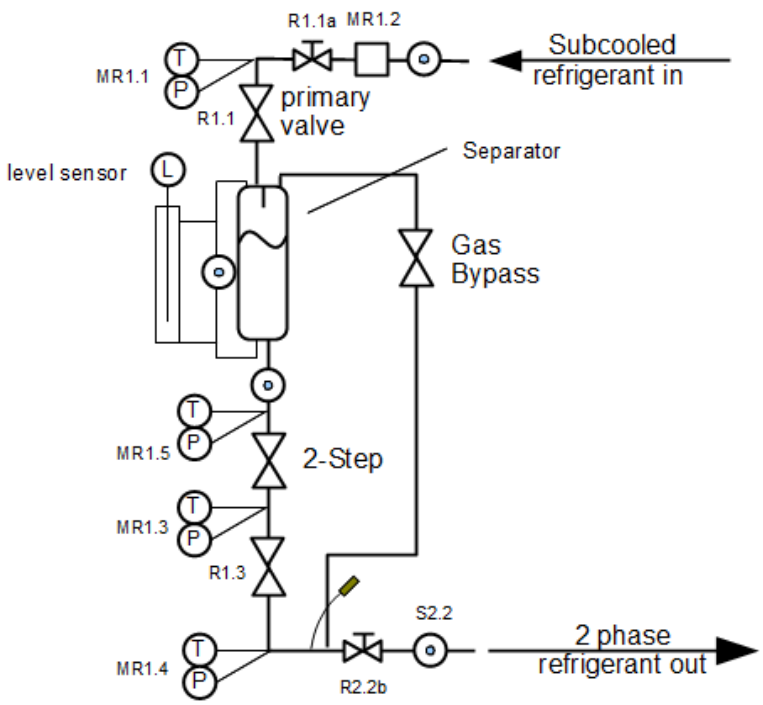

Figure 29: **Schematic of the test section modification of the EXV test stand**

Figure 30 shows a picture of the modified test stand. The oversized separator was well insulated to reduce heat gain from the ambient to less than 5% of the estimated per circuit capacity. This was done in order to reduce the influence of the ambient conditions onto the experiment.

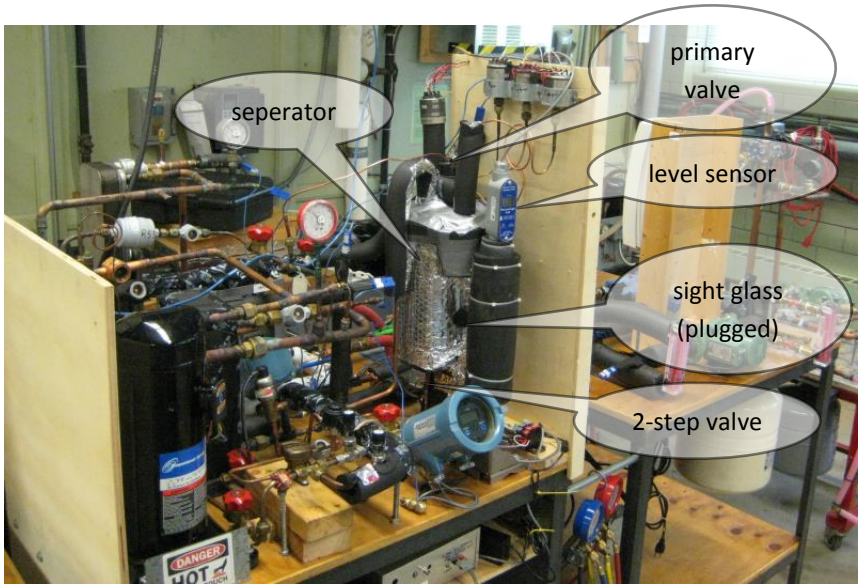

Figure 30: Picture of modified test stand.

To determine the required flow rates for the modified HP cycle with vapor injection, simulation data was used. A volumetric efficiency of 1.0 and an isentropic efficiency of 0.7 were used as a simplified assumption. Figure 31 shows the resulting capacity and flow rates. It can be noticed that the nominal capacity of 17.6 kW is exceeded at about -22°C evaporation temperature. At that point the saturated liquid flow rate from the vapor separator is approximately 55 g/s. In actual system operation, this mass flow rate will be the occurring maximum, since higher temperatures require a lower heating capacity for keeping the building temperature constant.

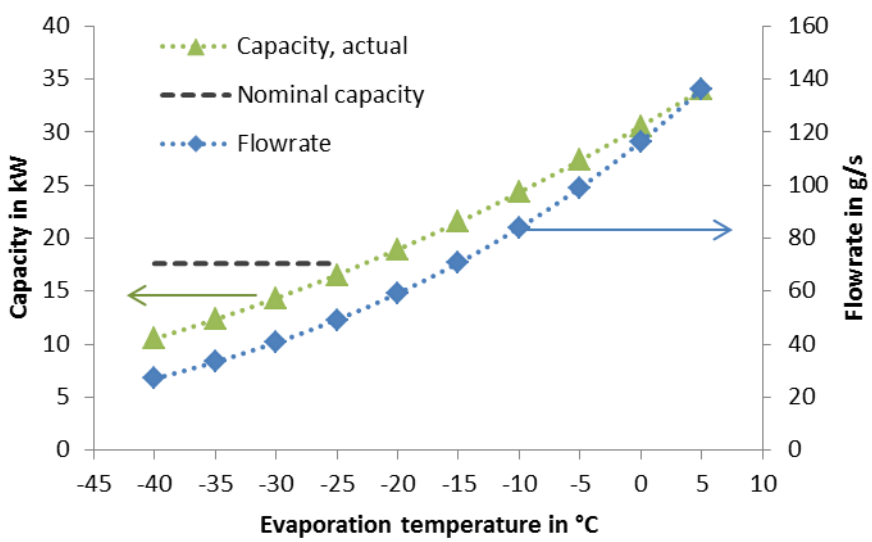

Figure 31: Liquid flow rate and heating capacity, vapor injected cycle

Figure 32 shows the injection pressure for the low pressure injection port along with the evaporation pressure and the pressure difference across the valve. The target of the adjustment of the two valve diameters is to obtain a flow rate of roughly 50 and 120 % of the one mentioned in Figure 31 over the operating range with those pressures. It might be necessary to implement an additional electronic expansion valve after the separator if that is not possible – which might be the case for part load operation.

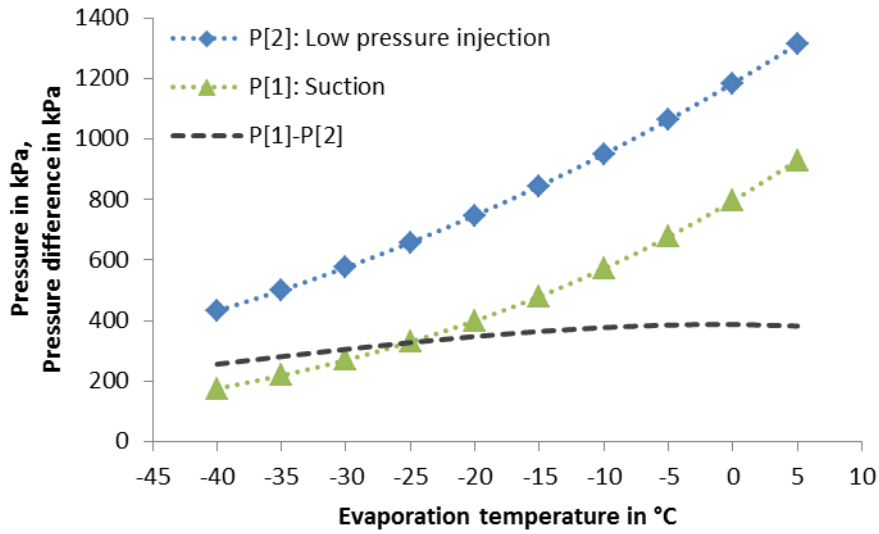

Figure 32: Pressures at low-pressure injection port and suction, vapor injected cycle

Initial testing of several different valve plunger dimensions was conducted to determine the necessary depth of the groove in the plunger. A test plan for the valve was developed to determine the performance of the valve. The test plan includes points with the valve in high and low flow rate position, Table 8. Additionally a limited number of points are tested under pulse width modulation mode to determine the relationship between duty cycle, period time, and flow rate of the valve, **Table 9**. **Table 10** includes different condensing pressures to determine the possible influence of a change in liquid composition after the first expansion at the inlet to the 2-step valve. Table 3 shows the data of the valve configurations used for determining the correlations.

Table 8: Test plan for steady state tests

	2-step valve						Primary valve		
Test #	**P_{in}**	**P_{in}**	**P_{out}**	**P_{out}**	**T_{eva}**	**Position**	**P_{in}**	**P_{in}**	**T_{in}**
	kPa	**PSIA**	**kPa**	**PSIA**	**C**		**kPa**	**PSIA**	**C**
1	748	108.5	400	58.0	-20.0	low/high	2618	379.7	38.4
2	871	126.3	504	73.1	-13.8	low/high	2618	379.7	38.4
3	1006	145.9	627	90.9	-7.5	low/high	2618	379.7	38.4
4	1153	167.3	767	111.3	-1.3	low/high	2618	379.7	38.4
5	1313	190.4	930	134.9	5.0	low/high	2618	379.7	38.4

Table 9: Test plan for steady state, pulse width modulated tests

Test #	1-a	1-b	1-c	1-d	1-e	1-f	1-g	1-h
Period [s]	0.5	1.5	3	6	0.5	1.5	3	6
Duty [%]	33.3	33.3	33.3	33.3	66.6	66.6	66.6	66.6

Table 10: Test plan for steady state tests

	2-step valve						Primary valve		
Test #	T_{eva}	P_{in}	P_{in}	P_{out}	P_{out}	**Position**	P_{in}	P_{in}	T_{in}
	C	**kPa**	**PSIA**	**kPa**	**PSIA**		**kPa**	**PSIA**	**C**
1-i	-20	748	108.5	400	58.0	low/high	2100	304.6	29.4
1-j	-7.5	1006	145.9	627	90.9	low/high	3100	449.6	45.7

Note: primary valve subcooling 5 K

4 Cold climate heat pump system development

The third phase of the project centered on integrating the proposed components into a high performance low temperature heat pump system.

4.1 Refine prototype components and develop prototype system

Based on the experimental results and model validation outcomes of Task 3, the prototype compressors and flow control valves were refined and the team developed a pre-manufacturing prototype system. This work was carried out by Purdue University in collaboration with Emerson Climate Technologies and Carrier Corporation.

4.1.1 Oil Flooded Compressor

The initial design of the oil flooded compressor had the injection ports being located too close to the suction which lead to flooding of the compressor sump. In the first design iteration, this issue was successfully fixed. In the second design iteration, the oil separator was integrated into the compressor. This component integration will lead to an overall cost reduction for series systems.

4.1.2 Vapor Injected Compressor

For the vapor injected compressor, no further refinement was necessary. However, the compressor employed in the prototype heat pump was equipped with removable plugs in the injection ports. This was done to prevent re-expansion losses for the conventional operating mode.

4.1.3 Flow Control Valves

The dimensions of the grooves in the 2-step flow control valves were modified to obtain the desired flow rates for the pressure differences of the vapor injected system. Besides from these changes, no further refinement was necessary.

4.1.4 Develop Prototype System – Overview

The purpose of the prototype systems is to show the system performance improvements. One main requirement was to use available standard components, where possible. This limited the selection of heat exchangers to the ones employed in the current systems of Carrier Cooperation.

For the vapor injected system, a split type heat pump was chosen, since no modifications are necessary on the indoor unit. The vapor injected system can therefore use existing indoor units.

For the oil injected system, an additional lineset to the indoor oil cooler is necessary. This will lead to additional installation as well as material costs and due to the larger oil charge to concerns about the flammability of the oil. Therefore a packaged system was chosen, where the lineset and oil charge are lower.

4.1.5 Develop Prototype System – Vapor Injected Compression

Figure 33 shows the system schematic of the cold climate heat pump. Two vapor separators S1 and S2 are used in the staged expansion process to generate the necessary vapor for the injection into the compressor. The system schematic also shows the hybrid evaporator coil schematically with 3 flow control valves. In air conditioning mode, the vapor separators are bypassed and the system is operated similar to a standard vapor compression system.

Commercially available components were used where possible. The employed outdoor HX is the one used in the 5-ton infinity series of Carrier – the largest available model in their residential range. The indoor unit is a 5-ton model. Both, indoor and outdoor unit are equipped with variable speed ECM motors. All employed valves in the system, with exception of the flow control valves for the evaporator are commercially available. The vapor separators are commercially available oil separators which were modified for vapor separation. The variable speed drive for the compressor is a commercially available model. All components, with exception of the variable speed drive of the compressor and some of the controls electronics, were mounted within the outdoor unit as shown in Figure 34. This was done in order to both, show that vapor injection can be integrated into the given envelope, and to show possible issues with this approach. As Figure 35 shows, there is no difference in appearance to the outdoor unit of a conventional system.

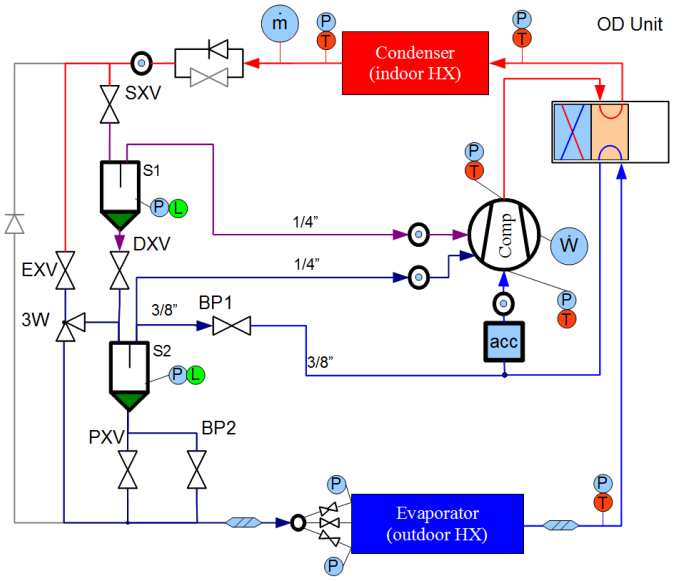

Figure 33: System schematic cold climate vapor injected heat pump.

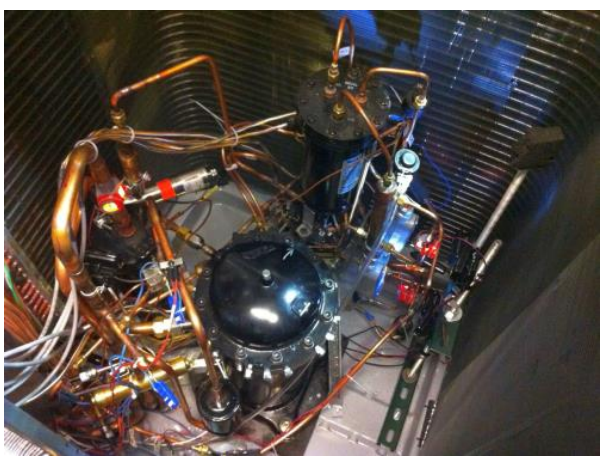

Figure 34: Interior of vapor injected HP OD Unit.

Figure 35: Outdoor unit of vapor injected heat pump

The outdoor coil consists of 10 parallel circuits. In order to reduce cost and complexity, these circuits are paired, such that only 5 flow control valves are necessary for the hybrid control scheme.

4.1.6 Develop Prototype System – Oil Flooded Compression

Figure 36 shows a simplified schematic for the oil flooded system. The system is based on a small packaged product (SPP), which is commercially available. All components, with exception of the prototype compressor are commercially available. Part of the original indoor coil is used as oil cooler.

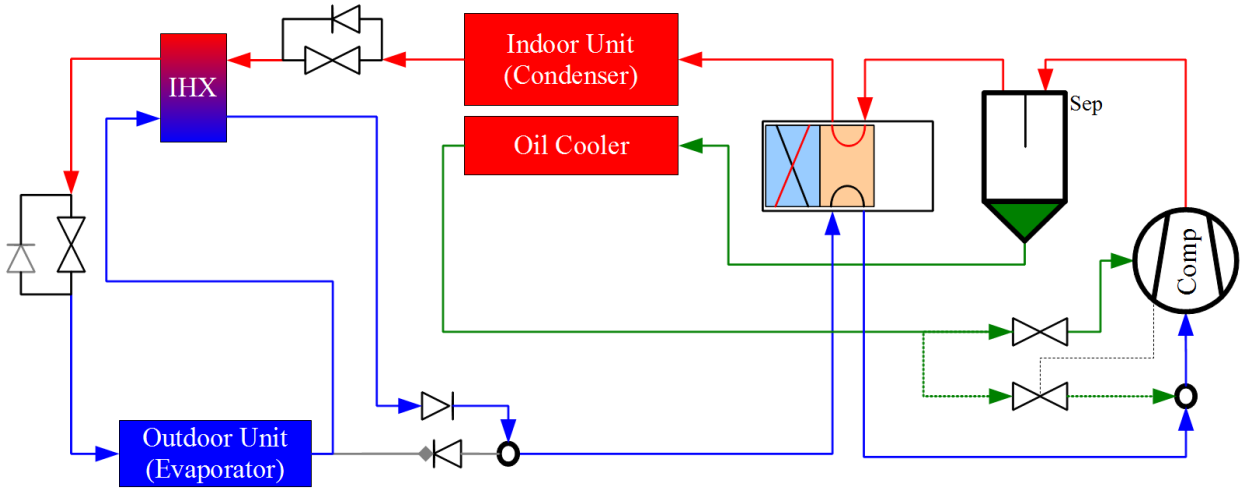

Figure 36: Simplified schematic for oil flooded system

4.2 Test and evaluate heat pump system

The pre-production heat pump systems were tested and evaluated over a range of conditions that would typically be encountered by a heat pump in a cold climate. The vapor injected heat pump was tested using a set of psychrometric chambers at the Herrick Labs that are capable of simulating the necessary indoor and outdoor conditions. The oil flooded heat pump was tested at the Carrier Corporation facilities in Indianapolis, Indiana.

4.2.1 Develop Prototype System – Vapor Injected Compression

The vapor injected system with economizing was tested in both vapor injected operating mode and conventional single-stage operation. The vapor injection ports were plugged for conventional single stage operating mode to prevent re-expansion losses. Table 11 shows the test plan for the vapor injected system. The test conditions for the H1, H2, and H3 tests are adopted from the AHRI 210/240 (2008) testing standard to provide comparability to published results. The target humidity was modified for the H2- and H3-tests. The HX tests are not specified in the standard and were added to evaluate the performance under cold climate conditions. All tests were conducted using the maximum outdoor fan speed of 850 RPM and with indoor fan speed set to HP comfort mode (≈330 cfm/ton).

Table 11: Test plan for vapor injected heat pump

Test description	Air Entering Indoor Unit Temperature [°C]			Air Entering Outdoor Unit Temperature [°C]			Compressor Speed/Capacity	Airside blockage
	Dry Bulb	Wet Bulb	Dew Point	Dry Bulb	Wet Bulb	Dew Point	[Hz]	-/light/severe
H1 - low - clean	21.1	≤15.6	≤12.06	8.3	6.1	3.7	40	-
H1 - low - light block	21.1	≤15.6	≤12.06	8.3	6.1	3.7	40	light
H1 - low - severe block	21.1	≤15.6	≤12.06	8.3	6.1	3.7	40	severe
H2 - mid - clean	21.1	≤15.6	≤12.06	1.7	min	min	55	-
H2 - mid - light block	21.1	≤15.6	≤12.06	1.7	min	min	55	light
H2 - mid - severe block	21.1	≤15.6	≤12.06	1.7	min	min	55	severe
H3 - full - clean	21.1	≤15.6	≤12.06	-8.3	min	min	70	-
H3 - full - light block	21.1	≤15.6	≤12.06	-8.3	min	min	70	light
H3 - full - severe block	21.1	≤15.6	≤12.06	-8.3	min	min	70	severe
HX - full - clean	21.1	≤15.6	≤12.06	-17.8	min	min	70	-
HX - full - light block	21.1	≤15.6	≤12.06	-17.8	min	min	70	light
HX - full - severe block	21.1	≤15.6	≤12.06	-17.8	min	min	70	severe

Notes:
Tests to be repeated with each different system configuration.
H1, H2, H3 adopted from AHRI 210/240; H2 modified huymidity compared to AHRI 210/240 (2008)

Baseline system compared to vapor injected system

Figure 37 shows the change of capacity and COP for the vapor injected system relative to the baseline system for the clean coil data that was taken according to the test plan. For the cases with fixed compressor speed, the capacity increases significantly, especially at lower ambient temperatures, e.g. by 28% at -8.33°C (17 F). This capacity increase leads to a similar increase in the temperature difference between return air temperature and condensing temperature, since the heat is rejected using identical indoor and outdoor unit heat exchanger size and air flow rate. As a result, the increase in COP is

between 0 and 4%, as shown in Figure 38. For a fairer comparison of the HP COP, the capacity of the baseline system and the vapor injected system was matched where possible. Figure 37 shows that this leads to an increased COP improvement for the lower ambient temperatures, especially at 1.67°C (35 F) and -8.33°C (17 F). Note that the available additional capacity of the vapor injected system reduces the need for electric auxiliary heat. This dependency is not reflected in the COP of the HP but can be seen if a bin-analysis for a given climate is conducted, as shown in paragraph 4.2.3, Figure 50.

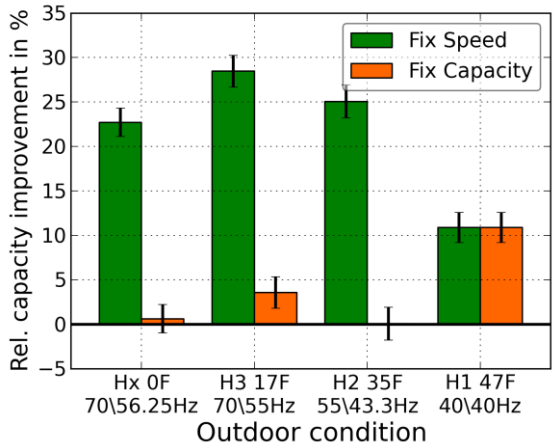

Figure 37: Capacity change relative to baseline system

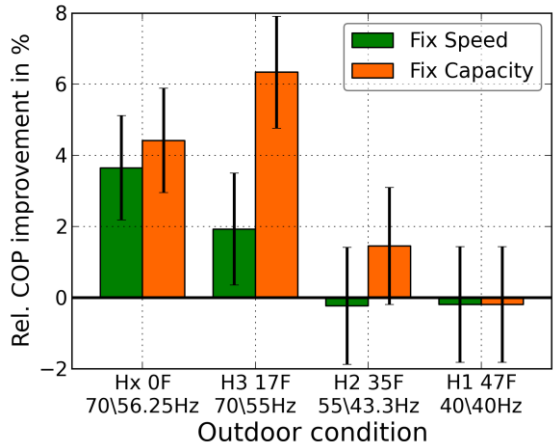

Figure 38: COP change relative to baseline system

Vapor injected system with and without hybrid control

Figure 39 shows the COP improvement of the vapor injected system with hybrid control outdoor heat exchanger relative to the same system with the baseline evaporator with standard distributor. Figure 40 shows the capacity improvement. COP and capacity improvement look similar, however, the capacity improvement for all comparisons is approximately twice as large as the COP improvement. For clean coil conditions, the performance change (COP, capacity) between the two systems is within the estimated uncertainty. COP and capacity improvement increase with blockage level from the HX to the H2 test. For the H2-test, a COP improvement of 17% along with a capacity improvement of nearly 40% was observed. The H1 test does not fit to the trend of performance improvement with increasing ambient temperature. Explanation for this behavior are the lower compressor speed (40 Hz instead of 55 Hz for H2 and 70 Hz for HX&H3) and lower inlet quality to the distributor in the baseline case which might have affected the distribution behavior.

Overall, the hybrid control scheme leads to a significant amount of performance improvement, if the air inlet conditions to the evaporator are maldistributed.

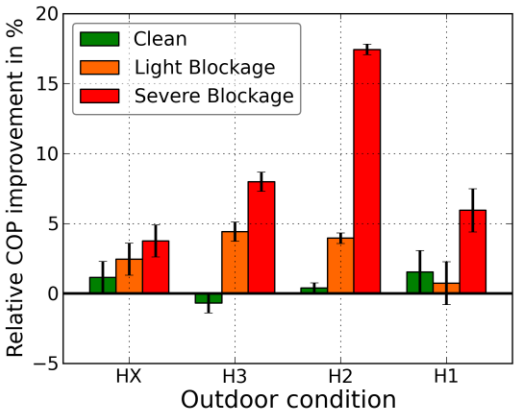

Figure 39: COP improvement of hybrid control relative to baseline

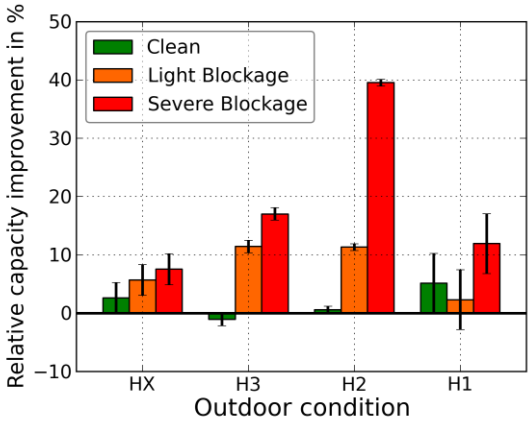

Figure 40: Capacity improvement of hybrid control relative to baseline

Future improvement of 2-step valves

The balancing valves in this project are 2-step solenoid valves, which are more cost effective than conventional EXV but have a limited control capability. While this was not a problem for all H3, H2, and H1 tests, it leads to issues for the HX tests. For all tests, a PI control scheme was employed to obtain uniform exit superheats. For the HX test without applied maldistribution, the bottom valve remained in low flow position during the entire test, indicating insufficient control range for the valve. For the HX tests with additional maldistribution, the bypass 2 was closed and the PXV was used to decrease the inlet pressure to the valves (see schematic in Figure 33) to be able to keep uniform exit superheats. This worked for the case with light blockage. For the case with severe blockage, Figure 41, the valve in the first branch saturated in open position while the valve in the bottom branch saturated in closed position. It was not possible to keep uniform exit superheats, which indicates that the limits of the control scheme were reached. To avoid this issue, the flowrate in closed position should be reduced while the flowrate in open position should be increased by modifying the valve plunger.

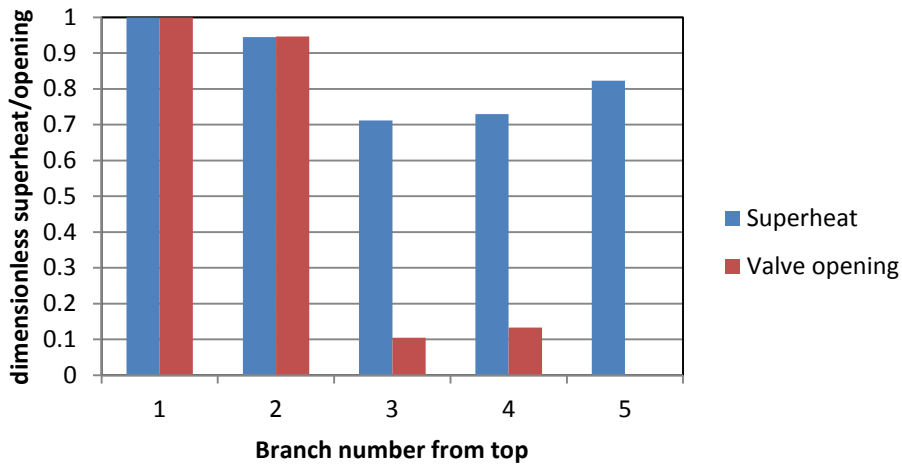

Figure 41: Dimensionless valve opening and dimensionless superheat.[1]

One potential issue of the 2-step valves is the pulsed operation. Therefore a test series under H1 operating conditions has been conducted to evaluate the influence of different PWM period duration. Figure 42 and Figure 43 show that the pressure fluctuations at the outlet of the evaporator depend on the chosen period duration. However, for a period duration of 4 seconds or less, these fluctuations about the mean value are smaller than the underlying variation of the evaporator pressure needed to control evaporator superheat.

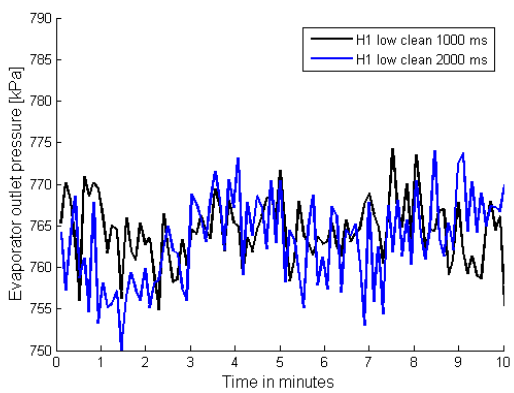

Figure 42: Evaporator outlet pressure for hybrid control with vapor injection, 1 and 2 s 2-step period

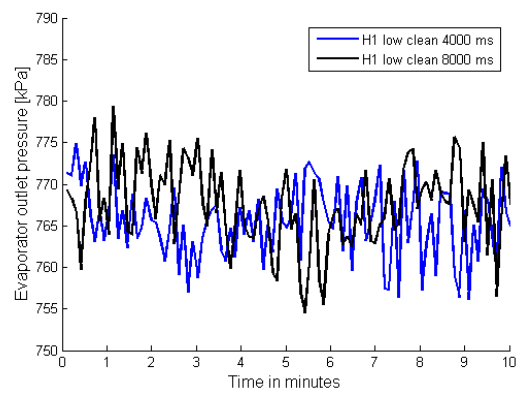

Figure 43: Evaporator outlet pressure for hybrid control with vapor injection, 4 and 8 s 2-step period

Figure 44 and Figure 45 show the pressure fluctuations at the inlet to circuit 1. There is no significant difference between the different PWM periods. However, the fluctuations are with approximately ±0.7 K much smaller than the air inlet temperature difference of 9.5 K at the evaporator exit.

[1] Superheat normalized to maximum occurring value.

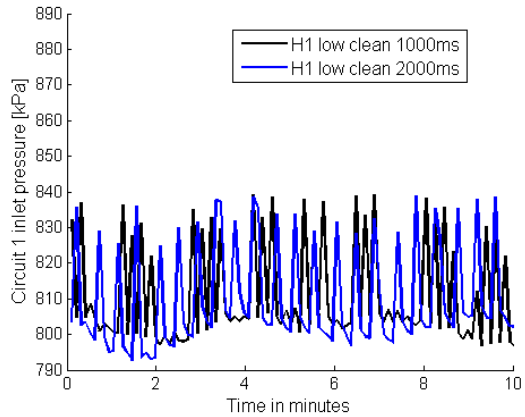

Figure 44: Circuit 1 inlet pressure for hybrid control with vapor injection, 1 and 2 s 2-step period

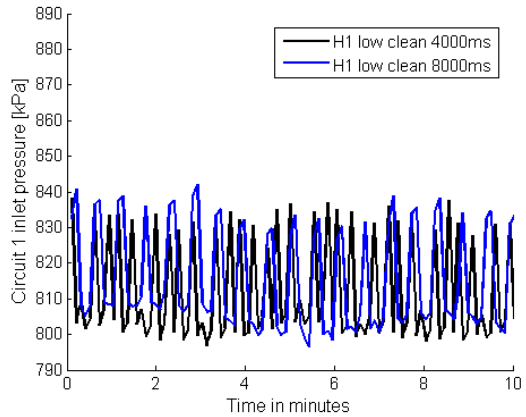

Figure 45: Circuit 1 inlet pressure for hybrid control with vapor injection, 1 and 2 s 2-step period

The operation of the 2-step valves without refrigerant flow leads to significant noise and vibration. This vibration caused the valve caps to partially unscrew which resulted in refrigerant leakage. The vibration is significantly reduced during operation, since the liquid refrigerant leads to hydraulic damping. Therefore the start-up procedure was modified to reduce valve operation without refrigerant flow. For a series production 2-step valve, welded valve caps should be used. These will significantly reduce the risk of leakage and lead to a lower large scale production cost.

4.2.2 Develop Prototype System – Oil Flooded Compression

The oil flooded system with regeneration was designed to run in oil injection mode during heating operation. Therefore, only a limited number of AC-mode operating conditions were tested as shown in Table 12. These conditions include the EER rating point at 95°F. For heating mode, an additional test was added to the standard test conditions in order to cover the entire range between 0°F and 47°F ambient temperature. Each point was measured at a wide range of oil injection rates to capture its effect onto COP and capacity.

Table 12: Test plan for oil flooded heat pump, AC mode

Test Name	Oil Mass Fraction	Evap. EDB (°F)	Evap. EWB (°F)	Cond. Entering Air Temperature (°F)	Indoor Air (CFM)
A	0	80	67	95	1750
B	0	80	67	82	

Table 13: Test plan for oil flooded heat pump, HP mode

Test Base Name	Indoor Unit (°F)		Outdoor Unit (°F)		Indoor Air (CFM)
	EDB	EWB	EDB	EWB	
H1	70	<=60	47	43	1750
H2			35	33	
H3			17	15	
H4*			0	min	

Note: For every test in heating mode, vary the oil mass fraction from 0.0 to 0.30, running at 0.0/0.05/0.10/0.15/0.20/0.30.

Legend:

* = Test not specified in AHRI 210/240

Figure 46 shows the measured COP improvement for different ambient temperatures and compressor superheat for the oil flooded system. Larger compressor superheat leads to a larger COP improvement – the maximum COP improvement for the 47°F ambient temperature is 6.6% for 25°F suction superheat and increases to 8.9% for 50°F suction superheat, since the suction temperature matches the oil return temperature better at these conditions. The experimental data did not cover the optimum oil flow rate for the 47°F tests. The achievable maximum improvement for 5°F and 17°F is approximately 8%. Figure 48 shows the capacity improvement for the same data. The maximum capacity improvement has a slightly decreasing trend with ambient temperature and was in the range of 1.6-3.3%.

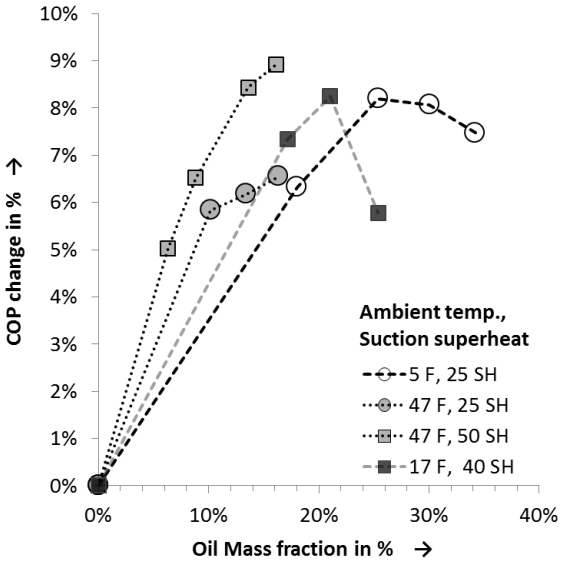

Figure 46: COP improvement for oil flooded system

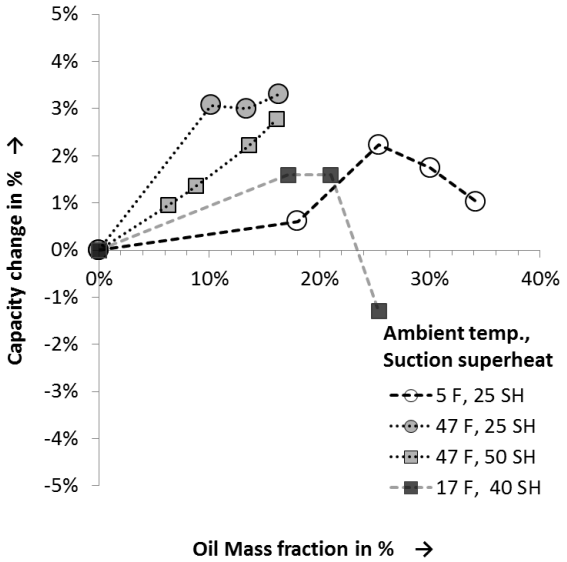

Figure 47: Capacity improvement for Oil flooded system

4.2.3 Evaluation of Test Results – Bin Analysis

A bin analysis was performed in order to evaluate the achievable benefits for the vapor injected system. The bin analysis is based on the method outlined in AHRI 210/240. The following modifications have been made to better suit the purpose of this analysis: (a) capacity and power consumption values are linearly interpolated based on nearest neighbor interpolation. For values outside the test range, data is linearly extrapolated based on the two nearest test points. (b) The design heating requirement value was adjusted to obtain a balance point of 14°F (-8.33°C) for both, the oil flooded (47160 Btu/hr) and the vapor injected system (60810 Btu/hr). (c) Bin temperature for Minneapolis (Minnesota) was added as an example for very cold climates.

The part load degradation factor was left as suggested in AHRI 210/240, since the system will go into intermittent operating mode for higher ambient temperatures.

For the variable speed vapor injected system it was assumed that the HP is run in continuous operating mode when possible rather than increased speed and intermittent operation. For ambient temperatures below the rating point, the data for maximum compressor frequency was used for both systems. For ambient temperature at and above the rating point, the data with matched capacity was used. For the highest tested point (47°F), the minimum frequency test data was used for both systems. Increased speed and intermittent operation might be of benefit when using thermostat setback, which is not considered in the method of the standard.

Vapor injected system

Figure 48 shows the resulting improvement in HSPF. The highest improvement of nearly 7% is achieved in region 5, while the energy savings in Minneapolis (6%) and region 4 (3%) are smaller.

Figure 49 shows that most of the electrical energy consumption reduction was obtained due to the larger heating capacity of the heat pump at low ambient temperatures, which is visible as a significant reduction in auxiliary heat. The heat pump power consumption increases for climate zone 5 and Minneapolis due to the larger heating capacity. Figure 50 shows that the COP of the HP increased by approximately 2% for all regions. However, this only is 32-53% of the HSPF improvement. Therefore, the COP improvement is largely caused by the reduction in auxiliary heat energy consumption (2.6-8%).

Note that the results for a differently chosen system design temperature will lead to different results. Specifically, a higher design temperature will lead to an increase in auxiliary reheat. This will be of benefit for the vapor injected system, since it will require less auxiliary reheat than the baseline system. The effects of the choice of system design point will be investigated for the final report

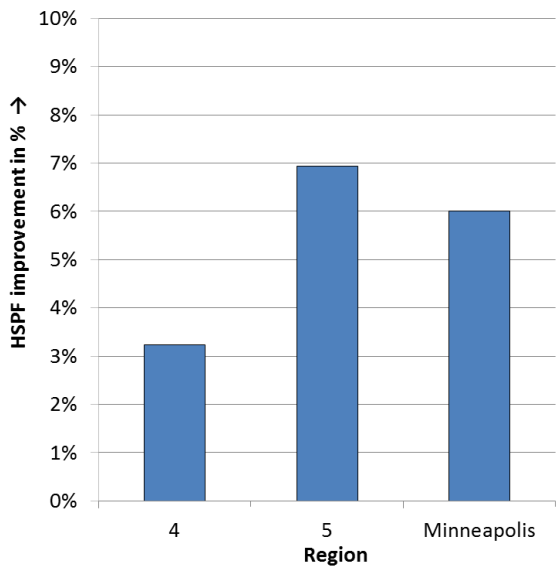

Figure 48: HSPF improvement, relative to baseline

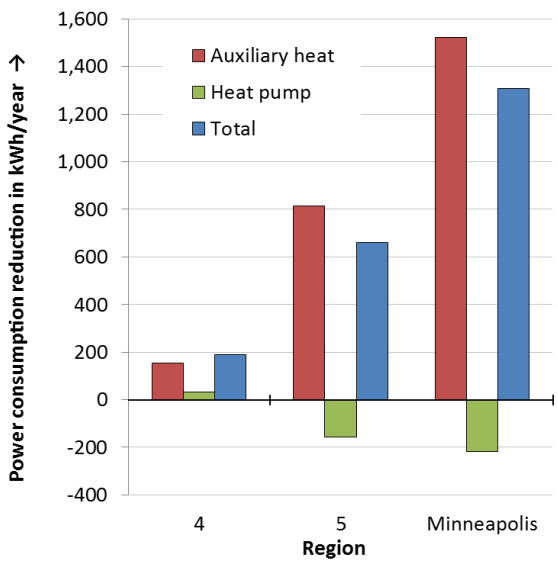

Figure 49: Power consumption reduction for system components.

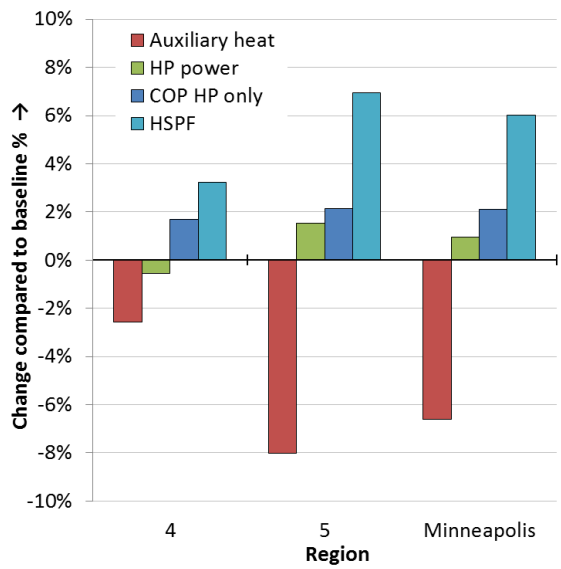

Figure 50: Power consumption change relative to total consumption of baseline for system components.

Oil flooded system

Figure 51 shows that the energy savings for the oil flooded system are 7.3% for region 5 and 7.4% for region 4 and Minneapolis. Note that, for the oil flooded tests, 1/6 of the indoor heat exchanger was used as oil cooler and 5/6 were used as condenser. This coil configuration was kept, even with no oil flooding, and therefore leads to a disadvantage for the tests without oil flooding. The performance improvement for the oil flooding is therefore larger than it would be if optimized systems would be compared against each other.

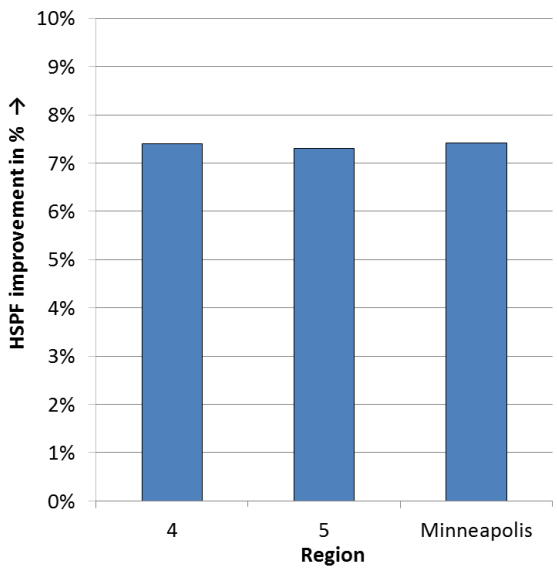

Figure 51: HSPF improvement, relative to baseline

Figure 52 shows that most of the power consumption reduction was obtained due to larger COP of the oil flooded configuration – the amount of auxiliary heat only changed by up to approximately 2% for regions 5 and Minneapolis. The heat pump power consumption decreases for all climate zones due to the larger COP of the oil flooded system. Figure 53 shows that the COP of the HP increased by more than 7.5% for region 4 and 7.6% for region 5 and Minneapolis. The increase in COP is the largest contributor to the increase in HSPF, since it reduces the power consumption of the compressor even though the fraction of the heating load covered by the HP increased compared to the baseline.

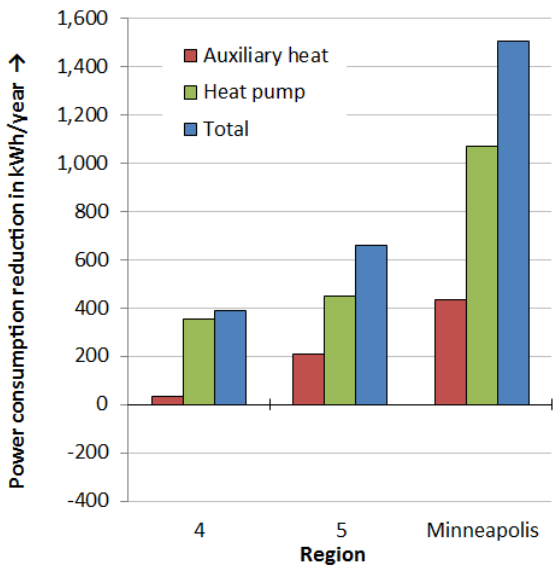

Figure 52: Power consumption reduction for system components.

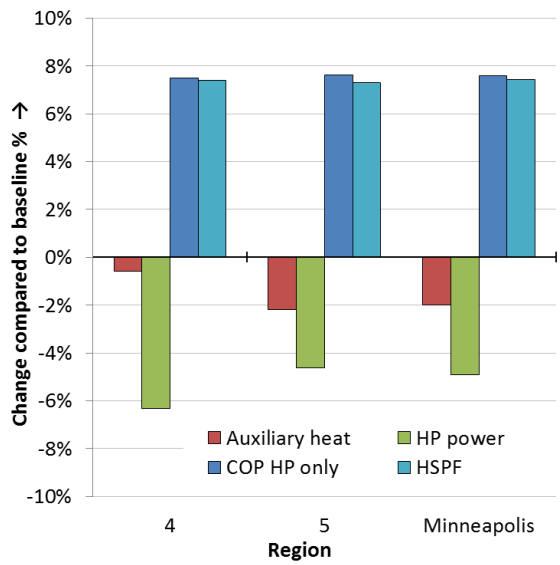

Figure 53: Power consumption change relative to total consumption of baseline for system components.

4.3 Perform economic analysis of the heat pump system

An economic analysis was performed for both, the vapor injected system with economizing and the oil flooded system with regeneration.

Energy savings for vapor injected system

Figure 54 shows the yearly energy costs savings along with the yearly energy cost. The greatest savings of $144 out of $2392 total heating costs are achieved in Minneapolis. In Region 5, $73 out of $1045 are saved with the vapor injected system, while in region 4, $21 of $641 are saved.

The system lifetime benefit for the vapor injected system is difficult to estimate, especially since there might be an influence of the vapor injection on the system lifetime. However, assuming a desired simple payback period of 3 years, the extra total cost of the vapor injection equipment should not exceed $62, $217 and $430 for regions 4, 5 and Minneapolis.

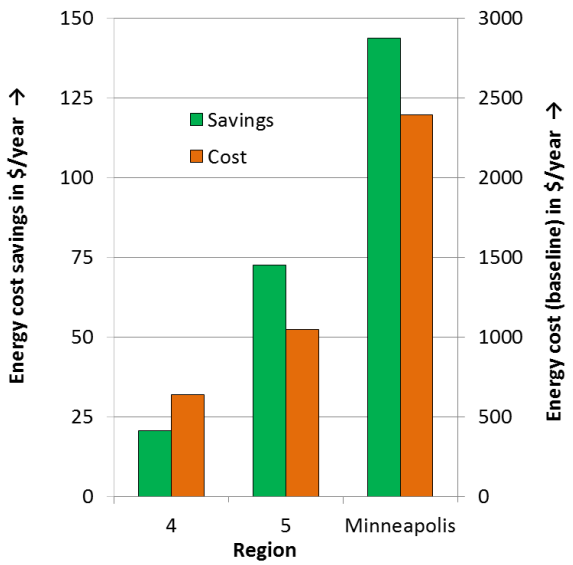

Figure 54: Energy cost and -savings per year, relative to baseline, for 0.11$/kWh.

Energy savings for oil flooded system

Figure 47 shows the yearly energy costs savings along with the yearly energy cost. The greatest savings of $165 out of $2230 are achieved in Minneapolis. In Region 5, $72 out of $991 are saved with the vapor injected system, while in region 4, $43 of $574 are saved.

Assuming a desired simple payback period of 3 years, the total additional cost of the oil flooded equipment should not exceed $127, $217 and $496 for regions 4, 5 and Minneapolis.

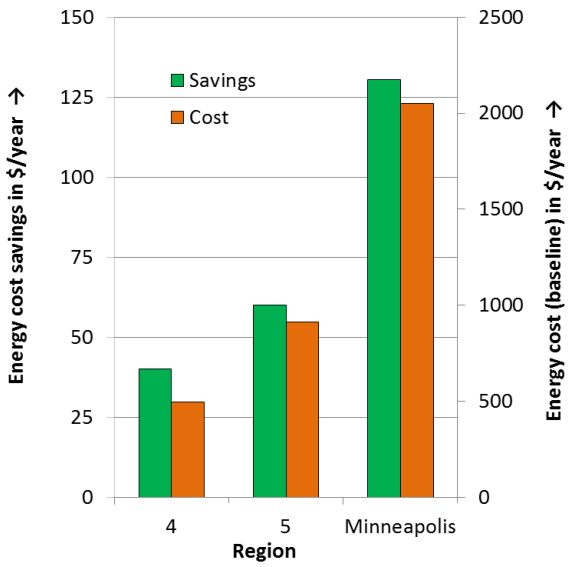

Figure 55: Energy cost and -savings per year, relative to baseline, for 0.11$/kWh.

Implementation challenges

Both, vapor injected and oil flooded system pose some technological challenges. For the vapor injected system, phase separators are required. The liquid level in these phase separators needs to be actively controlled. Currently it is unclear whether or not this can be achieved by using simple float valves. For the oil flooded system, an additional line-set is required for the oil cooler which needs to be located in the indoor unit. This additional lineset increases the material and installation cost and poses the risk of an indoor oil-leak. In contrast to refrigerants, oil is flammable, which leads to potential liability issues. Therefore the oil flooded approach seems only worth wile for packaged heat pumps.

Market Estimate for Cold Climate Heat Pumps

The following market estimate only considers the vapor injected cold climate heat pump, since the oil flooded approach will possible be restrained to packaged heat pumps.

The possible market for cold climate heat pumps can be divided into replacement of existing heat pumps and penetration into market shares dominated by electrical and combustion (mainly oil/gas) heating equipment.

For the replacement of existing heat pumps, only the incremental cost for changes towards a cold climate heat pump needs to be considered for the payback period. Previous researchers estimated the cost premium for a residential cold climate heat pump to be as low as $250 MSRP (Khowailed et al., 2011) and as high as $3000-$4000 (Meredith and Hales, 2007). The value estimated by Meredith and Hales (2007) was for an early commercially available heat pump. Roth et al. (2009) mentions an estimated cost premium of $1000, which will be applicable with more competition in the market.

For electric central air heating equipment, the additional cost is much larger, since there is either no refrigerant to air heat exchanger in the air handling unit or the existing air conditioning system needs to be replaced by a cold climate heat pump. The same is the case for the replacement of combustion heating equipment. Roth et al. (2009) estimates a cost premium of $2600 to $3700 relative to a 90% AFUE gas furnace. Based on our own research, the MSRP for electric and gas furnaces is comparable. Assuming that the installation cost is comparable as well, the cost premium will be comparable for both cases. Table 14 shows the incremental cost that we assumed for changing from the current standard to a CCHP.

Table 14: Incremental cost estimates for new homes.

Current system ->	**HP**	**AC**	**Furnace (el. or gas) only.**	**Furnace (el. or gas) only and AC, replace both**
CCHP	$1000	$1500	$3000	$0

For the subsequent analysis, average values for the electricity cost and natural gas cost were based on averages for the states within the regions were based upon the average of the states within these regions as supplied by EIA (2011a,b). For the average heating value, no such distinction was made, since

the standard deviation within the US data was 1.4% of the average value. Table 15 summarizes these assumptions. Note that these assumptions are based on 2011 values; gas prices might increase once the newly available shale gas is nearing depletion.

Table 15: Assumptions for cost analysis

Region	**4**	**5**	**Minneapolis**
Electricity cost ($/kWhr)	10.88	12.57	8.78
HP model	DOE Baseline 0/1	DOE Baseline 0/1	DOE Baseline 0/1
HP balance point [F]	14	14	14
Natural gas cost ($/1000ft³)	10.77	11.24	8.85
Furnace AFUE	90%	90%	90%
Heating value (Btu/ft³)	1024		
Furnace electricity consumption	not considered		

Case I: CCHP versus HP

If an existing heat pump is replaced due to failure, only the incremental cost needs to be considered as additional expense. The same is the case for new HP installations. This incremental cost with sufficient competition will be in the range of $250-$1000 as previously mentioned. Figure 56 shows that the achievable energy savings for region 4 are with $20 too small to justify the additional investment. However, $83 yearly savings for region 5 lead to a simple payback time of 3.1-12.5 years when considering the estimate for the incremental additional cost. These values are within the expected typical life expectancy and therefore would make the cold climate heat pump competitive for region 5. For Minneapolis the simple payback period is even shorter, since larger yearly electricity savings of nearly $144 are achieved.

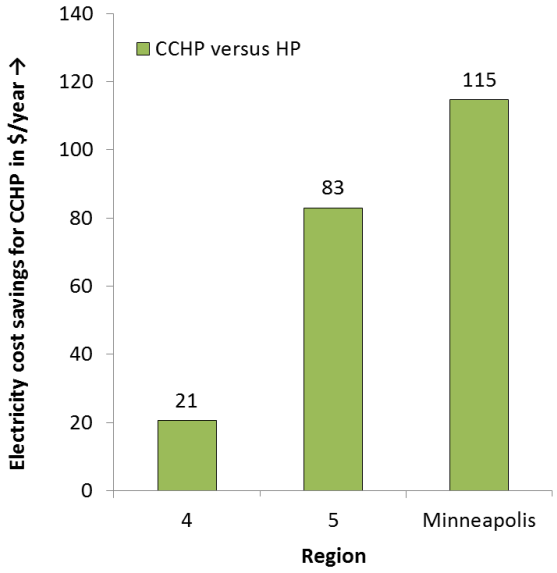

Figure 56: Energy savings cold climate heat pump versus heat pump

Case II: CCHP versus gas/electric furnace

If the heat pump is used instead of a furnace a significantly higher initial cost is applicable. However, in case of the electrical furnace, the cold climate heat pump also leads to significant savings of $940 in Region 4 and more than $1500 in region 5 as shown in Figure 57. For Minneapolis climate, the predicted savings are more than $2500 per year. Assuming an incremental cost of $3000 for the heat pump versus the electric furnace this corresponds to a simple payback period of 3.2, 2.0, and 1.2 years, respectively.

With the current gas and electricity cost, the cold climate heat pump seems not competitive with a gas furnace as heating option, and leads to an increase in operating cost. However, in region 4, the cold climate heat pump leads only to a minimal increase in operating cost. Therefore the cold climate heat pump might be interesting for areas where gas is relatively expensive.

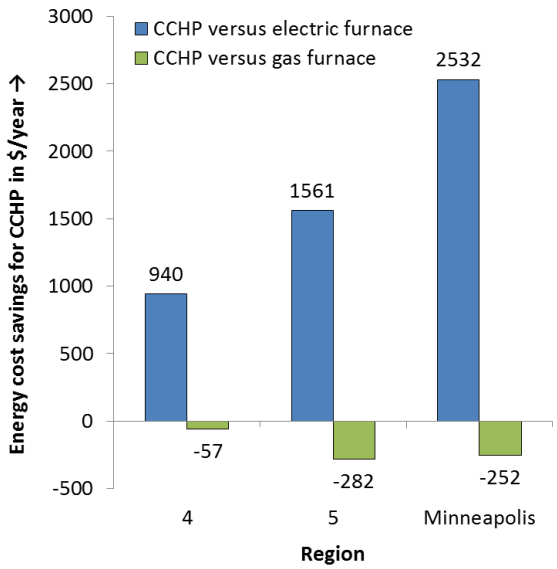

Figure 57: Energy savings compared to electric and gas furnace

Case III: CCHP versus gas/electric furnace with AC system

If the cold climate heat pump replaces a gas/electric furnace and the installation of AC is required, then the HP or CCHP can replace both systems. In that case, the same savings as outlined in Figure 57 are achieved when compare to an electric furnace.

Estimate of number of units to be manufactured

Based on the previous paragraphs, the cold climate heat pump is only of interest if it replaces a conventional heat pump in region 5 or an electric furnace that is combined with an AC system if no natural gas is available. Census data on which type of heating equipment is used in specific climate regions is available from the US energy administration information, e.g. EIA 2009. Unfortunately the EIA does use different climate regions than used in AHRI 210-240, and does not give more detailed information on where survey participants are located in their micro data. However, region 4 and 5 correspond roughly to the cold and very cold climate regions used by EIA. This can be seen by comparing Figure 58 and Figure 59. EIA (2009) states that for these regions, 4.2 million housing units use an electric warm air furnace or built in electric units as main heating equipment. In principle, all of these could potentially be replaced by a cold climate heat pump. However, this only will make financial sense if there is no natural gas available. A smaller market penetration of e.g. 1 million units seems reasonable and achievable. This corresponds to yearly shipments of less than 100,000 units per year. This does not include the additional units that could be used for the Case I scenario.

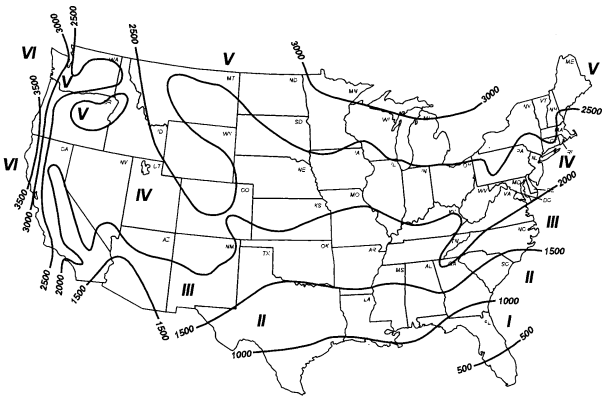

Figure 58: Climate regions (AHRI 210-240)

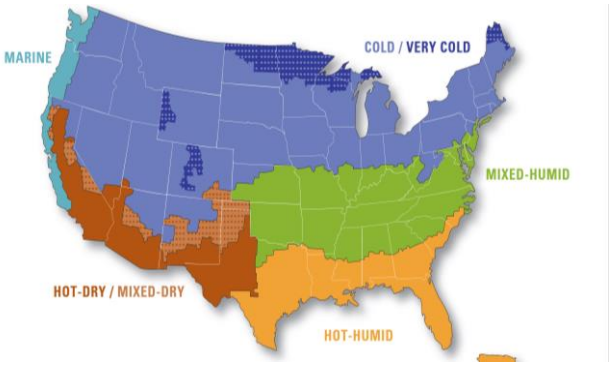

Figure 59: Climate regions (EERE, 2010)

5 Summary and future work

In this report, three technologies to improve the efficiency of vapor compression systems are described. These include a) vapor injected compression, b) oil flooded compression and c) hybrid flow control of the evaporator.

Compressor prototypes for both, oil flooded and vapor injected compression were developed by Emerson Climate Technologies. For the oil flooded compressor, the oil injection port location was optimized and an internal oil separator was added using several design iterations.

After initial testing at Emerson Climate Technologies, further testing was done at Purdue University, and compressor models were developed. These models were then integrated into a system model to determine the achievable improvement of seasonal energy efficiency (SEER) for Minneapolis (Minnesota) climate. For the oil flooded compression, a 34% improvement in seasonal energy efficiency was found while a 21% improvement in seasonal energy efficiency ratio was found for the vapor injected compression. It was found that one benefit of both tested compression technologies is a lower discharge temperature, which allows for continued operation at lower ambient temperatures.

A bin analysis of the vapor injected prototype cold climate heat pump predicts a 6% improvement in HSPF for Minneapolis. This improvement is mainly a result of the increased capacity of the system for active vapor injection. For the oil flooded system, a slightly larger performance improvement is predicted, in this case mostly caused by an increase in heating COP. Based on an economic analysis of these results, the maximum additional cost of the system changes, for the Minneapolis location, are $430 for the vapor injected system and $391 for the oil flooded system. These estimates assume that a 3-year simple payback period is accepted by the customer.

For the hybrid flow control of evaporators, a new type of balancing valve was developed together with Emerson Climate technologies to reduce the cost of the control scheme. In contrast to conventional stepper motor valves, this valve requires less cables and can be driven by a cheaper output circuit on the control board. The correct valve size was determined in a dedicated test stand in several design iterations.

The performance benefits of the hybrid control of the evaporator coil were determined for clean coil conditions as well as with partial blockage of the air inlet grille and under frosting conditions. For clean coil conditions, the benefits in terms of COP and capacity are negligible. However, significant benefits were noted for severely air-maldistributed operating conditions. For the H2-test, the maximum COP improvement of 17% along with a capacity improvement of nearly 40% was observed. Overall, the hybrid control scheme leads to a significant amount of performance improvement, if the air inlet conditions to the evaporator are maldistributed.

Future work should include an optimization of the control algorithms of the tested systems. Furthermore the effects of the different control schemes onto frost built up with repeated frost built-up and defrost should be evaluated. This should include laboratory studies under controlled operating conditions as well as field studies to include unforeseen effects. Frost built up

It would be beneficial for the market estimate to have more detailed data on the geographical distribution of number of housing units, their main heating equipment, the availability of natural gas, as well as the housing unit size. With that information it would be possible to give a more accurate market estimate.

6 References

I. H. Bell, 2011, *Theoretical and Experimental Analysis of Liquid Flooded Compression in Scroll compressors*, PhD-Thesis, Purdue University, West Lafayette, Indiana, USA

EERE (2010), *Building America Best Practice Series Volume 7.1 High-Performance Technologies: Guide to Determining Climate regions by County*, Office of Energy Efficiency & Renewable Energy, Washington D.C., USA

EIA (2009) *Table HC6.6: Space Heating in U.S. Homes, by Climate Region, 2009, U.S. Energy Information Administration*, Washington D.C., USA

EIA (2011 a), *Table 5.6.B. Average Retail Price of Electricity to Ultimate Customers by End-Use Sector,by State, Year-to-Date through September 2012 and 2011 (Cents per Kilowatthour)*, U.S. Energy Information Administration, Washington D.C., USA

EIA (2011 b), *Table 24. Average price of natural gas delivered to consumers by state and sector, 2011 (dollars per thousand cubic feet)*, U.S. Energy Information Administration, Washington D.C., USA

EIA (2011 c), *Heat Content of Natural Gas Consumed Heat Content of Natural Gas Consumed (Btu per Cubic Foot)*, U.S. Energy Information Administration, Washington D.C., USA

E. A. Groll, J. E. Braun, C. K. Bach (2011), *Optimizing Refrigerant Distribution in Evaporators*, Final report for California Energy Commission, CEC-500-2013-089, Purdue University, West Lafayette, Indiana, USA

G. Khowailed, K. Sikes, O. Abdelaziz (2011), *Preliminary Market Assessment for Cold Climate Heat Pumps*, ORNL Building Equipment Research Group, Oak Ridge National Laboratory, Springfield, Virginia, USA

M. Mathison, 2011, *Modeling and evaluation of advanced compression techniques for vapor compression equipment*, PhD-Thesis, Purdue University, West Lafayette, Indiana, USA

Appendix

A. Experimental Data Vapor Injected System

A.1 Calculation of Reported Values

Heating capacity is calculated as

$$\dot{Q} = \dot{Q}_{Cond,ref} + \dot{W}_{ID-Fan}, \quad \textbf{(A.1.1)}$$

where $\dot{Q}_{Cond,ref}$ is the condensing capacity evaluated at the inlet and outlet of the indoor unit and $\dot{W}_{ID-Fan}$ is the indoor fan power consumption. Both values are evaluated as arithmetic mean over the selected quasi-steady part of each test.

Heating coefficient of performance (COP) is calculated as

$$COP = \frac{\dot{Q}}{\dot{W}_{tot}}, \quad \textbf{(A.1.2)}$$

where $\dot{Q}$ is the heating capacity and $\dot{W}_{tot}$ is the sum of the power consumptions of indoor fan, outdoor fan, and compressor variable speed drive power consumption. All values are evaluated as arithmetic mean over the selected quasi-steady part of each test.

Reported uncertainties include sensor and first order uncertainty.

A.2 Detailed system schematic and documentation of measurement channels

Figure A 1 shows the schematic of the vapor injected system with hybrid control. Note that inlet pressures are not available for the baseline coil, which is instrumented according to Figure A 2. Additional instrumentation is listed in Table A 1.

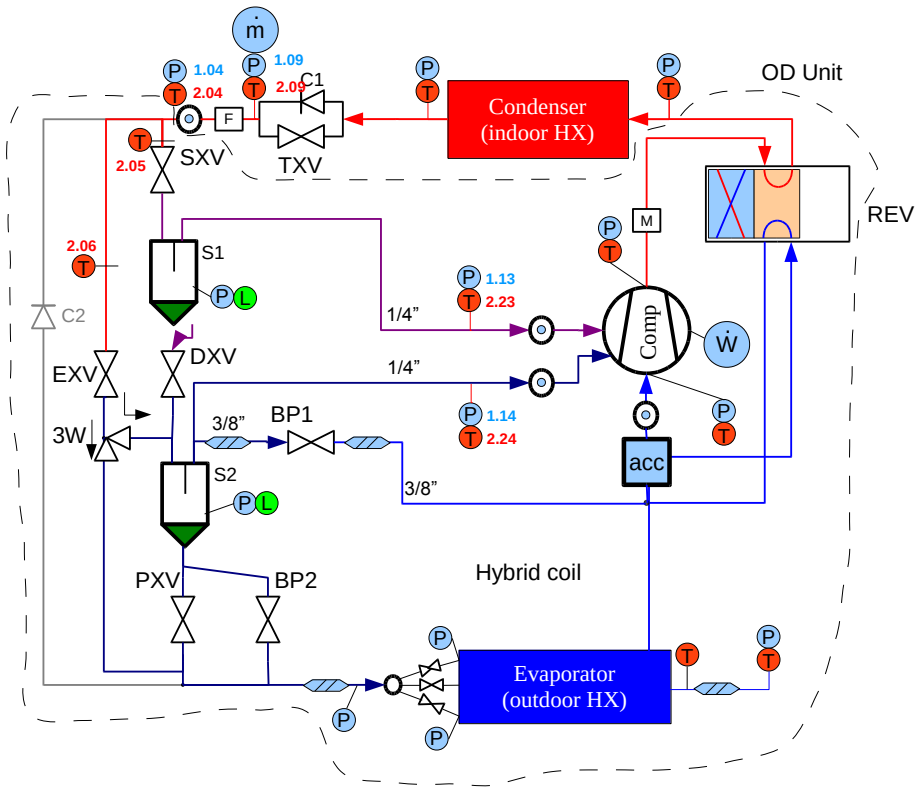

Figure A 1: Schematic with instrumentation locations \w hybrid coil

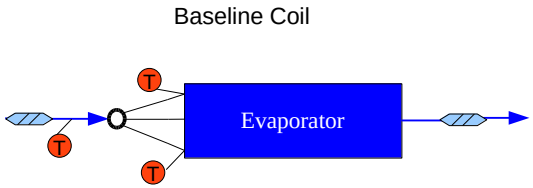

Figure A 2: Evaporator instrumentation for baseline coil

Table A 1: Measurement positions, type and location, part 1

Position	Description	Variable name	Signal
	Refrigerant side pressure		
1.01	Discharge port	p_dis	0-10 V
1.02	Condenser inlet	p_cond_in	0-10 V
1.03	Condenser outlet	p_cond_out	0-10 V
1.04	Condenser outlet2	p_cond_out2	0-10 V
1.05	Seperator 1	p_sep1	0-10 V
1.06	Seperator 2	p_sep2	0-10 V
1.07	Evaporator out	p_evap_out	0-10 V
1.08	Suction port	p_suc	0-10 V
1.09	Condenser outlet3	p_cond_out3	0-10 V
1.10	Evaporator inlet (before Distributor)	p_evap_in	0-10 V
1.11	Circuit1 (upper) inlet	p_cir1_in	0-10 V
1.12	Circuit2 (lower) inlet	p_cir10_in	0-10 V
1.13	Vapor injection, high pressure	p_vi_hp	0-10 V
1.14	Vapor injection, low pressure	p_vi_lp	0-10 V
	Refrigerant side temperature		
2.01	Discharge port	T_dis	TC (type T)
2.02	Condenser inlet	T_cond_in	TC (type T)
2.03	Condenser outlet	T_cond_out	TC (type T)
2.04	Condenser outlet2	T_cond_out2	TC (type T)
2.05	SXV inlet temperature	T_SXV_in	TC (type T)
2.06	EXV inlet temperature	T_EXV_in	TC (type T)
2.07	Evaporator outlet	T_evap_out	TC (type T)
2.08	Suction port	T_suc	TC (type T)
2.09	Condenser outlet3	T_cond_out3	TC (type T)
2.10	Evaporator inlet	T_evap_in	TC (type T)
2.11	Circuit1 inlet (upper)	T_cir1_in	TC (type T)
2.12	Circuit10 inlet (lower)	T_cir10_in	TC (type T)
2.13	Circuit1 (upper) outlet	T_cir1_out	TC (type T)
2.14	Circuit2 outlet	T_cir2_out	TC (type T)
2.15	Circuit3 outlet	T_cir3_out	TC (type T)
2.16	Circuit4 outlet	T_cir4_out	TC (type T)
2.17	Circuit5 outlet	T_cir5_out	TC (type T)
2.18	Circuit6 outlet	T_cir6_out	TC (type T)
2.19	Circuit7 outlet	T_cir7_out	TC (type T)
2.20	Circuit8 outlet	T_cir8_out	TC (type T)
2.21	Circuit9 outlet	T_cir9_out	TC (type T)
2.22	Circuit10 (lower) outlet	T_cir10_out	TC (type T)
2.23	Vapor injection, high pressure	T_vi_hp	TC (type T)
2.24	Vapor injection, low pressure	T_vi_lp	TC (type T)
	Refrigerant mass flow		
3.01	in liquid line	m_dot_r	0-10 V

Table A 2: Measurement positions, type and location, part 2

Position	Description	Variable name	Signal
	Refrigerant level in seperator		
4.01	Seperator 1	level_S1	0-10 V
4.02	Seperator 2	level_S2	0-10 V
xxx	Compressor oil levl switch		
	Power consumption		
5.00	Compressor and VSD	W_dot_comp_vsd	0-10 V
5.01	Compressor	W_dot_comp	0-10 V
5.02	Outdoor unit fan	W_dot_OU	0-10 V
5.03	Indoor unit fan	W_dot_IU	0-10 V
5.04	Read out VFD	VFD_out	0-10 V
5.05	PWM signal average	PWM_avg	0-10 V
	Air side temperature		
6.01	OU outlet: location according schematic	T_OU_out1	TC (type T)
6.02	OU outlet: location according schematic	T_OU_out2	TC (type T)
6.03	OU outlet: location according schematic	T_OU_out3	TC (type T)
6.04	OU outlet: location according schematic	T_OU_out4	TC (type T)
6.05	OU outlet: location according schematic	T_OU_out5	TC (type T)
6.06	OU outlet: location according schematic	T_OU_out6	TC (type T)
6.07	OU outlet: location according schematic	T_OU_out7	TC (type T)
6.08	OU outlet: location according schematic	T_OU_out8	TC (type T)
6.11	OU nord inlet: location according schematic	T_OU_in1	TC (type T)
6.12	OU nord inlet: location according schematic	T_OU_in2	TC (type T)
6.13	OU nord inlet: location according schematic	T_OU_in3	TC (type T)
6.14	OU nord inlet: location according schematic	T_OU_in4	TC (type T)
6.21	OU west inlet: location according schematic	T_OU_in5	TC (type T)
6.22	OU west inlet: location according schematic	T_OU_in6	TC (type T)
6.23	OU west inlet: location according schematic	T_OU_in7	TC (type T)
6.24	OU west inlet: location according schematic	T_OU_in8	TC (type T)
6.31	OU south inlet: location according schematic	T_OU_in9	TC (type T)
6.32	OU south inlet: location according schematic	T_OU_in10	TC (type T)
6.33	OU south inlet: location according schematic	T_OU_in11	TC (type T)
6.34	OU south inlet: location according schematic	T_OU_in12	TC (type T)
6.41	OU east inlet: location according schematic	T_OU_in13	TC (type T)
6.42	OU east inlet: location according schematic	T_OU_in14	TC (type T)
6.43	OU east inlet: location according schematic	T_OU_in15	TC (type T)
6.44	OU east inlet: location according schematic	T_OU_in16	TC (type T)

Table A 3: Measurement positions, type and location, part 3

Position	Description	Variable name	Signal
Air side temperature			
6.61	IU outlet: location according schematic	T_IU_out1	TC (type T)
6.62	IU outlet: location according schematic	T_IU_out2	TC (type T)
6.63	IU outlet: location according schematic	T_IU_out3	TC (type T)
6.64	IU outlet: location according schematic	T_IU_out4	TC (type T)
6.65	IU outlet: location according schematic	T_IU_out5	TC (type T)
6.66	IU outlet: location according schematic	T_IU_out6	TC (type T)
6.67	IU outlet: location according schematic	T_IU_out7	TC (type T)
6.68	IU outlet: location according schematic	T_IU_out8	TC (type T)
6.69	IU outlet: location according schematic	T_IU_out9	TC (type T)
6.71	IU inlet: location according schematic	T_IU_in1	TC (type T)
6.72	IU inlet: location according schematic	T_IU_in2	TC (type T)
6.73	IU inlet: location according schematic	T_IU_in3	TC (type T)
6.74	IU inlet: location according schematic	T_IU_in4	TC (type T)
6.75	IU inlet: location according schematic	T_IU_in5	TC (type T)
6.76	IU inlet: location according schematic	T_IU_in6	TC (type T)
6.77	IU inlet: location according schematic	T_IU_in7	TC (type T)
6.78	IU inlet: location according schematic	T_IU_in8	TC (type T)
6.79	IU inlet: location according schematic	T_IU_in9	TC (type T)
Airside pressure			
7.01	Inside OU vs. ambient	dp_OU	0-10 V
7.02	Inside IU vs. ambient	dp_IU	0-10 V
Dewpoint			
8.01	Outdoor unit inlet	DP_OU_in	0-10 V
8.02	Outdoor unit outlet	DP_OU_out	0-10 V
8.03	Indoor unit inlet	DP_IU_in	0-10 V
8.04	RH Outdoor unit inlet	RH_OU_in	0-10 V
8.05	RH Indoor unit inlet	RH_IU_in	0-10V
Air flow rate			
9.01	Nozzle box (for indoor unit)	dp_nozzle	0-10 V
Sensors initially installed on mother board of the unit			
10.01	Units discharge sensor	T_unit_dis	Ω
10.02	Units coil sensor	T_unit_coil	Ω
10.03	Units ambient sensor	T_unit_amb	Ω
Outputs			
11.10	set VFD frequency	VFD_freq_demand	0-10 V
11.20	set nozzle box fan frequency	Nozzle_freq_demand	0-10 V

A.3 Data Tables

The following tables show the measurement data for the different system configurations.

Table A 4: Baseline 0 data, part 1

	Date [MM/DD/YYYY]	Time [HH:MM:SS]	Test_duration [SS]	T_ambient [F]	DP [F]	T_return_air [F]	Speed [Hz]	Ref.charge [lb]	p_atm [kPa]	p_dis [kPa]
H1-low_clean_B0	8/1/2013	6:01:51 PM	2479.0	47.0	43.0	70.0	40.0	-9.8	99.5	2340.6
H1-low_light_B0	8/2/2013	4:02:17 PM	3415.0	47.0	43.0	70.0	40.0	-9.8	99.5	2302.1
H1-low_severe_B0	8/2/2013	5:41:30 PM	3104.0	47.0	43.0	70.0	40.0	-9.8	99.5	2237.5
H2_mid_clean_B0	7/10/2013	12:35:36 PM	1858.0	35.0	-999.0	70.0	55.0	9.8	98.9	2328.9
H2_mid_light_blocked_B0	7/10/2013	1:31:23 PM	1854.0	35.0	-999.0	70.0	55.0	9.8	98.9	2211.3
H2_mid_severe_blocked_B0	7/10/2013	2:24:39 PM	1854.0	35.0	-999.0	70.0	55.0	9.8	98.9	2080.4
H3_full_clean_B0	7/11/2013	10:23:44 AM	1855.0	17.0	-999.0	70.0	70.0	9.8	99.4	2247.8
H3_full_light_blocked_B0	7/11/2013	11:08:47 AM	1856.0	17.0	-999.0	70.0	70.0	9.8	99.4	2139.5
H3_full_severe_blocked_B0	7/11/2013	3:35:05 PM	1855.0	17.0	-999.0	70.0	70.0	9.8	99.4	1953.4
HX_full_clean_B0	7/15/2013	12:16:45 PM	1854.0	0.0	-999.0	70.0	70.0	9.8	100.2	2073.9
HX_full_light_blocked_B0	7/15/2013	1:23:47 PM	1854.0	0.0	-999.0	70.0	70.0	9.8	100.2	2040.6
HX_full_severe_blocked_B0	7/15/2013	2:51:44 PM	1855.0	0.0	-999.0	70.0	70.0	9.8	100.2	1930.0

	p_sep1 [kPa]	p_cond_in [kPa]	p_cond_out	p_cond_out2	p_sep2 [kPa]	p_cond_out3	p_evap_out	p_suc [kPa]	p_evap_in [kPa]	p_cir1_in [kPa]
H1-low_clean_B0	91.8	2332.8	2298.2	2273.6	96.6	2279.2	766.1	748.0	-999.0	-999.0
H1-low_light_B0	84.0	2305.1	2271.2	2249.6	95.3	2254.8	726.0	707.9	-999.0	-999.0
H1-low_severe_B0	84.7	2240.7	2208.4	2189.9	95.4	2194.0	680.6	662.4	-999.0	-999.0
H2_mid_clean_B0	63.7	2359.5	2322.0	2303.3	90.2	2302.8	546.4	518.3	-999.0	-999.0
H2_mid_light_blocked_B0	65.3	2242.3	2209.3	2202.0	90.4	2196.4	475.3	448.9	-999.0	-999.0
H2_mid_severe_blocked_B0	65.9	2114.8	2087.4	2089.7	90.5	2079.0	392.2	368.3	-999.0	-999.0
H3_full_clean_B0	28.9	2288.0	2252.8	2250.6	81.4	2239.0	403.4	366.1	-999.0	-999.0
H3_full_light_blocked_B0	30.1	2182.4	2150.5	2156.4	82.0	2141.7	352.7	318.6	-999.0	-999.0
H3_full_severe_blocked_B0	37.6	2001.3	1973.1	1988.4	83.7	1969.6	269.0	239.6	-999.0	-999.0
HX_full_clean_B0	75.5	2081.0	2051.4	2078.3	92.1	2047.1	310.7	269.4	-999.0	-999.0
HX_full_light_blocked_B0	78.8	2046.7	2018.7	2045.2	92.6	2014.3	297.6	257.7	-999.0	-999.0
HX_full_severe_blocked_B0	81.2	1937.6	1909.9	1941.3	92.9	1908.6	248.9	211.6	-999.0	-999.0

	p_cir10_in [kPa]	dp_IU [Pa]	dp_OU [Pa]	dp_nozzle [Pa]	dp_nozzle2 [Pa]	T_dis [C]	T_cond_in [C]	T_cond_out [C]	T_cond_out2 [C]	T_SXV_in [C]
H1-low_clean_B0	-999.0	51.0	24.8	195.3	195.3	87.6	82.6	33.9	29.3	6.9
H1-low_light_B0	-999.0	50.9	29.5	196.5	196.5	88.9	83.7	33.4	28.8	7.6
H1-low_severe_B0	-999.0	50.8	40.2	198.0	198.0	88.0	82.6	33.1	28.6	3.5
H2_mid_clean_B0	-999.0	51.0	38.7	201.0	201.0	93.2	87.6	34.3	28.8	0.8
H2_mid_light_blocked_B0	-999.0	51.0	48.5	201.1	201.1	96.2	89.5	32.4	26.9	0.4
H2_mid_severe_blocked_B0	-999.0	51.0	56.6	201.5	201.5	103.1	94.2	29.9	24.5	-0.9
H3_full_clean_B0	-999.0	51.0	45.9	200.8	200.8	103.5	95.9	32.8	25.8	-7.3
H3_full_light_blocked_B0	-999.0	51.0	56.3	200.9	200.9	108.4	99.2	31.0	24.0	-8.1
H3_full_severe_blocked_B0	-999.0	51.0	58.4	201.9	201.9	123.1	109.2	28.5	21.5	-10.3
HX_full_clean_B0	-999.0	51.0	31.3	193.2	193.2	114.0	102.8	28.9	20.7	-15.2
HX_full_light_blocked_B0	-999.0	51.0	45.5	193.8	193.8	116.2	104.3	28.8	20.5	-15.1
HX_full_severe_blocked_B0	-999.0	50.9	55.5	195.1	195.1	127.9	111.9	27.4	18.9	-16.1

Table A 5: Baseline 0 data, part 2

	T_EXV_in [C]	T_evap_out [C]	T_suc [C]	T_evap_distr_in [C]	T_cir1_in [C]	T_cir10_in [C]	T_cir1_out [C]	T_cir2_out [C]	T_cir3_out [C]	T_cir4_out [C]
H1-low_clean_B0	31.4	3.7	5.8	3.1	1.3	1.7	3.8	4.6	5.0	6.3
H1-low_light_B0	30.9	2.0	4.7	1.5	-0.3	0.0	5.1	6.2	5.0	6.5
H1-low_severe_B0	30.7	-0.1	2.6	-0.5	-2.4	-2.0	5.1	6.4	4.6	6.4
H2_mid_clean_B0	31.4	-6.4	-3.2	-3.4	-6.6	-6.0	-4.3	-3.3	-1.6	-0.4
H2_mid_light_blocked_B0	29.4	-10.4	-5.7	-7.7	-10.8	-10.4	-4.7	-3.7	-1.9	-0.4
H2_mid_severe_blocked_B0	26.7	-15.7	-8.3	-13.3	-15.9	-15.8	-4.3	-3.6	-2.2	-0.8
H3_full_clean_B0	29.1	-14.9	-11.6	-9.7	-14.0	-13.2	-12.9	-12.5	-11.3	-10.0
H3_full_light_blocked_B0	27.1	-18.6	-13.7	-13.7	-17.7	-17.1	-14.2	-13.7	-11.8	-10.3
H3_full_severe_blocked_B0	24.2	-25.1	-16.6	-21.4	-24.6	-24.6	-13.4	-14.7	-12.4	-11.2
HX_full_clean_B0	24.2	-21.5	-17.5	-18.3	-22.3	-21.5	-21.7	-21.6	-20.4	-19.7
HX_full_light_blocked_B0	24.0	-22.6	-18.1	-19.6	-23.6	-22.8	-22.6	-22.4	-20.3	-19.6
HX_full_severe_blocked_B0	22.2	-26.7	-20.5	-24.6	-27.8	-27.7	-22.7	-22.6	-20.8	-19.9

	T_cir5_out [C]	T_cir6_out [C]	T_cir7_out [C]	T_cir8_out [C]	T_cir9_out [C]	T_cir10_out [C]	T_cond_out3 [C]	T_OU_out [C]	T_OU_in [C]	T_IU_out [C]
H1-low_clean_B0	3.4	3.2	3.7	2.9	3.4	4.1	33.2	5.6	8.2	37.7
H1-low_light_B0	4.6	4.6	5.8	0.2	-0.3	-3.1	32.7	6.2	8.3	37.2
H1-low_severe_B0	3.6	-1.2	-1.5	-3.6	-2.7	-4.5	32.6	6.8	8.5	36.2
H2_mid_clean_B0	-6.9	-5.9	-3.8	-4.9	-4.1	-11.9	33.7	-1.1	1.6	38.3
H2_mid_light_blocked_B0	-10.1	-14.7	-7.8	-7.1	-6.7	-14.8	31.8	-0.7	1.8	36.3
H2_mid_severe_blocked_B0	-12.3	-21.1	-15.9	-9.2	-8.7	-12.1	29.3	-0.1	2.0	34.0
H3_full_clean_B0	-14.7	-20.0	-15.8	-13.3	-12.4	-17.4	32.1	-10.5	-8.3	37.3
H3_full_light_blocked_B0	-18.1	-23.0	-19.9	-15.4	-14.4	-20.4	30.3	-10.2	-8.2	35.4
H3_full_severe_blocked_B0	-21.0	-31.1	-28.6	-25.0	-22.5	-22.0	28.1	-9.7	-8.3	32.1
HX_full_clean_B0	-23.0	-22.1	-21.8	-20.7	-20.0	-20.9	28.4	-19.1	-17.8	33.4
HX_full_light_blocked_B0	-24.3	-23.2	-22.4	-22.3	-21.6	-24.1	28.3	-18.9	-17.4	32.9
HX_full_severe_blocked_B0	-26.7	-34.6	-31.4	-24.7	-23.6	-24.9	27.2	-18.4	-17.3	30.8

	T_IU_in [C]	m_dot_r [g/s]	level_S1 [%]	level_S2 [%]	W_dot_OU [kW]	W_dot_IU [kW]	W_dot_comp_vsd [kW]	W_dot_comp [kW]	DP_OU_in [C]	DP_IU_in [C]
H1-low_clean_B0	21.1	61.6	2.4	0.4	0.3	0.4	4.0	3.9	3.6	9.0
H1-low_light_B0	21.3	58.2	2.5	0.5	0.4	0.4	3.9	3.8	3.9	8.7
H1-low_severe_B0	21.3	54.9	2.4	0.4	0.4	0.4	3.7	3.6	3.7	8.8
H2_mid_clean_B0	21.1	62.3	2.3	0.2	0.4	0.4	4.6	4.5	-2.1	8.3
H2_mid_light_blocked_B0	21.1	53.4	2.1	0.2	0.3	0.4	4.2	4.2	-2.3	8.4
H2_mid_severe_blocked_B0	21.1	43.0	1.9	0.2	0.3	0.4	3.9	3.8	-2.4	8.5
H3_full_clean_B0	20.9	56.1	2.4	0.5	0.3	0.4	5.1	5.0	-7.8	5.0
H3_full_light_blocked_B0	20.8	48.3	2.3	0.5	0.3	0.4	4.8	4.7	-8.3	5.3
H3_full_severe_blocked_B0	20.9	35.0	2.0	0.5	0.3	0.4	4.2	4.1	-9.3	5.0
HX_full_clean_B0	20.8	40.7	1.7	0.1	0.4	0.4	4.5	4.4	-15.9	6.3
HX_full_light_blocked_B0	20.8	38.7	1.7	0.0	0.3	0.4	4.4	4.3	-16.3	6.4
HX_full_severe_blocked_B0	20.8	31.0	1.5	0.1	0.3	0.4	4.0	3.9	-16.7	6.3

Table A 6: Baseline 0 data, part 3

	DP_OU_out [C]	RH_OU_in [%]	RH_IU_in [%]	T_c_1 [C]	T_e_1 [C]	T_c_0 [C]	Q_dot_cond_1_3 [kW]	Q_dot_cond_2_3 [kW]	Q_dot_cond_2_9 [kW]	T_sc_3 [K]
H1-low_clean_B0	3.2	61.4	43.9	38.5	-1.3	37.5	14.4	14.1	14.2	4.3
H1-low_light_B0	2.9	63.9	41.8	38.0	-2.9	37.0	13.8	13.5	13.6	4.3
H1-low_severe_B0	2.6	65.5	42.0	36.9	-4.9	35.9	13.1	12.7	12.8	3.4
H2_mid_clean_B0	-3.5	61.1	41.1	39.0	-11.4	37.9	15.0	14.5	14.6	4.2
H2_mid_light_blocked_B0	-3.6	60.4	41.3	36.9	-15.3	36.0	13.3	12.8	12.9	4.1
H2_mid_severe_blocked_B0	-3.9	60.9	41.7	34.6	-20.5	33.8	11.2	10.8	10.9	4.4
H3_full_clean_B0	-11.5	74.2	33.1	37.7	-19.7	36.7	14.3	13.8	13.9	4.7
H3_full_light_blocked_B0	-12.0	73.2	33.9	35.8	-23.3	34.9	12.8	12.3	12.3	4.7
H3_full_severe_blocked_B0	-12.0	73.1	32.9	32.4	-30.0	31.6	10.0	9.5	9.5	3.5
HX_full_clean_B0	-20.3	77.5	36.3	33.9	-26.5	33.1	11.2	10.7	10.7	4.8
HX_full_light_blocked_B0	-20.5	76.2	36.7	33.3	-27.6	32.5	10.8	10.3	10.3	4.2
HX_full_severe_blocked_B0	-20.6	77.7	36.6	31.1	-31.9	30.4	9.1	8.6	8.6	3.2

	T_sc_XV [K]	T_sh_comp [K]	T_sh [K]	T_nozzle [C]	V_dot_IU [m3/s]	rho_a_nozzle [kg/m3]	V_dot_IU_standardair [kg/m3]	Q_dot_heat_airside [kW]	Q_dot_cond_airside [kW]	Q_dot_useful_airside [kW]
H1-low_clean_B0	5.9	7.8	5.0	37.2	0.8	1.1	0.7	14.8	14.4	14.8
H1-low_light_B0	6.0	8.4	5.0	36.7	0.8	1.1	0.7	14.2	13.8	14.2
H1-low_severe_B0	5.2	8.3	4.8	35.6	0.8	1.1	0.7	13.4	13.0	13.4
H2_mid_clean_B0	6.5	9.7	5.0	37.5	0.8	1.1	0.7	15.5	15.2	15.5
H2_mid_light_blocked_B0	6.7	11.2	4.8	35.8	0.8	1.1	0.7	13.7	13.4	13.8
H2_mid_severe_blocked_B0	7.3	13.8	4.8	33.7	0.8	1.1	0.7	11.6	11.3	11.7
H3_full_clean_B0	7.9	10.7	4.8	36.4	0.8	1.1	0.7	14.8	14.4	14.8
H3_full_light_blocked_B0	8.1	12.1	4.7	34.9	0.8	1.1	0.7	13.2	12.8	13.2
H3_full_severe_blocked_B0	7.8	16.2	4.9	31.9	0.8	1.1	0.7	10.2	9.9	10.2
HX_full_clean_B0	9.5	12.5	5.0	33.4	0.8	1.1	0.7	11.2	10.9	11.2
HX_full_light_blocked_B0	9.1	13.0	5.0	32.9	0.8	1.1	0.7	10.8	10.4	10.8
HX_full_severe_blocked_B0	8.9	15.2	5.2	31.1	0.8	1.1	0.7	9.0	8.7	9.1

	Q_dot_useful_refside [kW]	COP_h_airside [-]	COP_h_refside [-]	DT_air_on_eva7 [K]	T_dew_suc [C]	T_dew_dis [C]	T_bub_cond [C]	T_dew_evap [C]	DT_air_on_cond3 [K]	Q_dot_evap [kW]
H1-low_clean_B0	14.6	3.1	3.1	9.5	-2.0	38.7	37.6	-1.3	16.5	11.1
H1-low_light_B0	13.9	3.0	3.0	11.3	-3.7	38.0	37.1	-2.9	15.8	10.5
H1-low_severe_B0	13.2	3.0	2.9	13.4	-5.7	36.8	36.0	-4.9	14.7	9.8
H2_mid_clean_B0	15.0	2.9	2.8	12.9	-12.9	38.4	38.0	-11.4	16.9	11.0
H2_mid_light_blocked_B0	13.3	2.8	2.7	17.1	-16.8	36.3	36.1	-15.3	15.0	9.5
H2_mid_severe_blocked_B0	11.2	2.5	2.4	22.5	-22.1	33.9	33.9	-20.5	12.8	7.7
H3_full_clean_B0	14.3	2.5	2.4	11.5	-22.3	37.0	36.9	-19.7	16.0	10.0
H3_full_light_blocked_B0	12.7	2.4	2.3	15.1	-25.8	35.0	35.1	-23.3	14.3	8.7
H3_full_severe_blocked_B0	9.9	2.1	2.0	21.7	-32.8	31.4	31.7	-30.0	10.9	6.3
HX_full_clean_B0	11.1	2.2	2.1	8.7	-30.0	33.8	33.3	-26.5	12.5	7.5
HX_full_light_blocked_B0	10.7	2.1	2.1	10.1	-31.1	33.1	32.6	-27.6	11.8	7.1
HX_full_severe_blocked_B0	9.0	1.9	1.9	14.6	-35.7	30.9	30.5	-31.9	9.7	5.7

Table A 7: Baseline 0 data, part 4

	m_dot_OU_air [kg/s]	T_sh_cir1 [K]	T_sh_cir2 [K]	T_sh_cir3 [K]	T_sh_cir4 [K]	T_sh_cir5 [K]	T_sh_cir6 [K]	T_sh_cir7 [K]	T_sh_cir8 [K]	T_sh_cir9 [K]
H1-low_clean_B0	3.6	5.0	5.9	6.2	7.6	4.7	4.5	5.0	4.1	4.7
H1-low_light_B0	3.4	8.0	9.2	7.9	9.5	7.5	7.5	8.8	3.1	2.7
H1-low_severe_B0	3.5	10.0	11.3	9.5	11.3	8.5	3.7	3.4	1.3	2.2
H2_mid_clean_B0	2.9	7.1	8.0	9.7	10.9	4.4	5.4	7.6	6.4	7.2
H2_mid_light_blocked_B0	2.7	10.5	11.6	13.4	14.8	5.2	0.5	7.4	8.1	8.6
H2_mid_severe_blocked_B0	2.3	16.2	16.9	18.3	19.7	8.1	-0.6	4.6	11.3	11.8
H3_full_clean_B0	2.8	6.8	7.3	8.5	9.7	5.0	-0.3	3.9	6.4	7.3
H3_full_light_blocked_B0	2.5	9.0	9.5	11.5	12.9	5.2	0.2	3.3	7.9	8.8
H3_full_severe_blocked_B0	2.7	16.6	15.3	17.6	18.9	9.0	-1.0	1.5	5.0	7.5
HX_full_clean_B0	3.4	4.7	4.9	6.1	6.8	3.5	4.4	4.7	5.8	6.5
HX_full_light_blocked_B0	3.2	5.0	5.2	7.2	8.0	3.2	4.3	5.2	5.3	6.0
HX_full_severe_blocked_B0	3.3	9.2	9.3	11.1	12.0	5.2	-2.7	0.5	7.2	8.3

	T_sh_cir10 [K]
H1-low_clean_B0	5.4
H1-low_light_B0	-0.1
H1-low_severe_B0	0.4
H2_mid_clean_B0	-0.6
H2_mid_light_blocked_B0	0.5
H2_mid_severe_blocked_B0	8.4
H3_full_clean_B0	2.3
H3_full_light_blocked_B0	2.8
H3_full_severe_blocked_B0	8.0
HX_full_clean_B0	5.6
HX_full_light_blocked_B0	3.5
HX_full_severe_blocked_B0	7.0

Table A 8: Notes to measurement data for vapor injected heat pump

Refrigerant Charge	A negative number indicates that a negligible loss of charge had occurred, which was compensated for by recharging to the same level of subcooling according to a previous test
All columns	-999.0 indicates that the measurement was not available
Injection flowrates	"mb" stands for mass balance, "YP" uses the correlation developed as part of the compressor testing

Table A 9: Baseline 1 data, part 1

	Date [MM/DD/YYYY]	Time [HH:MM:SS]	Test_duration [SS]	T_ambient [F]	DP [F]	T_return_air [F]	Speed [Hz]	Ref.charge [lb]	p_atm [kPa]	p_dis [kPa]
H1_low_clean_B1	8/29/2013	12:38:23 PM	3187.0	47.0	43.0	70.0	40.0	14.9	99.6	2477.0
H1_low_light_blocked_B1	8/29/2013	2:03:58 PM	2610.0	47.0	43.0	70.0	40.0	14.9	99.6	2443.7
H1_low_severe_blocked_B1	8/29/2013	2:47:58 PM	1590.0	47.0	43.0	70.0	40.0	14.9	99.6	2336.1
H2_mid_clean_B1	8/30/2013	1:08:31 PM	3092.0	35.0		70.0	55.0	14.9	99.2	2637.2
H2_mid_light_blocked_B1	8/30/2013	2:13:50 PM	1135.0	35.0		70.0	55.0	14.9	99.2	2437.9
H2_mid_severe_blocked_B1	8/30/2013	3:38:00 PM	1264.0	35.0		70.0	55.0	14.9	99.2	2121.5
H2_xHz_clean_B1	9/6/2013	1:11:26 PM	1872.0	35.0		70.0	43.3	14.9	100.0	2357.7
H2_yHz_clean_B1	9/6/2013	2:21:15 PM	1587.0	35.0		70.0	50.0	14.9	100.0	2534.5
H3_full_clean_B1	9/3/2013	9:59:28 AM	1264.0	17.0		70.0	70.0	14.9	99.6	2586.0
H3_full_light_blocked_B1	9/3/2013	11:05:52 AM	302.0	17.0		70.0	70.0	14.9	99.6	2333.4
H3_full_severe_blocked_B1	9/3/2013	11:42:18 AM	616.0	17.0		70.0	70.0	14.9	99.6	2137.5
H3_full_severe_blocked_B1	9/3/2013	11:34:15 AM	625.0	17.0		70.0	70.0	14.9	99.6	2158.7
H3_xHz_clean_B1	9/9/2013	10:37:08 AM	622.0	17.0		70.0	55.0	14.9	99.3	2341.8
HX_full_clean_B1	9/4/2013	10:03:40 AM	2098.0	0.0		70.0	70.0	14.9	99.8	2248.3
HX_full_light_blocked_B1	9/4/2013	10:52:02 AM	1135.0	0.0		70.0	70.0	14.9	99.8	2199.3
HX_full_severe_blocked_B1	9/4/2013	11:46:33 AM	1584.0	0.0		70.0	70.0	14.9	99.8	2137.0
HX_xHz_clean_B1	9/10/2013	10:49:25 AM	1263.0	0.0		70.0	56.3	14.9	99.6	2108.1
HX_xHz_clean_retest_B1	9/13/2013	10:33:42 AM	1841.0	0.0		70.0	56.2	14.9	99.6	2088.4

	p_sep1 [kPa]	p_vi_hp [kPa]	p_cond_in [kPa]	p_cond_out [kPa]	p_cond_out2 [kPa]	p_sep2 [kPa]	p_cond_out3 [kPa]	p_evap_out [kPa]	p_suc [kPa]	p_evap_in [kPa]
H1_low_clean_B1	1630.9	1623.4	2470.2	2427.2	2400.0	1268.2	2405.2	756.6	741.0	-999.0
H1_low_light_blocked_B1	1585.7	1574.9	2434.7	2393.5	2369.7	1221.7	2373.0	726.7	711.7	-999.0
H1_low_severe_blocked_B1	1471.0	1460.2	2326.1	2288.5	2272.8	1092.1	2273.1	637.7	623.1	-999.0
H2_mid_clean_B1	1399.6	1387.5	2654.9	2599.6	2557.7	1010.8	2569.4	574.1	550.1	-999.0
H2_mid_light_blocked_B1	1178.3	1168.5	2458.2	2414.2	2396.6	820.8	2394.9	469.6	447.8	-999.0
H2_mid_severe_blocked_B1	807.5	798.2	2144.5	2114.1	2121.9	525.6	2107.6	301.6	282.5	-999.0
H2_xHz_clean_B1	1370.2	1355.3	2385.1	2345.5	2331.9	1028.1	2329.4	607.6	589.5	-999.0
H2_yHz_clean_B1	1409.4	1400.6	2561.6	2511.6	2481.4	1038.7	2487.4	599.1	578.8	-999.0
H3_full_clean_B1	1123.0	1092.7	2599.1	2547.0	2529.7	729.3	2523.3	411.1	376.5	-999.0
H3_full_light_blocked_B1	913.2	884.2	2342.6	2303.9	2310.3	558.4	2292.5	316.7	285.9	-999.0
H3_full_severe_blocked_B1	727.3	704.6	2148.1	2115.9	2137.6	420.6	2112.2	245.5	216.6	-999.0
H3_full_severe_blocked_B1	753.2	730.2	2170.4	2136.6	2157.0	440.1	2132.3	254.6	225.9	-999.0
H3_xHz_clean_B1	1077.7	1069.8	2351.0	2311.3	2312.9	735.0	2297.7	429.1	400.6	-999.0
HX_full_clean_B1	817.4	807.3	2255.0	2219.3	2242.3	495.4	2211.2	294.6	257.4	-999.0
HX_full_light_blocked_B1	772.8	763.3	2203.8	2170.0	2197.2	462.0	2164.0	275.5	239.4	-999.0
HX_full_severe_blocked_B1	711.8	701.7	2138.9	2106.0	2137.7	414.5	2101.8	251.0	215.8	-999.0
HX_xHz_clean_B1	777.6	779.2	2114.4	2086.1	2115.2	495.8	2081.1	303.8	269.8	-999.0
HX_xHz_clean_retest_B1	748.1	768.3	2116.0	2088.9	2116.2	497.3	2083.9	307.8	272.9	-999.0

Table A 10: Baseline 1 data, part 2

	p_cir1_in [kPa]	p_cir10_in [kPa]	p_vi_lp [kPa]	dp_IU [Pa]	dp_OU [Pa]	dp_nozzle [Pa]	dp_nozzle2 [Pa]	T_dis [C]	T_cond_in [C]	T_cond_out [C]
H1_low_clean_B1	-999.0	-999.0	1266.4	51.0	28.0	194.7	194.7	88.0	83.6	35.4
H1_low_light_blocked_B1	-999.0	-999.0	1219.9	51.0	30.4	194.9	194.9	88.9	84.3	34.8
H1_low_severe_blocked_B1	-999.0	-999.0	1092.6	51.0	40.2	194.9	194.9	88.8	83.4	34.3
H2_mid_clean_B1	-999.0	-999.0	1008.5	50.9	33.7	196.8	196.8	94.3	89.7	38.3
H2_mid_light_blocked_B1	-999.0	-999.0	821.0	51.0	47.7	194.5	194.5	98.9	93.1	35.0
H2_mid_severe_blocked_B1	-999.0	-999.0	524.9	51.0	59.0	196.0	196.0	109.2	98.9	29.1
H2_xHz_clean_B1	-999.0	-999.0	1032.5	51.0	29.0	194.3	194.3	90.2	85.0	34.2
H2_yHz_clean_B1	-999.0	-999.0	1041.5	50.9	28.4	195.1	195.1	92.8	88.1	36.8
H3_full_clean_B1	-999.0	-999.0	736.5	50.9	39.7	195.1	195.1	103.4	97.7	37.1
H3_full_light_blocked_B1	-999.0	-999.0	562.8	51.1	64.6	193.3	193.3	108.0	99.9	33.8
H3_full_severe_blocked_B1	-999.0	-999.0	428.5	51.0	66.6	193.9	193.9	116.9	105.7	30.3
H3_full_severe_blocked_B1	-999.0	-999.0	447.5	51.0	66.6	193.8	193.8	115.3	104.5	30.9
H3_xHz_clean_B1	-999.0	-999.0	746.2	51.0	48.2	194.8	194.8	95.5	89.3	33.7
HX_full_clean_B1	-999.0	-999.0	506.1	50.9	31.7	195.3	195.3	107.5	99.1	32.0
HX_full_light_blocked_B1	-999.0	-999.0	471.2	51.0	39.7	194.2	194.2	112.2	102.9	31.1
HX_full_severe_blocked_B1	-999.0	-999.0	423.6	51.0	51.9	194.2	194.2	116.7	105.9	29.9
HX_xHz_clean_B1	-999.0	-999.0	508.0	51.0	31.4	195.2	195.2	100.1	90.9	29.4
HX_xHz_clean_retest_B1	-999.0	-999.0	509.8	51.0	30.8	194.9	194.9	100.5	91.4	29.5

	T_cond_out2 [C]	T_SXV_in [C]	T_EXV_in [C]	T_evap_out [C]	T_suc [C]	T_evap_distr_in [C]	T_cir1_in [C]	T_cir10_in [C]	T_vi_hp [C]	T_vi_lp [C]
H1_low_clean_B1	31.1	32.8	32.9	3.3	5.5	1.9	0.7	1.5	23.2	15.6
H1_low_light_blocked_B1	30.5	32.2	32.3	2.1	4.7	0.6	-0.6	0.3	22.1	14.3
H1_low_severe_blocked_B1	30.3	32.0	32.1	-2.0	0.0	-3.3	-4.4	-3.6	19.4	10.9
H2_mid_clean_B1	33.1	35.6	35.6	-5.3	-2.5	-3.7	-5.5	-4.3	17.6	7.0
H2_mid_light_blocked_B1	29.6	31.9	31.9	-9.0	-4.6	-9.9	-11.3	-10.2	11.8	0.5
H2_mid_severe_blocked_B1	24.1	25.7	25.9	-22.1	-13.8	-22.0	-22.1	-22.4	0.1	-10.6
H2_xHz_clean_B1	29.3	31.3	31.4	-3.3	-0.7	-4.2	-5.5	-4.5	17.4	8.3
H2_yHz_clean_B1	31.7	34.0	34.1	-3.9	-1.3	-3.4	-5.0	-3.9	18.2	8.1
H3_full_clean_B1	30.8	33.9	33.9	-14.1	-10.7	-11.9	-13.7	-12.5	9.4	-3.8
H3_full_light_blocked_B1	27.4	30.2	30.2	-26.6	-17.8	-19.6	-20.9	-20.2	2.6	-11.0
H3_full_severe_blocked_B1	23.9	26.2	26.3	-28.6	-19.6	-26.3	-27.0	-26.6	-4.1	-17.2
H3_full_severe_blocked_B1	24.5	26.9	27.0	-28.9	-19.5	-25.2	-26.0	-25.7	-3.1	-16.3
H3_xHz_clean_B1	27.4	30.2	30.2	-13.6	-10.3	-13.0	-14.6	-13.4	8.5	-3.0
HX_full_clean_B1	24.6	27.7	27.9	-22.4	-18.5	-21.8	-23.3	-22.3	-0.7	-14.7
HX_full_light_blocked_B1	23.6	26.7	26.8	-24.1	-19.1	-23.8	-25.2	-24.3	-2.7	-16.6
HX_full_severe_blocked_B1	22.2	25.2	25.2	-26.6	-20.6	-26.6	-27.9	-27.2	-5.2	-19.1
HX_xHz_clean_B1	22.0	24.9	25.1	-22.1	-18.5	-22.5	-23.8	-22.8	-1.9	-14.3
HX_xHz_clean_retest_B1	22.2	25.1	25.2	-21.8	-18.1	-22.2	-23.5	-22.5	-1.7	-14.0

Table A 11: Baseline 1 data, part 3

	T_cir1_out [C]	T_cir2_out [C]	T_cir3_out [C]	T_cir4_out [C]	T_cir5_out [C]	T_cir6_out [C]	T_cir7_out [C]	T_cir8_out [C]	T_cir9_out [C]	T_cir10_out [C]
H1_low_clean_B1	3.8	4.8	4.4	5.8	3.2	2.8	3.3	2.4	2.8	3.7
H1_low_light_blocked_B1	5.1	6.3	4.8	6.4	3.6	3.6	4.7	0.1	-0.2	-2.8
H1_low_severe_blocked_B1	4.8	6.2	4.1	6.1	3.4	-2.3	-2.4	-4.6	-4.0	-4.2
H2_mid_clean_B1	-3.8	-3.1	-3.9	-3.0	-4.8	-4.0	-3.3	-4.5	-4.1	-8.8
H2_mid_light_blocked_B1	-5.5	-4.0	-5.1	-3.0	-9.2	-6.3	-4.8	-8.9	-8.8	-14.3
H2_mid_severe_blocked_B1	-3.8	-2.5	-3.2	-1.9	-15.3	-12.8	-10.0	-21.1	-23.4	-28.6
H2_xHz_clean_B1	-2.5	-1.7	-2.4	-1.2	-2.9	-3.4	-2.9	-3.9	-3.4	-5.1
H2_yHz_clean_B1	-3.0	-2.7	-3.2	-2.6	-3.3	-3.5	-3.1	-3.9	-3.5	-5.6
H3_full_clean_B1	-13.0	-12.4	-13.0	-12.2	-14.1	-13.5	-12.8	-13.3	-13.2	-16.0
H3_full_light_blocked_B1	-15.1	-14.4	-14.5	-12.7	-19.5	-21.2	-18.5	-21.1	-21.4	-27.0
H3_full_severe_blocked_B1	-16.8	-16.3	-15.0	-13.4	-23.0	-26.7	-26.5	-31.7	-29.8	-33.4
H3_full_severe_blocked_B1	-16.7	-16.3	-15.5	-13.7	-22.3	-26.6	-25.9	-30.3	-28.6	-32.5
H3_xHz_clean_B1	-13.3	-12.4	-13.3	-12.0	-14.8	-14.4	-12.7	-13.5	-12.9	-13.2
HX_full_clean_B1	-22.0	-21.4	-22.2	-21.5	-22.1	-22.5	-22.1	-22.8	-22.4	-21.4
HX_full_light_blocked_B1	-23.1	-22.0	-23.2	-21.7	-23.2	-23.7	-22.9	-25.1	-25.3	-25.6
HX_full_severe_blocked_B1	-23.1	-21.8	-23.1	-21.4	-26.5	-27.3	-26.7	-28.1	-28.2	-30.1
HX_xHz_clean_B1	-21.1	-20.3	-21.3	-20.3	-22.0	-22.9	-22.3	-23.1	-22.6	-21.5
HX_xHz_clean_retest_B1	-20.9	-20.2	-21.3	-20.3	-21.8	-22.5	-21.9	-22.7	-22.3	-21.2

	T_cond_out3 [C]	T_OU_out [C]	T_OU_in [C]	T_IU_out [C]	T_IU_in [C]	m_dot_r [g/s]	level_S1 [%]	level_S2 [%]	W_dot_OU [kW]	W_dot_IU [kW]
H1_low_clean_B1	34.6	5.3	8.2	39.7	21.0	69.4	57.1	57.1	0.4	0.4
H1_low_light_blocked_B1	34.1	5.5	8.2	39.2	21.0	66.8	57.5	57.5	0.4	0.4
H1_low_severe_blocked_B1	33.9	6.3	8.5	37.6	21.0	60.3	58.8	60.6	0.4	0.4
H2_mid_clean_B1	37.6	-1.8	1.6	42.9	21.1	81.1	55.5	56.7	0.4	0.4
H2_mid_light_blocked_B1	34.2	-1.2	1.8	39.8	21.1	66.2	59.5	60.0	0.3	0.4
H2_mid_severe_blocked_B1	28.6	-0.2	1.9	34.1	21.1	42.4	65.0	65.1	0.3	0.4
H2_xHz_clean_B1	33.5	-1.0	1.7	38.4	21.1	63.1	53.4	53.5	0.4	0.4
H2_yHz_clean_B1	36.0	-1.4	1.6	41.3	21.1	74.9	50.3	50.5	0.4	0.4
H3_full_clean_B1	36.3	-11.3	-8.3	42.3	21.1	75.3	60.0	59.9	0.4	0.4
H3_full_light_blocked_B1	33.1	-10.5	-8.0	38.3	21.0	57.7	60.6	61.0	0.3	0.4
H3_full_severe_blocked_B1	29.8	-10.6	-8.4	34.7	20.9	43.7	67.0	67.2	0.3	0.4
H3_full_severe_blocked_B1	30.3	-10.7	-8.4	35.2	20.9	45.6	66.3	66.6	0.3	0.4
H3_xHz_clean_B1	33.0	-10.7	-8.3	38.0	20.9	60.6	51.2	51.7	0.3	0.4
HX_full_clean_B1	31.3	-19.8	-17.8	36.5	20.9	52.4	69.8	69.7	0.4	0.4
HX_full_light_blocked_B1	30.5	-19.6	-17.7	35.7	20.8	48.4	69.8	69.7	0.3	0.4
HX_full_severe_blocked_B1	29.2	-19.6	-17.5	34.4	20.8	43.4	68.9	69.1	0.3	0.4
HX_xHz_clean_B1	28.9	-19.4	-17.7	33.6	20.9	43.3	50.4	50.4	0.4	0.4
HX_xHz_clean_retest_B1	28.9	-19.3	-17.7	33.7	20.8	43.5	31.3	31.2	0.4	0.4

Table A 12: Baseline 1 data, part 4

	W_dot_comp_vsd [kW]	W_dot_comp [kW]	DP_OU_in [C]	DP_IU_in [C]	DP_OU_out [C]	RH_OU_in [%]	RH_IU_in [%]	T_c_1 [C]	T_e_1 [C]	T_c_0 [C]
H1_low_clean_B1	4.5	4.4	3.7	9.1	3.2	66.6	43.3	40.9	-1.7	39.7
H1_low_light_blocked_B1	4.4	4.3	3.7	9.1	2.9	66.5	43.2	40.3	-2.9	39.1
H1_low_severe_blocked_B1	4.2	4.1	3.6	9.0	2.7	65.7	43.2	38.4	-6.8	37.3
H2_mid_clean_B1	5.9	5.8	-1.9	8.3	-3.4	65.2	41.1	43.9	-9.9	42.4
H2_mid_light_blocked_B1	5.3	5.2	-2.2	8.3	-4.1	62.6	41.2	40.7	-15.6	39.5
H2_mid_severe_blocked_B1	4.3	4.2	-1.9	8.3	-3.7	66.4	41.3	35.1	-27.2	34.3
H2_xHz_clean_B1	4.5	4.4	-2.4	8.2	-3.4	65.3	41.1	39.4	-8.3	38.3
H2_yHz_clean_B1	5.4	5.2	-2.5	8.3	-3.5	65.2	41.0	42.4	-8.7	41.0
H3_full_clean_B1	6.6	6.5	-8.4	5.1	-11.9	75.0	32.7	43.0	-19.2	41.6
H3_full_light_blocked_B1	5.7	5.6	-8.4	4.9	-12.1	77.7	32.7	38.7	-26.0	37.7
H3_full_severe_blocked_B1	5.0	4.9	-9.1	5.1	-12.5	76.2	33.2	35.2	-32.2	34.4
H3_full_severe_blocked_B1	5.1	5.0	-8.8	5.0	-12.4	76.2	33.1	35.6	-31.4	34.8
H3_xHz_clean_B1	5.0	4.9	-8.2	5.1	-11.4	77.7	33.3	38.8	-18.1	37.8
HX_full_clean_B1	5.4	5.3	-14.8	6.0	-20.1	71.4	35.7	37.1	-27.8	36.2
HX_full_light_blocked_B1	5.2	5.1	-15.7	6.3	-20.6	70.8	36.6	36.2	-29.4	35.4
HX_full_severe_blocked_B1	4.9	4.8	-15.8	6.2	-21.3	70.8	36.3	35.0	-31.7	34.2
HX_xHz_clean_B1	4.3	4.2	-15.1	6.0	-20.0	68.0	35.6	34.6	-27.0	33.8
HX_xHz_clean_retest_B1	4.3	4.2	-16.1	6.1	-20.1	70.5	36.1	34.6	-26.7	33.9

	Q_dot_cond_1_3 [kW]	Q_dot_cond_2_3 [kW]	Q_dot_cond_2_9 [kW]	T_sc_3 [K]	T_sc_XV [K]	T_sh_comp [K]	T_sh [K]	T_nozzle [C]	V_dot_IU [m3/s]	rho_a_nozzle [kg/m3]
H1_low_clean_B1	16.0	15.7	15.8	5.0	6.7	7.8	5.0	39.0	0.8	1.1
H1_low_light_blocked_B1	15.6	15.2	15.3	5.0	6.8	8.2	5.0	38.6	0.8	1.1
H1_low_severe_blocked_B1	14.2	13.8	13.9	3.5	5.2	7.5	4.8	37.3	0.8	1.1
H2_mid_clean_B1	18.7	18.3	18.4	4.8	6.6	8.7	4.6	41.7	0.8	1.1
H2_mid_light_blocked_B1	16.2	15.7	15.8	5.2	7.6	12.3	6.7	39.3	0.8	1.1
H2_mid_severe_blocked_B1	11.4	10.9	11.0	5.7	8.7	15.1	5.1	34.1	0.8	1.1
H2_xHz_clean_B1	14.9	14.5	14.6	4.9	7.0	8.4	4.9	37.8	0.8	1.1
H2_yHz_clean_B1	17.4	17.0	17.1	5.0	6.9	8.3	4.8	40.3	0.8	1.1
H3_full_clean_B1	18.4	17.9	18.0	5.3	7.9	10.9	5.1	41.0	0.8	1.1
H3_full_light_blocked_B1	14.9	14.3	14.4	4.6	7.9	10.7	0.0	37.6	0.8	1.1
H3_full_severe_blocked_B1	12.0	11.5	11.5	4.6	8.5	15.6	3.6	34.7	0.8	1.1
H3_full_severe_blocked_B1	12.4	11.9	11.9	4.4	8.2	14.7	2.5	35.1	0.8	1.1
H3_xHz_clean_B1	14.8	14.3	14.4	4.7	7.8	9.6	4.5	37.4	0.8	1.1
HX_full_clean_B1	13.7	13.2	13.3	4.9	8.9	12.6	5.4	35.9	0.8	1.1
HX_full_light_blocked_B1	13.0	12.5	12.6	4.9	9.2	13.7	5.4	35.4	0.8	1.1
HX_full_severe_blocked_B1	12.0	11.5	11.5	5.0	9.7	14.7	5.1	34.2	0.8	1.1
HX_xHz_clean_B1	11.2	10.8	10.8	4.9	9.4	11.4	4.9	33.5	0.8	1.1
HX_xHz_clean_retest_B1	11.3	10.8	10.9	5.0	9.3	11.6	4.9	33.5	0.8	1.1

Table A 13: Baseline 1 data, part 5

	V_dot_IU_standardair [kg/m3]	Q_dot_heat_airside [kW]	Q_dot_cond_airside [kW]	Q_dot_useful_airside [kW]	Q_dot_useful_refside [kW]	COP_h_airside [-]	COP_h_refside [-]	DT_air_on_eva7 [K]	T_dew_suc [C]	T_dew_dis [C]
H1_low_clean_B1	0.7	16.5	16.2	16.6	16.1	3.2	3.1	9.9	-2.3	41.0
H1_low_light_blocked_B1	0.7	16.1	15.8	16.1	15.7	3.1	3.0	11.2	-3.5	40.4
H1_low_severe_blocked_B1	0.7	14.7	14.4	14.8	14.2	3.0	2.9	15.3	-7.5	38.6
H2_mid_clean_B1	0.7	19.2	18.9	19.2	18.8	2.9	2.8	11.5	-11.2	43.6
H2_mid_light_blocked_B1	0.7	16.5	16.2	16.6	16.2	2.8	2.7	17.4	-16.9	40.3
H2_mid_severe_blocked_B1	0.7	11.6	11.3	11.6	11.3	2.3	2.3	29.1	-28.8	34.7
H2_xHz_clean_B1	0.7	15.3	15.0	15.4	15.0	2.9	2.9	10.0	-9.2	39.0
H2_yHz_clean_B1	0.7	17.9	17.5	17.9	17.5	2.9	2.9	10.3	-9.7	41.9
H3_full_clean_B1	0.7	18.7	18.4	18.8	18.4	2.6	2.5	10.9	-21.6	42.8
H3_full_light_blocked_B1	0.7	15.2	14.8	15.2	14.8	2.4	2.3	18.0	-28.5	38.5
H3_full_severe_blocked_B1	0.7	12.2	11.9	12.3	11.9	2.2	2.1	23.8	-35.2	35.0
H3_full_severe_blocked_B1	0.7	12.7	12.3	12.7	12.3	2.2	2.1	22.9	-34.2	35.4
H3_xHz_clean_B1	0.7	15.1	14.7	15.1	14.8	2.7	2.6	9.8	-19.9	38.7
HX_full_clean_B1	0.7	13.9	13.6	14.0	13.6	2.3	2.2	10.0	-31.1	37.0
HX_full_light_blocked_B1	0.7	13.2	12.8	13.2	12.9	2.2	2.2	11.8	-32.8	36.1
HX_full_severe_blocked_B1	0.7	12.1	11.8	12.2	11.9	2.2	2.1	14.2	-35.3	35.0
HX_xHz_clean_B1	0.7	11.4	11.0	11.4	11.2	2.3	2.2	9.3	-30.0	34.4
HX_xHz_clean_retest_B1	0.7	11.5	11.1	11.5	11.3	2.3	2.2	9.0	-29.7	34.1

	T_bub_cond [C]	T_dew_evap [C]	DT_air_on_cond3 [K]	T_sh_vi_hp [K]	T_sh_vi_lp [K]	m_dot_vi_hp_mb [g/s]	m_dot_vi_lp_mb [g/s]	Q_dot_evap [kW]	m_dot_OU_air [kg/s]	m_dot_VI_H_YP [g/s]
H1_low_clean_B1	39.8	-1.7	18.7	-1.1	0.2	4.1	4.9	12.2	3.6	12.6
H1_low_light_blocked_B1	39.2	-2.9	18.2	-1.1	0.3	4.2	4.7	11.8	3.3	12.2
H1_low_severe_blocked_B1	37.5	-6.8	16.5	-1.0	0.7	5.0	4.5	10.6	3.6	11.8
H2_mid_clean_B1	42.5	-9.9	21.4	-1.0	-0.6	9.8	6.0	13.8	3.0	17.6
H2_mid_light_blocked_B1	39.6	-15.6	18.5	-0.7	-0.4	8.9	4.8	11.6	2.6	14.4
H2_mid_severe_blocked_B1	34.4	-27.2	13.4	0.1	1.9	7.2	2.8	7.6	2.2	9.5
H2_xHz_clean_B1	38.5	-8.3	17.4	-0.4	0.0	5.9	4.3	11.2	3.2	11.8
H2_yHz_clean_B1	41.2	-8.7	20.1	-0.7	-0.5	8.0	5.4	12.9	3.3	15.3
H3_full_clean_B1	41.8	-19.2	20.7	-0.9	-1.3	11.7	6.1	12.9	3.0	18.9
H3_full_light_blocked_B1	37.8	-26.0	16.8	-0.7	-0.5	9.9	4.6	10.4	2.7	15.1
H3_full_severe_blocked_B1	34.5	-32.2	13.6	-0.2	0.9	8.2	3.4	7.7	2.3	11.6
H3_full_severe_blocked_B1	34.9	-31.4	14.0	-0.3	0.6	8.5	3.5	8.0	2.3	12.1
H3_xHz_clean_B1	37.9	-18.1	17.0	-1.1	-0.9	8.3	4.4	10.7	3.0	13.4
HX_full_clean_B1	36.3	-27.8	15.5	-1.1	-1.2	9.0	4.0	9.3	3.1	13.7
HX_full_light_blocked_B1	35.5	-29.4	14.7	-1.3	-1.1	8.4	3.7	8.7	3.1	12.7
HX_full_severe_blocked_B1	34.3	-31.7	13.5	-1.2	-0.7	7.8	3.3	7.8	2.5	11.5
HX_xHz_clean_B1	33.9	-27.0	13.1	-1.1	-0.9	7.0	3.0	7.9	3.1	9.9
HX_xHz_clean_retest_B1	34.0	-26.7	13.2	-0.5	-0.7	7.4	2.7	7.9	3.4	9.6

Table A 14: Baseline 1 data, part 6

	m_dot_VI_L_YP [g/s]	T_sh_cir1 [K]	T_sh_cir2 [K]	T_sh_cir3 [K]	T_sh_cir4 [K]	T_sh_cir5 [K]	T_sh_cir6 [K]	T_sh_cir7 [K]	T_sh_cir8 [K]	T_sh_cir9 [K]
H1_low_clean_B1	-1.6	5.4	6.4	6.0	7.4	4.9	4.5	5.0	4.1	4.5
H1_low_light_blocked_B1	-1.5	8.0	9.2	7.7	9.3	6.5	6.5	7.6	3.1	2.7
H1_low_severe_blocked_B1	-1.2	11.6	13.0	10.9	12.9	10.3	4.6	4.4	2.3	2.8
H2_mid_clean_B1	-0.8	6.2	6.9	6.0	6.9	5.1	5.9	6.6	5.4	5.8
H2_mid_light_blocked_B1	-1.1	10.1	11.6	10.5	12.6	6.4	9.3	10.8	6.7	6.8
H2_mid_severe_blocked_B1	-1.0	23.4	24.7	24.0	25.3	11.9	14.4	17.2	6.2	3.8
H2_xHz_clean_B1	-1.3	5.8	6.6	5.9	7.1	5.4	4.9	5.3	4.4	4.8
H2_yHz_clean_B1	-1.0	5.7	6.0	5.5	6.1	5.4	5.2	5.6	4.8	5.1
H3_full_clean_B1	0.0	6.3	6.9	6.2	7.1	5.1	5.7	6.4	5.9	6.0
H3_full_light_blocked_B1	-0.4	10.9	11.6	11.5	13.3	6.5	4.8	7.5	4.9	4.6
H3_full_severe_blocked_B1	-0.6	15.4	15.9	17.2	18.9	9.2	5.5	5.7	0.6	2.5
H3_full_severe_blocked_B1	-0.6	14.7	15.1	15.9	17.6	9.0	4.8	5.5	1.1	2.8
H3_xHz_clean_B1	-0.8	4.8	5.6	4.8	6.0	3.2	3.7	5.4	4.6	5.2
HX_full_clean_B1	-0.6	5.8	6.4	5.6	6.3	5.8	5.3	5.7	5.0	5.4
HX_full_light_blocked_B1	-0.6	6.3	7.4	6.2	7.8	6.3	5.7	6.5	4.3	4.2
HX_full_severe_blocked_B1	-0.7	8.6	9.9	8.6	10.3	5.2	4.4	5.0	3.6	3.5
HX_xHz_clean_B1	-0.9	5.9	6.8	5.7	6.7	5.0	4.2	4.8	3.9	4.4
HX_xHz_clean_retest_B1	-1.0	5.8	6.6	5.4	6.4	4.9	4.2	4.8	4.0	4.4

	T_sh_cir10 [K]
H1_low_clean_B1	5.3
H1_low_light_blocked_B1	0.1
H1_low_severe_blocked_B1	2.7
H2_mid_clean_B1	1.1
H2_mid_light_blocked_B1	1.3
H2_mid_severe_blocked_B1	-1.4
H2_xHz_clean_B1	3.2
H2_yHz_clean_B1	3.1
H3_full_clean_B1	3.2
H3_full_light_blocked_B1	-1.0
H3_full_severe_blocked_B1	-1.2
H3_full_severe_blocked_B1	-1.1
H3_xHz_clean_B1	4.9
HX_full_clean_B1	6.4
HX_full_light_blocked_B1	3.9
HX_full_severe_blocked_B1	1.6
HX_xHz_clean_B1	5.5

Table A 15: Baseline 1H data, part 1

	Date [MM/DD/YYYY]	Time [HH:MM:SS]	Test_duration [SS]	T_ambient [F]	DP [F]	T_return_air [F]	Speed [Hz]	Ref.charge [lb]	p_atm [kPa]	p_dis [kPa]
H1_low_clean_1000ms_B1H	10/29/2013	12:21:05 PM	1273.0	47.0	43.0	70.0	40.0	14.0	100.4	2495.2
H1_low_clean_2000ms_B1H	10/29/2013	12:49:59 PM	1461.0	47.0	43.0	70.0	40.0	14.0	100.4	2493.3
H1_low_clean_4000ms_B1H	10/29/2013	1:25:42 PM	950.0	47.0	43.0	70.0	40.0	14.0	100.4	2494.3
H1_low_clean_8000ms_B1H	10/29/2013	1:52:58 PM	1086.0	47.0	43.0	70.0	40.0	14.0	100.4	2498.6
H1_low_clean_B1H	11/14/2013	10:11:49 AM	1930.0	47.0	43.0	70.0	40.0	14.9	100.1	2564.1
H1_low_clean_REP_B1H	11/19/2013	2:37:21 PM	1301.0	47.0	43.0	70.0	40.0	14.9	100.7	2451.9
H1_low_light_blocked_B1H	11/19/2013	3:55:24 PM	971.0	47.0	43.0	70.0	40.0	14.9	100.7	2461.4
H1_low_severe_blocked_B1H	11/19/2013	4:31:16 PM	971.0	47.0	43.0	70.0	40.0	14.9	100.7	2453.9
H2_mid_clean_B1H	11/15/2013	10:15:11 AM	646.0	35.0		70.0	55.0	14.9	99.8	2689.5
H2_mid_light_blocked_B1H	11/15/2013	10:43:32 AM	971.0	35.0		70.0	55.0	14.9	99.8	2609.4
H2_mid_severe_blocked_B1H	11/15/2013	11:33:44 AM	971.0	35.0		70.0	55.0	14.9	99.8	2443.7
H3_full_clean_unstable_B1H	11/6/2013	10:22:04 AM	496.0	17.0		70.0	70.0	14.0	99.2	2537.6
H3_light_blocked_B1H	11/18/2013	2:10:19 PM	642.0	17.0		70.0	70.0	14.9	99.2	2437.3
H3_severe_blocked_B1H	11/18/2013	2:34:44 PM	641.0	17.0		70.0	70.0	14.9	99.2	2253.5
HX_full_clean_B1H	11/19/2013	9:55:52 AM	1302.0	17.0		70.0	70.0	14.9	101.2	2290.6
HX_full_light_blocked_B1H	11/19/2013	10:31:03 AM	647.0	17.0		70.0	70.0	14.9	101.2	2268.6
HX_full_severe_blocked_B1H	11/19/2013	10:53:31 AM	644.0	17.0		70.0	70.0	14.9	101.2	2206.3

	p_sep1 [kPa]	p_vi_hp [kPa]	p_cond_in [kPa]	p_cond_out [kPa]	p_cond_out2 [kPa]	p_sep2 [kPa]	p_cond_out3 [kPa]	p_evap_out [kPa]	p_suc [kPa]	p_evap_in [kPa]
H1_low_clean_1000ms_B1H	1628.9	1621.3	2473.3	2431.3	2398.5	1254.1	2406.9	763.9	745.3	1210.9
H1_low_clean_2000ms_B1H	1629.0	1615.4	2472.2	2429.9	2397.2	1253.5	2405.8	763.8	745.0	1205.3
H1_low_clean_4000ms_B1H	1630.9	1626.2	2472.4	2430.1	2397.0	1257.7	2405.8	765.4	745.9	1202.6
H1_low_clean_8000ms_B1H	1636.7	1630.5	2476.7	2433.6	2400.8	1263.7	2409.5	766.9	748.2	1196.2
H1_low_clean_B1H	1730.2	1724.9	2549.5	2503.2	2454.8	1349.3	2473.2	818.0	796.4	1290.4
H1_low_clean_REP_B1H	1594.1	1588.7	2463.0	2419.8	2380.0	1234.3	2397.2	747.7	727.6	1191.7
H1_low_light_blocked_B1H	1606.9	1596.5	2471.9	2427.5	2388.0	1250.7	2405.9	753.2	733.2	1210.4
H1_low_severe_blocked_B1H	1598.8	1590.2	2463.5	2419.5	2380.7	1236.4	2398.0	743.2	724.6	1199.3
H2_mid_clean_B1H	1428.8	1413.9	2681.6	2626.3	2571.7	1015.7	2593.4	583.0	553.3	954.5
H2_mid_light_blocked_B1H	1354.4	1340.0	2600.2	2549.2	2503.2	953.3	2520.0	548.3	519.7	903.4
H2_mid_severe_blocked_B1H	1180.9	1166.3	2435.3	2393.1	2364.6	801.4	2373.2	463.7	436.2	772.1
H3_full_clean_unstable_B1H	1092.2	1085.2	2584.0	2532.8	2495.3	713.3	2504.5	403.8	366.7	677.8
H3_light_blocked_B1H	1001.3	990.9	2470.0	2424.5	2402.1	631.6	2404.7	361.6	326.0	609.5
H3_severe_blocked_B1H	830.2	824.2	2286.6	2248.0	2241.3	501.6	2236.4	294.2	261.1	492.2
HX_full_clean_B1H	857.7	843.9	2293.6	2256.2	2259.1	514.5	2244.0	308.2	268.3	501.5
HX_full_light_blocked_B1H	832.4	818.0	2266.0	2229.5	2232.6	493.0	2218.4	300.6	258.7	479.5
HX_full_severe_blocked_B1H	776.5	764.4	2201.5	2167.1	2174.7	452.6	2158.0	276.4	236.3	433.2

Table A 16: Baseline 1H data, part 2

	p_cir1_in [kPa]	p_cir10_in [kPa]	p_vi_lp [kPa]	dp_IU [Pa]	dp_OU [Pa]	dp_nozzle [Pa]	dp_nozzle2 [Pa]	T_dis [C]	T_cond_in [C]	T_cond_out [C]
H1_low_clean_1000ms_B1H	810.8	959.7	1248.4	51.0	29.5	193.1	193.1	87.7	83.4	35.4
H1_low_clean_2000ms_B1H	810.1	958.3	1248.2	51.0	29.8	193.1	193.1	87.7	83.4	35.4
H1_low_clean_4000ms_B1H	811.9	958.2	1255.0	51.0	30.0	193.2	193.2	87.5	83.2	35.4
H1_low_clean_8000ms_B1H	814.7	954.7	1260.9	51.0	30.0	193.2	193.2	87.4	83.1	35.4
H1_low_clean_B1H	846.1	969.7	1340.9	51.0	27.3	193.6	193.6	85.5	81.5	36.7
H1_low_clean_REP_B1H	819.8	871.0	1232.1	50.9	26.1	195.7	195.7	87.0	82.7	35.3
H1_low_light_blocked_B1H	755.4	964.7	1249.2	51.0	31.6	194.4	194.4	88.4	84.1	35.4
H1_low_severe_blocked_B1H	737.4	971.4	1239.5	51.0	42.2	194.3	194.3	89.1	84.6	35.3
H2_mid_clean_B1H	669.0	789.6	1013.3	50.9	36.2	196.1	196.1	93.8	89.4	38.6
H2_mid_light_blocked_B1H	588.4	714.8	948.6	50.9	49.2	193.3	193.3	95.4	90.6	37.4
H2_mid_severe_blocked_B1H	487.4	600.1	797.5	51.0	62.0	193.6	193.6	98.0	92.2	35.0
H3_full_clean_unstable_B1H	474.1	587.5	718.8	50.8	41.5	196.8	196.8	101.6	96.0	37.5
H3_light_blocked_B1H	387.1	517.3	637.6	50.7	62.3	194.6	194.6	106.3	99.6	35.6
H3_severe_blocked_B1H	352.1	423.9	505.4	51.4	70.3	194.1	194.1	111.3	102.8	32.4
HX_full_clean_B1H	301.6	460.1	524.6	50.9	29.9	195.1	195.1	107.2	99.3	32.6
HX_full_light_blocked_B1H	289.7	436.9	499.2	51.2	39.8	193.8	193.8	110.4	102.0	32.0
HX_full_severe_blocked_B1H	263.1	432.5	457.9	51.2	52.0	193.8	193.8	114.5	105.1	30.9

	T_cond_out2 [C]	T_SXV_in [C]	T_EXV_in [C]	T_evap_out [C]	T_suc [C]	T_evap_distr_in [C]	T_cir1_in [C]	T_cir10_in [C]	T_vi_hp [C]	T_vi_lp [C]
H1_low_clean_1000ms_B1H	30.7	32.8	32.9	3.6	5.7	13.1	4.6	1.3	22.8	15.5
H1_low_clean_2000ms_B1H	30.7	32.8	32.9	3.6	5.7	12.8	4.3	1.1	22.6	15.4
H1_low_clean_4000ms_B1H	30.8	32.8	32.9	3.7	5.8	12.6	4.3	1.1	22.6	15.2
H1_low_clean_8000ms_B1H	30.8	32.9	33.0	3.7	5.8	12.4	4.2	1.2	22.8	15.3
H1_low_clean_B1H	32.0	34.2	34.3	5.5	5.4	15.4	5.5	3.1	25.2	17.7
H1_low_clean_REP_B1H	30.6	32.7	32.8	2.9	4.7	12.2	1.5	1.6	22.8	15.0
H1_low_light_blocked_B1H	30.7	32.9	32.9	3.1	5.2	12.9	4.7	-1.0	23.0	15.6
H1_low_severe_blocked_B1H	30.5	32.8	32.9	3.0	5.3	12.8	4.9	-1.8	23.0	15.3
H2_mid_clean_B1H	32.8	35.9	35.9	-4.1	-1.9	5.4	-1.7	-4.4	17.7	7.0
H2_mid_light_blocked_B1H	31.5	34.6	34.6	-5.8	-3.1	3.7	-4.6	-8.0	15.9	5.1
H2_mid_severe_blocked_B1H	29.3	32.0	32.1	-9.3	-5.4	-0.9	-9.9	-13.0	11.1	-0.2
H3_full_clean_unstable_B1H	30.4	34.3	34.4	-14.5	-11.4	-4.5	-10.6	-13.6	9.3	-4.2
H3_light_blocked_B1H	28.6	32.3	32.3	-17.2	-13.0	-7.6	-14.3	-18.8	6.1	-7.2
H3_severe_blocked_B1H	25.5	28.6	28.7	-23.5	-17.5	-13.5	-19.6	-21.2	0.2	-13.4
HX_full_clean_B1H	24.5	28.4	28.6	-21.1	-18.1	-13.8	-18.5	-26.2	0.2	-13.5
HX_full_light_blocked_B1H	23.7	27.7	27.8	-21.8	-18.0	-14.5	-19.3	-26.5	-0.8	-14.6
HX_full_severe_blocked_B1H	22.4	26.4	26.6	-23.0	-18.6	-17.1	-19.8	-28.8	-3.0	-16.9

Table A 17: Baseline 1H data, part 3

	T_cir1_out [C]	T_cir2_out [C]	T_cir3_out [C]	T_cir4_out [C]	T_cir5_out [C]	T_cir6_out [C]	T_cir7_out [C]	T_cir8_out [C]	T_cir9_out [C]	T_cir10_out [C]
H1_low_clean_1000ms_B1H	4.2	4.7	4.0	4.9	4.7	4.2	5.3	3.6	4.4	4.5
H1_low_clean_2000ms_B1H	4.2	4.7	4.0	4.9	4.7	4.2	5.3	3.6	4.4	4.5
H1_low_clean_4000ms_B1H	4.2	4.8	4.1	4.9	4.7	4.3	5.4	3.6	4.4	4.6
H1_low_clean_8000ms_B1H	4.2	4.8	4.2	4.8	4.7	4.3	5.3	3.7	4.4	4.7
H1_low_clean_B1H	6.1	6.7	6.1	6.3	6.3	6.1	6.5	5.9	5.9	6.3
H1_low_clean_REP_B1H	3.9	4.3	3.7	4.2	4.6	3.8	4.8	3.5	3.3	4.0
H1_low_light_blocked_B1H	4.0	4.8	3.9	4.6	4.6	4.3	5.3	3.5	3.9	4.0
H1_low_severe_blocked_B1H	3.6	4.9	4.0	4.3	5.2	3.3	4.1	3.8	3.5	3.7
H2_mid_clean_B1H	-3.5	-1.6	-3.0	-2.1	-2.5	-2.7	-2.1	-2.8	-2.5	-2.4
H2_mid_light_blocked_B1H	-5.3	-3.4	-4.5	-3.8	-4.2	-4.7	-4.2	-4.8	-4.2	-3.8
H2_mid_severe_blocked_B1H	-9.5	-6.2	-7.8	-7.4	-6.7	-9.3	-8.0	-7.9	-7.6	-7.0
H3_full_clean_unstable_B1H	-13.7	-11.6	-13.3	-12.3	-12.6	-13.5	-12.6	-13.6	-12.9	-13.3
H3_light_blocked_B1H	-15.5	-14.6	-14.4	-16.4	-16.2	-15.7	-15.5	-16.0	-14.0	-12.9
H3_severe_blocked_B1H	-20.6	-20.5	-22.2	-22.2	-21.2	-21.2	-21.3	-20.1	-19.6	-18.3
HX_full_clean_B1H	-20.1	-19.2	-20.1	-19.7	-20.0	-19.7	-19.7	-19.6	-19.2	-19.6
HX_full_light_blocked_B1H	-19.4	-19.0	-19.5	-19.6	-20.0	-20.3	-19.7	-20.3	-20.0	-19.9
HX_full_severe_blocked_B1H	-19.8	-19.5	-20.1	-20.3	-20.9	-24.0	-22.9	-21.7	-21.4	-21.4

	T_cond_out3 [C]	T_OU_out [C]	T_OU_in [C]	T_IU_out [C]	T_IU_in [C]	m_dot_r [g/s]	level_S1 [%]	level_S2 [%]	W_dot_OU [kW]	W_dot_IU [kW]
H1_low_clean_1000ms_B1H	34.7	5.6	8.2	39.6	21.1	69.4	42.2	42.3	0.4	0.4
H1_low_clean_2000ms_B1H	34.6	5.7	8.2	39.6	21.1	69.4	41.7	41.8	0.4	0.4
H1_low_clean_4000ms_B1H	34.6	5.7	8.2	39.6	21.1	69.5	41.3	41.3	0.4	0.4
H1_low_clean_8000ms_B1H	34.6	5.7	8.3	39.7	21.1	69.8	41.1	41.0	0.4	0.4
H1_low_clean_B1H	35.8	5.4	8.3	40.6	21.1	74.9	37.4	37.4	0.4	0.4
H1_low_clean_REP_B1H	34.5	5.3	8.3	39.3	21.0	68.9	54.0	54.0	0.4	0.4
H1_low_light_blocked_B1H	34.7	5.3	8.3	39.5	21.1	68.9	46.7	46.7	0.4	0.4
H1_low_severe_blocked_B1H	34.6	4.7	8.4	39.4	21.1	68.1	39.3	39.2	0.4	0.4
H2_mid_clean_B1H	37.8	-1.6	1.6	42.9	21.2	82.0	47.7	47.9	0.4	0.4
H2_mid_light_blocked_B1H	36.6	-1.7	1.8	41.9	21.0	76.6	45.0	45.0	0.4	0.4
H2_mid_severe_blocked_B1H	34.2	-1.2	1.8	39.2	21.0	64.7	48.2	48.2	0.3	0.4
H3_full_clean_unstable_B1H	36.8	-10.9	-8.3	41.9	21.2	75.2	44.5	44.6	0.4	0.4
H3_light_blocked_B1H	34.8	-11.0	-8.3	40.2	21.1	65.7	56.1	56.2	0.3	0.4
H3_severe_blocked_B1H	31.6	-11.6	-8.3	36.9	20.9	52.9	59.6	59.6	0.3	0.4
HX_full_clean_B1H	31.8	-19.8	-17.7	36.9	21.0	54.1	64.9	64.9	0.4	0.4
HX_full_light_blocked_B1H	31.2	-19.7	-17.6	36.5	20.9	51.9	64.2	64.4	0.4	0.4
HX_full_severe_blocked_B1H	30.2	-19.7	-17.6	35.4	20.8	47.4	65.7	65.7	0.3	0.4

Table A 18: Baseline 1H data, part 4

	W_dot_comp_vsd [kW]	W_dot_comp [kW]	DP_OU_in [C]	DP_IU_in [C]	DP_OU_out [C]	RH_OU_in [%]	RH_IU_in [%]	T_c_1 [C]	T_e_1 [C]	T_c_0 [C]
H1_low_clean_1000ms_B1H	4.5	4.4	3.7	9.1	8.9	66.7	43.2	40.9	-1.4	39.7
H1_low_clean_2000ms_B1H	4.5	4.3	3.6	9.1	8.2	66.9	43.2	40.9	-1.4	39.7
H1_low_clean_4000ms_B1H	4.5	4.3	3.7	9.1	6.4	66.8	43.2	40.9	-1.3	39.7
H1_low_clean_8000ms_B1H	4.5	4.4	3.8	9.0	5.0	66.8	43.3	41.0	-1.2	39.7
H1_low_clean_B1H	4.7	4.5	3.8	9.1	4.1	71.9	43.4	42.2	0.8	40.8
H1_low_clean_REP_B1H	4.5	4.3	3.8	9.2	2.8	63.1	43.9	40.8	-2.0	39.5
H1_low_light_blocked_B1H	4.5	4.4	3.8	9.3	3.3	62.6	43.9	40.9	-1.8	39.7
H1_low_severe_blocked_B1H	4.5	4.3	3.7	9.3	3.3	62.1	43.9	40.8	-2.2	39.5
H2_mid_clean_B1H	5.9	5.8	-2.0	8.3	-3.0	64.5	40.7	44.3	-9.5	42.8
H2_mid_light_blocked_B1H	5.7	5.6	-2.1	8.0	-3.5	62.6	40.7	43.0	-11.2	41.6
H2_mid_severe_blocked_B1H	5.2	5.1	-2.1	8.1	-4.1	63.6	40.9	40.3	-16.0	39.1
H3_full_clean_unstable_B1H	6.6	6.4	-8.7	5.0	-11.9	70.7	32.2	42.7	-19.7	41.3
H3_light_blocked_B1H	6.1	6.0	-8.6	4.9	-12.6	76.4	32.6	40.9	-22.6	39.6
H3_severe_blocked_B1H	5.5	5.3	-8.6	4.7	-13.4	78.8	32.2	37.7	-27.8	36.7
HX_full_clean_B1H	5.5	0.0	-17.6	5.9	-20.5	66.4	35.1	37.8	-26.7	36.8
HX_full_light_blocked_B1H	5.4	0.0	-17.9	6.0	-19.3	65.9	35.5	37.3	-27.3	36.4
HX_full_severe_blocked_B1H	5.1	0.0	-16.9	6.1	-19.3	65.9	35.7	36.2	-29.4	35.2

	Q_dot_cond_1_3 [kW]	Q_dot_cond_2_3 [kW]	Q_dot_cond_2_9 [kW]	T_sc_3 [K]	T_sc_XV [K]	T_sh_comp [K]	T_sh [K]	T_nozzle [C]	V_dot_IU [m3/s]	rho_a_nozzle [kg/m3]
H1_low_clean_1000ms_B1H	16.0	15.6	15.7	5.0	6.6	7.8	5.0	38.9	0.8	1.1
H1_low_clean_2000ms_B1H	16.0	15.6	15.7	5.0	6.6	7.9	5.0	38.9	0.8	1.1
H1_low_clean_4000ms_B1H	16.0	15.7	15.8	5.1	6.6	7.9	5.0	38.9	0.8	1.1
H1_low_clean_8000ms_B1H	16.0	15.7	15.8	5.1	6.6	7.8	5.0	38.9	0.8	1.1
H1_low_clean_B1H	16.8	16.5	16.6	5.0	6.2	5.5	4.8	39.8	0.8	1.1
H1_low_clean_REP_B1H	15.9	15.5	15.6	5.0	6.4	7.6	4.9	38.7	0.8	1.1
H1_low_light_blocked_B1H	15.9	15.6	15.7	5.0	6.4	7.9	4.9	39.0	0.8	1.1
H1_low_severe_blocked_B1H	15.8	15.5	15.6	5.0	6.4	8.3	5.3	38.9	0.8	1.1
H2_mid_clean_B1H	18.8	18.4	18.5	5.0	6.5	9.1	5.4	41.8	0.8	1.1
H2_mid_light_blocked_B1H	17.9	17.5	17.6	5.0	6.7	9.7	5.4	40.9	0.8	1.1
H2_mid_severe_blocked_B1H	15.7	15.3	15.4	4.9	6.9	12.2	6.6	38.7	0.8	1.1
H3_full_clean_unstable_B1H	18.2	17.7	17.8	4.5	6.8	10.8	5.2	40.9	0.8	1.1
H3_light_blocked_B1H	16.5	16.0	16.1	4.8	7.3	12.3	5.4	39.6	0.8	1.1
H3_severe_blocked_B1H	14.0	13.5	13.5	5.0	8.1	13.3	4.3	36.5	0.8	1.1
HX_full_clean_B1H	14.0	13.6	13.6	5.0	8.5	12.0	5.5	36.5	0.8	1.1
HX_full_light_blocked_B1H	13.7	13.2	13.3	5.1	8.8	13.0	5.5	36.1	0.8	1.1
HX_full_severe_blocked_B1H	12.8	12.4	12.4	5.0	9.0	14.5	6.4	35.1	0.8	1.1

Table A 19: Baseline 1H data, part 5

	V_dot_IU_standardair [kg/m3]	Q_dot_heat_airside [kW]	Q_dot_cond_airside [kW]	Q_dot_useful_airside [kW]	Q_dot_useful_refside [kW]	COP_h_airside [-]	COP_h_refside [-]	DT_air_on_eva7 [K]	T_dew_suc [C]	T_dew_dis [C]
H1_low_clean_1000ms_B1H	0.7	16.4	16.0	16.4	16.1	3.1	3.1	9.6	-2.1	41.3
H1_low_clean_2000ms_B1H	0.7	16.3	16.0	16.4	16.1	3.1	3.1	9.6	-2.1	41.3
H1_low_clean_4000ms_B1H	0.7	16.4	16.0	16.4	16.1	3.1	3.1	9.5	-2.1	41.3
H1_low_clean_8000ms_B1H	0.7	16.5	16.1	16.5	16.2	3.1	3.1	9.5	-2.0	41.3
H1_low_clean_B1H	0.7	17.2	16.9	17.3	17.0	3.2	3.1	7.5	-0.1	42.4
H1_low_clean_REP_B1H	0.7	16.3	15.9	16.3	16.0	3.1	3.1	10.3	-2.9	40.6
H1_low_light_blocked_B1H	0.7	16.4	16.0	16.4	16.1	3.1	3.1	10.1	-2.6	40.7
H1_low_severe_blocked_B1H	0.7	16.3	15.9	16.3	15.9	3.1	3.1	10.6	-3.0	40.6
H2_mid_clean_B1H	0.7	19.2	18.8	19.2	18.9	2.9	2.8	11.1	-11.0	44.4
H2_mid_light_blocked_B1H	0.7	18.4	18.0	18.4	18.0	2.9	2.8	13.1	-12.8	43.2
H2_mid_severe_blocked_B1H	0.7	16.1	15.8	16.1	15.8	2.7	2.7	17.8	-17.6	40.4
H3_full_clean_unstable_B1H	0.7	18.3	18.0	18.4	18.2	2.5	2.5	11.4	-22.2	42.0
H3_light_blocked_B1H	0.7	16.8	16.5	16.9	16.5	2.5	2.4	14.3	-25.3	40.3
H3_severe_blocked_B1H	0.7	14.1	13.8	14.1	13.9	2.3	2.3	19.5	-30.8	37.1
HX_full_clean_B1H	0.7	14.3	13.9	14.3	14.0	2.3	2.3	9.0	-30.1	37.8
HX_full_light_blocked_B1H	0.7	13.9	13.6	14.0	13.7	2.3	2.2	9.7	-31.0	37.4
HX_full_severe_blocked_B1H	0.7	13.0	12.6	13.0	12.8	2.2	2.2	11.8	-33.1	36.3

	T_bub_cond [C]	T_dew_evap [C]	DT_air_on_cond3 [K]	T_sh_vi_hp [K]	T_sh_vi_lp [K]	m_dot_vi_hp_mb [g/s]	m_dot_vi_lp_mb [g/s]	Q_dot_evap [kW]	m_dot_OU_air [kg/s]	m_dot_VI_H_YP [g/s]
H1_low_clean_1000ms_B1H	39.8	-1.4	18.7	-1.5	0.6	3.9	5.0	12.3	4.6	12.4
H1_low_clean_2000ms_B1H	39.8	-1.4	18.7	-1.6	0.5	3.9	5.0	12.3	4.8	12.4
H1_low_clean_4000ms_B1H	39.8	-1.3	18.7	-1.8	0.2	3.9	5.0	12.3	4.8	12.5
H1_low_clean_8000ms_B1H	39.8	-1.2	18.8	-1.7	0.1	3.9	5.0	12.3	4.7	12.6
H1_low_clean_B1H	40.9	0.8	19.8	-1.4	0.4	3.6	5.5	13.1	4.4	13.6
H1_low_clean_REP_B1H	39.6	-2.0	18.6	-0.8	0.6	4.3	4.8	12.2	3.2	12.4
H1_low_light_blocked_B1H	39.8	-1.8	18.7	-0.7	0.7	4.2	4.7	12.2	3.5	12.3
H1_low_severe_blocked_B1H	39.6	-2.2	18.6	-0.5	0.7	4.1	4.8	12.1	2.9	12.3
H2_mid_clean_B1H	42.9	-9.5	21.7	-1.6	-0.7	9.3	6.5	14.0	3.5	18.2
H2_mid_light_blocked_B1H	41.7	-11.2	20.7	-1.5	-0.5	8.9	6.0	13.2	2.9	17.0
H2_mid_severe_blocked_B1H	39.2	-16.0	18.2	-1.4	-0.2	8.5	5.0	11.4	2.6	14.6
H3_full_clean_unstable_B1H	41.4	-19.7	20.3	-0.7	-0.9	11.9	5.9	12.9	3.4	19.4
H3_light_blocked_B1H	39.8	-22.6	18.7	-0.9	-0.4	10.7	5.2	11.4	2.8	17.2
H3_severe_blocked_B1H	36.8	-27.8	15.9	-0.9	0.2	9.3	4.1	9.3	1.9	14.0
HX_full_clean_B1H	36.9	-26.7	16.0	-1.5	-1.0	8.8	4.4	9.7	3.7	14.3
HX_full_light_blocked_B1H	36.5	-27.3	15.6	-1.6	-0.7	8.4	4.2	9.3	3.8	13.7
HX_full_severe_blocked_B1H	35.4	-29.4	14.5	-1.7	-0.6	7.8	3.8	8.6	3.5	12.7

Table A 20: Baseline 1H data, part 6

	m_dot_VI_L_YP [g/s]	T_sh_cir12 [K]	T_sh_cir34 [K]	T_sh_cir56 [K]	T_sh_cir78 [K]	T_sh_cir910 [K]	T_sh_cir1 [K]	T_sh_cir2 [K]	T_sh_cir3 [K]	T_sh_cir4 [K]
H1_low_clean_1000ms_B1H	-2.1	5.8	5.8	5.8	5.8	5.8	5.5	6.1	5.4	6.2
H1_low_clean_2000ms_B1H	-2.1	5.8	5.8	5.8	5.8	5.8	5.6	6.1	5.4	6.3
H1_low_clean_4000ms_B1H	-2.0	5.8	5.8	5.8	5.8	5.8	5.5	6.1	5.4	6.2
H1_low_clean_8000ms_B1H	-1.9	5.8	5.7	5.7	5.7	5.7	5.5	6.1	5.4	6.1
H1_low_clean_B1H	-2.0	5.6	5.5	5.4	5.4	5.4	5.3	5.9	5.4	5.6
H1_low_clean_REP_B1H	-1.8	6.1	6.0	6.2	6.2	5.7	5.9	6.4	5.8	6.3
H1_low_light_blocked_B1H	-1.6	6.2	6.1	6.3	6.2	5.7	5.8	6.6	5.7	6.4
H1_low_severe_blocked_B1H	-1.6	6.5	6.4	6.4	6.2	5.8	5.8	7.1	6.2	6.6
H2_mid_clean_B1H	-0.9	6.9	7.0	6.9	7.0	7.1	5.9	7.9	6.5	7.4
H2_mid_light_blocked_B1H	-1.1	6.9	7.1	6.8	6.8	7.2	6.0	7.9	6.7	7.5
H2_mid_severe_blocked_B1H	-1.2	8.1	8.3	8.0	8.0	8.6	6.4	9.7	8.1	8.5
H3_full_clean_unstable_B1H	-0.1	7.1	6.9	6.7	6.6	6.6	6.0	8.1	6.4	7.4
H3_light_blocked_B1H	-0.4	7.5	7.2	6.7	6.9	9.2	7.1	8.0	8.2	6.2
H3_severe_blocked_B1H	-0.9	7.3	5.6	6.7	7.2	8.9	7.3	7.4	5.6	5.6
HX_full_clean_B1H	-0.7	7.0	6.8	6.8	7.0	7.3	6.5	7.4	6.6	6.9
HX_full_light_blocked_B1H	-1.0	8.1	7.8	7.1	7.3	7.3	7.9	8.3	7.8	7.7
HX_full_severe_blocked_B1H	-1.0	9.7	9.2	6.9	7.1	8.0	9.5	9.9	9.2	9.1

	T_sh_cir5 [K]	T_sh_cir6 [K]	T_sh_cir7 [K]	T_sh_cir8 [K]	T_sh_cir9 [K]	T_sh_cir10 [K]
H1_low_clean_1000ms_B1H	6.1	5.6	6.7	5.0	5.8	5.9
H1_low_clean_2000ms_B1H	6.1	5.6	6.7	5.0	5.8	5.9
H1_low_clean_4000ms_B1H	6.0	5.6	6.7	4.9	5.7	5.9
H1_low_clean_8000ms_B1H	6.0	5.5	6.6	4.9	5.6	5.9
H1_low_clean_B1H	5.5	5.3	5.7	5.1	5.2	5.6
H1_low_clean_REP_B1H	6.6	5.9	6.9	5.6	5.4	6.0
H1_low_light_blocked_B1H	6.4	6.1	7.1	5.3	5.7	5.8
H1_low_severe_blocked_B1H	7.4	5.5	6.3	6.0	5.7	5.9
H2_mid_clean_B1H	7.0	6.8	7.3	6.7	7.0	7.1
H2_mid_light_blocked_B1H	7.1	6.5	7.0	6.5	7.0	7.5
H2_mid_severe_blocked_B1H	9.2	6.7	7.9	8.1	8.3	8.9
H3_full_clean_unstable_B1H	7.2	6.2	7.1	6.1	6.8	6.4
H3_light_blocked_B1H	6.4	6.9	7.1	6.6	8.6	9.7
H3_severe_blocked_B1H	6.7	6.7	6.6	7.8	8.2	9.5
HX_full_clean_B1H	6.7	7.0	6.9	7.1	7.5	7.1
HX_full_light_blocked_B1H	7.3	7.0	7.6	7.0	7.3	7.4
HX_full_severe_blocked_B1H	8.5	5.3	6.5	7.7	8.0	8.0

B. Appendix B: Oil Flooded System

B.1 Calculation Methods

For the oil flooded system, capacity was measured on the airside of the indoor unit and therefore includes the heat-loss of the fan. Heating COP is calculated in the same way than for the vapor injected system.

B.2 Data Tables

Table B 1: Measurement data for oil flooded system

Date	T_OU_in C	EXV1	EXV2	Oil MFR kg/s	Oil MFR Stable	Oil Fraction	EXV3 Steps	Capacity Btu/h	Q_dot_useful_airside kW	Pwr_comp W	ID&OD fan power W	T_dis F	T_suc F	MFR lb/h	SH_suc F	SH_dis F	System COP	P_dis Psig	P_suc Psig
8/29/2013	8.33	0	0	0		0	370	61605	18.1	5901	879.7	194.84	51.1	732.4	25.1	81.31	2.65	383.81	89.68
8/29/2013	8.33	0	111	0.0044	No.	5%	277	63510	18.6	5871	880.9	187.54	50.8	735.0	25.1	72.74	2.75	390.5	89.0
8/29/2013	8.33	0	114	0.0105	Yes.(15min)	10%	360	63497	18.6	5747	883.0	175.26	50.6	734.5	25.4	61.49	2.80	385.0	88.1
8/29/2013	8.33	0	160	0.0143	Yes.(>5min)	13%	367	63451	18.6	5724	884.3	170.93	51.0	731.4	25.8	57.57	2.80	382.9	88.1
8/29/2013	8.33	0	200	0.018	Yes.(15min)	16%	372	63639	18.7	5721	886.1	166.89	50.7	730.4	25.8	53.92	2.81	380.9	87.5
8/29/2013	8.33	0	215	NA			372	63655	18.7	5724	885.8	166.3	50.8	729.8	25.8	53.33	2.81	380.9	87.8
8/29/2013	8.3	0	0	0		0%	160	66480	19.5	6293	884.5	231.46	75.5	664.4	50.3	112.52	2.71	412.8	88.1
8/29/2013	8.33	0	79	0.0057	No.	6%	165	67114	19.7	6049	885.4	214.27	74.6	672.9	50.0	95.71	2.83	410.7	86.9
8/29/2013	8.33	0	97	0.0082	Yes.(14min)	9%	167	67384	19.7	5988	885.4	204.74	74.5	673.6	50.0	86.82	2.86	407.2	86.7
8/29/2013	8.33	0	135	0.0135	Yes.(25min)	14%	173	67954	19.9	5932	885.1	195.36	74.9	680.3	50.3	78.02	2.91	404.1	87.0
8/29/2013	8.33	0	190	0.0166	Yes.(>10min)	16%	177	68327	20.0	5938	885.1	190.56	75.3	684.8	50.5	73.42	2.92	403.0	87.3
8/29/2013	8.33	0	210	NA			176	68485	20.1	5942	885.2	189.67	75.4	683.8	50.6	72.55	2.93	402.8	87.3
8/29/2013	8.33						175	64217	18.8	6060	885.3	211.4	59.6	694.4	34.5	95.3	2.70	397.3	87.9
8/29/2013	8.33						500	61320	18.0	5869	883.9	189.0	41.5	747.4	15.9	75.9	2.65	381.6	89.0
Date	T_OU_in C	EXV1	EXV2	Oil MFR kg/s	Oil MFR Stable	Oil Fraction	EXV3 Steps	Capacity Btu/h	Q_dot_useful_airside kW	Pwr_comp W	ID&OD fan power W	T_dis F	T_suc F	MFR kg/s	SH_suc F	SH_dis F	System COP	P_dis Psig	P_suc Psig
8/30/2013	-8.33	0	0	0			103	39800	11.7	4675	927.8	199.3	26.6		25.4	98.7	2.07	320.4	50.2
9/4/2013	-8.33	0	0	0		0%	105	39935	11.7	4696	924.6	223.5	50.4		49.5	121.6	2.07	326.6	49.7
9/4/2013	-8.33	0	85	0.0032	No.	6%	103	38629	11.3	4394	924.5	200.5	40.4	0.05246	41.5	100.2	2.12	319.4	47.1
9/4/2013	-8.33	0	85	0.0038	No.	7%	101	37129	10.9	4306	933.7	188.4	31.6	0.05205	35.0	89.3	2.07	313.9	44.2
9/4/2013	-8.33	0	95	0.0054	Yes.(20min)	9%	99	36706	10.8	4297	926.7	188.4	38.6	0.05400	42.6	89.3	2.05	313.9	43.5
9/4/2013	-8.33	0	120	0.0108	Yes.(20min)	17%	109	40571	11.9	4445	924.6	174.5	39.7	0.05217	39.08	74.41	2.20	318.1	49.3
9/4/2013	-8.33	0	160	0.014	Yes.(10min)	21%	109	40570	11.9	4408	915.2	165.7	39.6	0.05263	39.63	66.69	2.22	313.4	48.5
9/4/2013	-8.33	0	205	0.018	Yes.(15min)	25%	109	39417	11.6	4382	924.2	158.1	34.1	0.05294	34.93	59.79	2.17	310.2	47.5
Date	T_OU_in C	EXV1	EXV2	Oil MFR kg/s	Oil MFR Stable	Oil Fraction	EXV3 Steps	Capacity Btu/h	Q_dot_useful_airside kW	Pwr_comp W	OD fan power W	T_dis F	T_suc F	MFR kg/s	SH_suc F	SH_dis F	System COP	P_dis Psig	P_suc Psig
9/6/2013	-15	0	0	0		0	86	25342	7.4	4301	437.39	227.72	44.48		53.85	130.1	1.559	307.2	37.3
9/6/2013	-15	0	91	0.0037	No.	9%	90	25585	7.5	4103	440.3	202.93	45.35	0.03700	54.9	105.32	1.641	307.2	37.1
9/6/2013	-15	0	99	0.0075	Yes (15m)	18%	89	25495	7.5	4070	436.46	184.09	43.17	0.03409	52.99	87.81	1.649	301.3	36.8
9/6/2013	-15	0	132	0.0118	Yes (30m)	25%	89	25907	7.6	4064	443.12	173.88	41.12	0.03456	50.72	78.1	1.675	299.1	37.0
9/6/2013	-15	0	160	0.0145	Yes(30m)	30%	89	25783	7.6	4050	442.77	166.64	38.94	0.03372	48.7	71.54	1.673	296.2	36.9
9/6/2013	-15	0	200	0.018	Yes(>15min)	34%	88	25602	7.5	4043	441.83	162.24	42.2	0.03462	52.49	67.39	1.663	295.1	36.3